Technische Universität Braunschweig

Thermophysical Properties of a Moist Porous Material

Von der Fakultät für Maschinenbau
der Technischen Universität Carolo–Wilhelmina zu Braunschweig

zur Erlangung der Würde

eines Doktor–Ingenieurs (Dr.–Ing.)

genehmigte Dissertation

von: Muhammad Abid

aus: Multan, Pakistan

Thermophysical Properties of a Moist Porous Material

Von der Fakultät für Maschinenbau
der Technischen Universität Carolo–Wilhelmina zu Braunschweig

zur Erlangung der Würde

eines Doktor–Ingenieurs (Dr.–Ing.)

genehmigte Dissertation

von: Muhammad Abid
aus: Multan, Pakistan

eingereicht am: 21. November 2011
mündliche Prüfung am: 17. Februar 2012

Referenten: Prof. Dr.–Ing. Jürgen Köhler
Prof. Dr.–Ing. habil. Ulrich Groß
Dr. Ulf Hammerschmidt

Vorsitzender: Prof. Dr.–Ing. Ferit Küçükay

2012

Preface

This thesis is based on the experimental work carried out at thermal conductivity group (AG 1.74) at Physikalisch-Technische Bundesanstalt (PTB) Braunschweig, Germany. Financial support of this research work is given by Higher Education Commission (HEC), Pakistan and Deutscher Akademischer Austausch Dienst (DAAD), Germany, through a mutual co-operation. In year 2006, PTB has patented a new thermoelectric sensor to measure the thermal transport properties of a wide variety of materials. This sensor is known as Transient hot-bridge (THB) sensor. Since, there exists a large deviation in the uncertainty of thermophysical properties of porous materials as measured in the past, therefore; an accurate measurement method is needed to measure thermophysical properties of solid porous materials with low uncertainty values in the output data. This thesis is based on the measurement of thermophysical properties namely, thermal conductivity, thermal diffusivity and specific heat capacity of some porous materials especially of Sander sandstone because of its model porous structure.

Muhammad Abid
Braunschweig, February 2012

Acknowledgements

I would not have been able to finish this research work without the strong support and encouragement of a number of people to whom following paragraphs are dedicated. First, I would like to express my sincere gratitude to my advisor Dr. Ulf Hammerschmidt for supervising me throughout my PhD work and always keeping his doors open for discussions. I believe that his guidance will prove a valuable source of inspiration throughout my life. I owe my indescribable special indebtedness to my university supervisor Prof. Dr.–Ing. Jürgen Köhler, for his support and thesis supervision. I am very thankful to Prof. Dr. Werner Scholl for providing me a fascinating research place in PTB and keeping an eye on my research progress. I am also very thankful to him for his polite and friendly assistance. I want to thank Prof. Dr.–Ing. habil. Ulrich Groß and Prof. Dr.–Ing. Ferit Küçükay for their interest in my research work and also as being a second referee and chairman of the examination board for my thesis, respectively.

I am indebted to my colleges Mr. Manfred Rasper and Mr. Jörg Matthies who helped me at each time during my experiments and proved as a good language teacher for me in learning German language. It is all because of them that, today I am able to understand and speak German language. I would like to pay special thanks to Dipl.–Ing. Vladislav Meier who was very benevolent and ready to discuss experimental results at any time with me. I learn a lot from his experience concerning Transient hot-bridge (THB) theory and Finite Element simulations. I am grateful to Dr. Ingolf Bork for his help in FEM simulations. I want to thank our secretary Mrs. Marion Wittwer for her affectionate behavior and help during any official matters. I also thank her for arranging get together parties and outing trips. Furthermore, I am thankful to all staff members of the working group 1.72 in PTB for providing me a nice friendly atmosphere.

I am very grateful to Mr. Hermann Graser for providing me the sandstone samples. I would like to thank to Mr. Peter Hardi from TU Braunschweig, who performed SEM images and MIP on Sandstone sample. I am also thankful to the technical staff in PTB, especially Mr. Maik Röhr who helped me in preparing the samples.

My family is the source of all my happiness in this world. It is all because of my

parents who brought me up and gave me courage that, today I am going to complete my PhD degree. A countless bundle of thanks to my parents, brothers and sisters. With all my heart, I would like to thank my wife who always provides me a generous supply of sharing, understanding and so many things that I have realized in her presence. A very special thank to my loving sweet daughters, Huda Abid and Sarah Abid, whose presence removes all my tiredness in an eye blink. Finally, I want to thank Higher Education Commission (HEC), Pakistan and Deutscher Ackademischer Austausch Dienst (DAAD) Germany for financially supporting my doctoral studies.

Abstract

This dissertation is based on the experimental and empirical determination of the thermophysical properties namely, thermal conductivity, thermal diffusivity and specific heat capacity of moist porous materials, especially of Sander sandstone, using a state of the art thermoelectric sensor. In this work, Transient hot-bridge (THB) sensor, which is a new-patented thermoelectric sensor recently developed by Physikalisch-Technische Bundesanstalt (PTB) Braunschweig, is used to measure the thermal properties. Finite Element Method (FEM) is used to describe the complete geometry of the sensor and its working validity is checked by using a porous material. The investigated porous specimen of Sander sandstone is chosen from the southeast part, "Hermannsberg (Sand am Main)", Haßberge, of Germany. To explore the internal pore structure in Sander sandstone, its physical characterization is done by using Scanning Electron Microscopy (SEM) and Mercury Intrusion Porosimetry (MIP) methods. Porosity of the sample is also determined using free-saturation method (Archimedes principle).

Temperature dependence of thermal properties of Sander sandstone, bricks, cellular concrete and unconsolidated sand are measured in a temperature range of -20 to +40 °C. To understand freeze-thaw process in the porous structures, a very slow cooling rate is applied to see the possible variations in the thermal properties during phase transition of water into ice at freezing temperatures. To obtain more details on the simultaneous transport of heat and matter inside sandstone, measurements are carried out by filling the porous sandstone structure one by one with six different fluids of different thermal conductivities and next with six different gases also having different thermal conductivities. Three thermal parameters are measured simultaneously for each saturation state. Purpose of saturating sandstone with different stagnant fluids is to analyze the effect of these fluids on the overall effective thermal properties of the sandstone. Moreover, effect of applied dilute gas pressure on the thermal conductivity of sandstone is also presented. Results on significantly reduced thermal conduction due to low pressure in the pores are discussed on the basis of Knudsen-effect. For building application point of view, determination of the effect of relative humidity (RH) from 0 to 90 % on thermal performance of Sander sandstone is observed accord-

ing to the temperature and humidity conditions in Europe. For comparison reasons, thermal conductivity, thermal diffusivity and specific heat capacity values are also determined using few other standard methods like steady-state method, laser flash method and differential calorimetric method, respectively. To become a part of these efforts, an empirical model for the determination of effective thermal conductivity of porous materials in terms of easily measurable parameters such as porosity, thermal conductivity of the solid matrix (λ_{matrix}) i.e., mineral components and the thermal conductivity of the saturating fluids (λ_f) is also proposed.

Kurzfassung

Diese Dissertation behandelt die experimentellen und empirischen Bestimmungen der thermophysikalischen Eigenschaften Wärmeleitfähigkeit, Temperaturleitfähigkeit und spezifische Wärmekapazität von feuchtebeladenen porösen Materialien. Mit einem neuartigen Sensor wurden vor allem Sander Sandstein aber auch Ziegel, Porenbeton und Sand untersucht. Die gewonnenen Ergebnisse lassen sich mit einem phänomenologischen Transportmodell mit sehr guter Genauigkeit beschreiben. Der in der Physikalisch-Technischen Bundesanstalt entwickelte thermoelektrische Transient-Hot-Bridge (THB) Sensor wurdefür die experimentellen Untersuchungen eingesetzt. Zuvor ist mit der Finite-Elemente-Methode (FEM) seine komplette Geometrie und die thermische Arbeitsweise kritisch validiert worden. Die numerischen Ergebnisse der diversen Simulationen wurden an den genannten porösen Materialien erfolgreich überprüft. Die untersuchten Sandsteinproben sind aus Sander Sandstein und stammen direkt vom Steinbruch "Hermannsberg (Sand am Main)", Haßberge, Deutschland. Zur Erkundung ihrer inneren Porenstruktur, wurde die Rasterelektronen Mikroskopie (SEM) und Quecksilberdruck-porosimetrie (MIP) eingesetzt. Die Porositaet der Proben wurde auch nach der Sättigungsmethode (Archimedes-Prinzip) bestimmt. Die Temperaturabhängigkeit der genannten thermischen Eigenschaften von Sander Sandstein, Ziegel, Porenbeton und lockerem Sand sind in einem Temperaturbereich von -20 bis +40 °C gemessen worden. Hierbei konnten Phasenumwandlungen in den porösen feuchtebeladenen Strukturen bei Temperaturen unter dem Gefrierpunkt von Wasser beobachtet werden. Zur besseren Auflösung der Frost-Tau-Zyklen, wurden sehr langsame Abkühl-und Aufheizraten gewählt. Der wesentliche Teil der Arbeit beschäftigt sich mit den physikalischen Vorgängen beim gleichzeitigen Transport von Wärme und Materie in Sandstein als Folge eines äusseren Temperaturgradienten. Hierzu wurde der Sandstein nacheinander mit sechs verschiedenen Flüssigkeiten und sechs verschiedenen Gasen von jeweils unterschiedlicher Wärmeleitfähigkeit jeweils bis zur freien Sättigung gefüllt. Für jedes Füllfluid wurden die drei genannten thermophysikalischen Eigenschaften des erzeugten Festkörper-Fluid-Systems gemessen. Darüberhinaus konnte an gasgefülltem Sandstein der Knudsen-Effekt nachgewiesen werden, die stark verminderte thermische Leitfähigkeitskomponente des verdünnten

Gases in den Poren. Von besonderer Bedeutung, insbesondere für die Bauphysik, sind die Ergebnisse der Messungen mit dem Füllfluid als feuchte Luft. In der Klimakammer wurden Sandsteine bei relativen Feuchten zwischen 0 % und 90 % (RH) gemessen. Die erhaltenen Ergebnisse unterscheiden sich signifikant von denen der anderen (trockenen) Füllfluide.

Die experimentell ermittelten Daten zur Wärmeleitfähigkeit, Temperaturleitfähigkeit und spezifischen Wärmekapazität wurden verglichen mit den Ergebnissen anderer Messverfahren, z.B. Plattenverfahren, Laser-Flash-Verfahren und DSC (differential scanning calorimetry). Auch wurden sie an bekannte theoretische Modelle aus der Literatur angepaßt. Während der reine Datenvergleich recht gute Ergebnisse lieferte, konnte keines der ausgewählten Modelle die hier gewonnenen Daten zufriedenstellend beschreiben. Es wird daher ein eigenes phänomenologisches Modell vorgeschlagen, dass den Einfluss des Füllfluids auf die Wärmeleitfähigkeit des Sandsteins mit sehr guter Genauigkeit wiedergibt.

Contents

Chapter 1

Introduction

Determination of thermophysical properties of porous materials is of great importance in a wide variety of applications. The main thermal properties include thermal conductivity, thermal diffusivity and specific heat capacity (or volumetric heat capacity). Whereas, physical properties mainly include porosity, density and pore size distribution in case of porous materials. Heat transfer applications can be found in many areas, for example: automotive engines, gas turbines, electronics, aerospace, chemical reactions, food and bio-engineering, environment, underground storage of heat, buildings etc. The importance of thermophysical parameters depends directly on the materials and their appropriate use. These are particularly important when the behavior of materials changes with temperature, pressure and fluid-saturation. In porous consolidated materials heat transfer mechanism may occur in all of its three forms (conduction, convection and radiation) depending on the pore sizes and temperature. In this chapter, the choice of a model porous material, the motivations, and the aims of the work are presented.

1.1 Motivations

Thermophysical properties of consolidated porous rocks/stones are needed in a wide variety of applications whether these are underground or on the surface of earth. In all underground applications, like underground buried steam and hot water pipes, heat dissipation from underground nuclear explosions and disposal of nuclear wastes, rate of heat loss from the earth due to geothermal gradient [1], construction of buildings on permafrost zones, dissipation of heat through porous rocks, oil and gas recovery through underground reservoirs etc, all require accurate determination of the thermal properties of the surrounding medium. To store solar energy in summer season,

underground aquifers are built which uses rock surroundings as temporary storage of heat or cold [2]. Accurate measurement of thermal properties are also necessary to estimate the ability of the surrounding rock reservoirs (aquifers) to store thermal energy. A recent example is underground heat and cold storage system underneath the German Reichstag in Berlin [3]. Therefore, knowledge of thermal conductivity, thermal diffusivity and specific heat capacity is of prime importance for all kinds of underground energy storage systems. Different types of rocks are present underneath the earth surface. Among these rock types, Sandstone is commonly used as aquifers because of its prevalent availability, porosity, permeability and high capacity to store fluids/gases.

On the other hand, on earth surface applications, uses of porous stones and rocks are highly important in the areas of building physics. Thermal insulation of a building depends on the type of the building material used. For higher thermal insulations, porous materials are best choice. But at the same time, these may be worse if the porous structure is filled with some liquid (let say, water). Therefore, study of thermophysical properties of porous stones/rocks play a vital role when we apply this study on building insulations where fluid saturation can affect the thermal performance of the buildings made from porous stones. Generally, thermal properties of porous materials depend on many factors such as thermal properties of its mineral constituents, saturating fluid, porosity and distribution of pores within the medium, size and shape of pores, tortuosity, temperature etc. Among all of these factors, the amount of pores in a porous materials acts as one of the most important parameter.

Accurate determination of thermophysical properties has always been a challenging problem. Production and applications of porous building materials has largely increased in last two decades. The improvement of new experimental methods for measurement of thermophysical properties, particularly transient methods, and their application to the modern non-homogeneous and homogeneous porous materials has generated a large amount of published thermophysical data so far. Unfortunately, there are many discrepancies in the data obtained through the various experimental methods and these discrepancies need corrections. Particularly, very less reliable data is available in the case of fluid-saturated porous media. Therefore, there is an imperative need of accurate determination of thermophysical data, especially for saturated porous materials. This is only possible if measurements are done using some state of the art instrument having most advantages and least disadvantages as compared to its predecessors.

1.2 Aims of the Work

There are three main objectives of this work as following,

1. Determination of thermophysical properties namely, thermal conductivity, thermal diffusivity and specific heat capacity of moist porous materials (a special case study of Sander sandstone) using the newly developed Transient Hot-Bridge (THB) sensor at various environmental conditions. It consists further,

    - Investigation of the temperature dependent thermal properties of Sander sandstone in a temperature range of -20 to +40 °C, especially, during phase transition of water into ice at freezing temperatures (to understand the freeze-thaw process in the porous structure of sandstone).
    - Determination of the thermal properties of Sander sandstone depending on different fluid-saturations and pressure (in the context of underground applications of sandstone reservoirs)
    - Determination of the effect of moisture (0 to 90 % RH) on thermal performance of Sander sandstone from -20 to +40 °C (in the context of building applications).
    - Complete understanding of the heat transfer mechanism is not possible without having knowledge on the internal pore structure and pore size distribution of the stone; therefore, physical characterization of the Sander Sandstone is also done using Scanning Electron Microscopy (SEM) and Mercury Intrusion Porosimetry (MIP) methods.

2. The second aim of this study is to check the validity of the newly developed THB sensor using Finite Element Simulations (COMSOL Multiphysics version 3.4) and comparing the experimental results with the simulated ones.

3. The third aim of this work is to develop an empirical model for the determination of the effective thermal conductivity of porous materials in terms of easily measurable parameters such as porosity, thermal conductivity of the saturating fluids (λ_f) and the thermal conductivity of the solid matrix (λ_{matrix}) i.e., mineral components.

1.3 Structure of the Thesis

Chapter 2 of this thesis is based on the theory of main thermal parameters and chapter 3 describes some state of the art in thermophysical property measurement

methods, their comparison and at the end choice of a best measurement technique. Chapter 4 is based on Finite Element Simulations (FEM) of the transient hot-bridge method and its measurement validity for porous materials. Chapter 5 describes the physical characterization of Sander sandstone using some standard characterizing methods. Chapter 6 describes the temperature dependent thermophysical properties of Sander sandstone using transient hot-bridge method. Chapter 7 is based on the determination of thermophysical properties of Sander sandstone depending on different liquid/gas saturations and pressure. Since, different porous structures may behave (thermally) in different ways therefore, in chapters 6 and 7, we discussed thermophysical properties of a homogeneous (macroscopically) porous structure i.e., Sander sandstone, while chapter 8 of this thesis describes the thermal conductivity of heterogeneous porous structure of bricks and aerated concrete (cellular/foam concrete), both having different pore structures as compared to Sander sandstone. In chapter 9, an empirical model is proposed to estimate the effective thermal conductivity of porous materials. This chapter also explains few already existing theoretical and empirical models for the determination of the effective thermal conductivity. In addition, a comparison of the experimental results with the results obtained through various existing models are also given. Last section (chapter 10) provides conclusions and recommendations from this work.

1.4 Choice of a Model Porous Material

Figure 1.1: Place of chosen Sander sandstone.

There are different types of porous materials depending on several parameters like porosity, density and mineral components. The most commonly used porous building materials are sandstone, bricks, foam concrete (for light weight buildings). In order to carry out experimental work we had to choose one of these porous materials. Sandstone is widely used as a masonry material for the construction of monuments and restoration of old historical buildings because its soft characteristics makes it easy to cut into regular shapes and to work with it. In this work, we have chosen Sander sandstone for experimentation because of four main reasons, (1) its widespread availability compared to other consolidated rocks/stones, (2) its vast use in monumental and historical buildings, particularly in Germany when, after the second world war thousands of old and historical buildings are reconstructed with Sander sandstone, (3) its use as aquifers in underground storage of thermal energy, (4) its exemplary macroscopic homogeneous pore structure [4]. Apart from these facts, its excellent porous features like its average range of porosity, tortuosity, pore size distribution and pore inter-connectivity also motivated us to consider it as a model porous substance to study the thermal transport properties of porous rocks/stone system. Sander sandstone is named after the German village "Sand am Main" and is spread at different sites near the river Main in the state of Bavaria in south part of Germany.

1.5 State of the Art in Thermophysical Property Measurements

Numerous experimental methods are used for the determination of thermophysical properties and each method has its own limited working range and suitability for a particular type of material. Nevertheless, a state of the art instrument is always needed to meet all the requirements (accurate measurement, less uncertainty, less measuring time, multiple thermal parameters in a single run).

Physikalisch-Technische Bundesanstalt (PTB) is a worldwide renowned national metrological institute of Federal Republic of Germany and is involved in the invention and calibration of new instruments. In year 2006, PTB has invented a new state of the art thermoelectric sensor for the determination of thermophysical properties of a wide variety of materials. The sensor is known as Transient Hot-bridge Sensor (THB) and is based on the transient technique of measurements. A detailed theory of THB sensor and its comparison with few other well-known transient methods is given in chapter 2.

1.6 Main Thermal Properties of Materials

Thermophysical properties of porous materials (especially building materials) are mainly determined by the following three parameters:

- Thermal conductivity (λ)
- Thermal diffusivity (a)
- Specific heat capacity (c_p)

First two parameters determine the ability of a material to conduct heat and how fast thermal energy is transmitted through the material respectively, while the third parameter determines the ability of materials to store the thermal energy. In the following chapter, we will discuss each of these properties in details.

Chapter 2

A Short Theory on Main Thermophysical Parameters

Thermophysical properties are the material properties which affect the transfer and storage of heat without changing the chemical characteristics of the material. These properties mainly include thermal conductivity, thermal diffusivity and heat capacity. In any material, heat can be transferred in three major ways: conduction, convection and radiation. A brief description on each of these modes [5] and above mentioned three thermal properties is given in this chapter.

2.1 Different Modes of Heat Transfer

2.1.1 Conduction

Thermal conduction is the transfer of heat from more energetic particles of a substance to the adjacent less energetic ones. Conduction can take place in solids, liquids and gases. In solids, conduction is due to the presence of free electrons or phonons[1]. Transfer of heat through a medium occurs whenever there exist a temperature gradient across the medium. The first clear statement of the relationship between heat flow and the temperature gradient is given by Joseph Fourier in 1822 [6]. Fourier's law (or law of heat conduction) is defined as, "the time rate of heat transfer through a material is proportional to the negative gradient in the temperature and to the area, at right angles to the gradient through which the heat is flowing".

[1]Lattice vibrations in solids are treated as sound waves obeying harmonic oscillator equation ($E_n = (n + 1/2)\,\hbar w$). These harmonic oscillators are found to posses energy only in discrete energy units of $hv = \hbar w$. These quanta of energy are called phonons.

2.1.2 Convection

Transfer of heat by the movements of the particles of a liquid or gas is termed as convection. Convection is one of the major modes of heat and mass transfer in liquids and gases. There can be two types of convection, i.e., natural convection and forced convection. Natural convection is a type of heat transfer in which the fluid motion is due to the density variations within the fluid occurring as a result of a temperature difference. Whereas, in forced convection, fluid motion is done by using some external sources like a fan, pump, etc.

In general, convective heat transfer is expressed by Newton's law of cooling. It states that, "the transfer of heat per second from the surface of a body is proportional to the difference in the temperatures between the body and its surroundings". Mathematically, we can write it as:

$$\frac{dQ_{conv}}{dt} = -hA\left(T_s - T_{env}\right) \tag{2.1}$$

where Q_{conv} is the amount of thermal energy in Joules, h is the convection heat transfer coefficient in units of $\mathrm{W.m^{-2}.K^{-1}}$, A is the surface area through which convective heat transfer takes place, T_s is the surface temperature of the body and T_{env} is the temperature of the surrounding environment.

2.1.3 Radiation

Emission of electromagnetic waves from a body at temperatures greater than absolute zero ($T > 0$ K) is called thermal radiation. Unlike conduction and convection, the transfer of heat by radiation does not require the presence of an intervening medium.

All objects at temperatures greater than absolute zero continuously radiate and absorb energy in the form of electromagnetic waves. Total amount of energy that can be emitted from any surface at an absolute temperature is given by Stefan-Boltzmann law. It states that, "the amount of heat energy radiated from a surface is proportional to the fourth power of its absolute temperature".

$$\frac{dQ_{rad}}{dt} = \sigma A T_s^4 \tag{2.2}$$

In equation 2.2, Q_{rad} is the amount of thermal energy radiated by the body and $\sigma = 5.67\times10^{-8}$ $\mathrm{W.m^{-2}.K^{-4}}$ is the Stefan-Boltzmann constant. The idealized surface that emits and absorbs radiation at maximum rate is called a black body, and the radiations emitted by a black body are called black body radiations. Radiations emitted by all real surfaces are less than the radiations emitted by a black body at the same temperature. If a body at temperature $T_1 > 0$ K is radiating energy to an

other body at temperature T_2 (where, $T_1 > T_2$) then, the net amount of radiation transfered between the two real bodies can be expressed by Stefan-Boltzmann law as:

$$\frac{dQ_{rad}}{dt} = \epsilon\sigma A \left(T_1^4 - T_2^4\right) \tag{2.3}$$

where ϵ is the emissivity of the surfaces and its value is in the range $0 \leq \epsilon \leq 1$. For an ideal radiator (black body), the value of emissivity is 1 (i.e., $\epsilon = 1$).

2.2 Main Thermophysical Properties

2.2.1 Thermal Conductivity

Consider a slab of a material of thickness dx and cross-sectional area A. One face of the slab is at temperature T_1, and the other face is at temperature T_2, with $T_2 > T_1$ as shown in figure 2.1. Experimentally, it is found that the amount of heat transferred (Q) in a time (dt) flows from the hotter face to the colder one. The rate (Q/dt) at which this heat flows is found to be proportional to the cross-sectional area and and the temperature difference ($dT = T_2 - T_1$), and inversely proportional to the thickness:

$$\frac{Q}{dt} = \lambda A \frac{dT}{dx} \tag{2.4}$$

where, λ is a constant of proportionality and is called the thermal conductivity. Thermal conductivity of a material is defined as, "the quantity of heat transmitted due to unit temperature gradient in unit time, under steady-state conditions in a direction normal to the surface of unit area of cross-section".

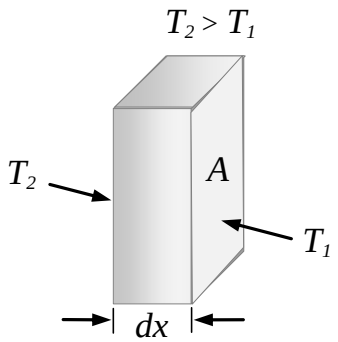

Figure 2.1: Transfer of heat through a conducting slab [7].

In simple words, thermal conductivity is the ability of a material to transfer heat and it is an intrinsic property of the materials. It is measured in the units of $\mathrm{W.m^{-1}.K^{-1}}$.

In metals, heat is transported both by electrons and phonons. From different points of view [6], phonons are regarded as pseudo particles and a solid is considered as a gas of such pseudo particles. Therefore, transmission of heat appears as a diffusion of phonons from a hot region where they are more in number to a cold region where they are less. In semi-metals such as bismuth or in metals containing large amounts of impurities (alloys), the phononic conductivity may be important. In insulators, heat is transmitted almost entirely by phonons, since there are no free electrons in the substance.

From kinetic theory of gases, thermal conductivity of a system of phonons (solids, liquids and gases) can be computed using the following relation [11]:

$$\lambda = \frac{1}{3} n.c_v.\overline{v}.\bar{l} \tag{2.5}$$

where n is the molecular density of the gas, c_v is the specific heat capacity at constant volume, $\overline{v}$ is the mean velocity and $\bar{l}$ is mean free path of the particles (atoms or molecules).

In context of this work, we shall confine ourselves more towards the thermal conductivity of insulators to obtain some insight into the phononic conductivity for the reason that our stone samples are insulators. Thermal conductivity values of insulating materials such as polymers, ceramics and glasses typically lie in the range of 0.1 to 2 $W.m^{-1}.K^{-1}$. Dry porous rocks/stones are poor conductors of heat and have a narrow range of thermal conductivity (0.1 – 7 $W.m^{-1}.K^{-1}$) as compared to the metals. Thermal conductivity of rocks/stones mainly depend on their constituent minerals and mineral arrangements. However, porosity and the amount of liquid saturation in the case of moist porous rocks/stones may have an immense effect on the thermal conductivity values. For example, thermal conductivity of water-saturated clay increases six times as compared to its dry state values.

2.2.2 Theory of Thermal Conductivity

The overall thermal conductivity in solids consists of two entirely independent terms, that are, the contribution due to phonons and the contribution due to electrons. However, there are few other minute excitations in the structure of solids, such as spin waves but they have a small contribution in the overall conduction of heat.

$$\lambda = \lambda_{electron} + \lambda_{phonon} \tag{2.6}$$

2.2.2.1 Electronic Thermal Conductivity

It is seen that, metals which are good electrical conductors are also good thermal conductors. According to the Wiedemann–Franz law "the ratio of the thermal conductivity to the electrical conductivity of a metal is proportional to the temperature".

$$\frac{\lambda_{electron}}{\sigma} = LT \tag{2.7}$$

Where, L is a constant of proportionality and is called Lorenz number, T is the temperature, σ is the electrical conductivity and $\lambda_{electron}$ is the thermal conductivity due to electrons. The numerical value of L is 2.4453×10^{-8} W.Ω.K^{-2}.

2.2.2.2 Phononic Thermal Conductivity

In nonmetals, transport of heat due to phonons is the leading thermal conduction mechanism. If a temperature gradient exists in a body, phonons are considered to flow down the temperature gradient. The thermal conductivity of the body is determined by inelastic collisions of phonons or, according to the kinetic theory, by the mean free path of phonons [14].

In a system of phonon gas, there may be three types of collisions.

1. The collision of phonons with other phonons.
2. The collision of the phonons with imperfections in crystal such as impurities and dislocations.
3. The collision of phonons with the external boundaries of the sample.

Suppose that two phonons of wave vectors K_1 and K_2 collide elastically inside first Brillouin zone and produce a third phonon of wave vector K_3. If, the wave vector K_3 also lies inside the first Brillouin zone, then the total momentum and energy of the system will be conserved (i.e., elastic scattering) and we get $K_3 = K_1 + K_2$. Such a process has no effect on the overall thermal conductivity of the system. It is called, "Normal process or N-process".

By contrast, if two phonons having wave vectors K_1 and K_2 but with increased momentum collide inelastically inside the first Brillouin zone and produce a third phonon with wave vector K_3 which appears outside the first Brilloin zone then, the total momentum of the system may not be conserved (i.e., inelastic scattering). The kinematics of the collision between two phonons is described as [8]:

$$K_1 + K_2 = K_3 + G \tag{2.8}$$

where G is the reciprocal lattice vector as shown in figures 2.2. Processes or collisions in which $G \neq 0$ are called, "Umklapp processes or U-processes" [9]. This term refers to the circumstances that a collision of two phonons both having a positive K_x can, by Umklapp, give after collision a phonon with negative K_x, i.e., the propagation direction is changed. At high temperatures ($T > \theta_D$; where θ_D is the Debye temperature) and consequently due to high momentum change after collisions, a substantial portion of all phonon collisions will be then U-process. The thermal conductivity of the material determined by umklapp process may be considered as a fundamental property and is called lattice thermal conductivity [14].

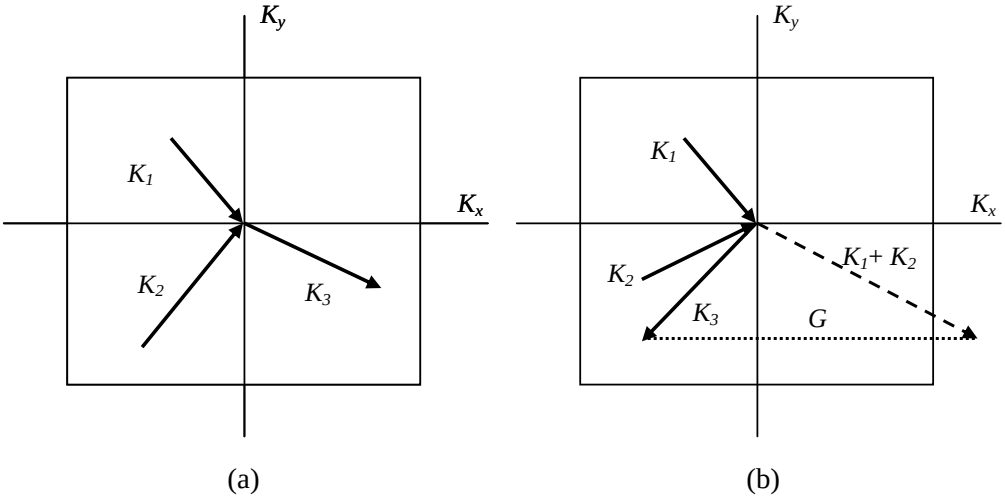

Figure 2.2: (a) Normal process (b) Umklapp process

The density of phonons is directly proportional to the temperature T while the mean free path l of a given phonon is inversely proportional to the density due to all other phonons with which it interacts.

$$l \propto T^{-1} \quad for \quad T >> \theta_D \tag{2.9}$$

Therefore, according to equation 2.5, the thermal conductivity for an insulating material where U-process are dominant varies as $1/T$ dependence.

Crystal imperfections such as impurities and defects also scatter phonons because they partially destroy the perfect periodicity. For instance, a substitutional point impurity, having a mass different from that of the host atom causes scattering of the wave. The greater the difference in the mass and greater the density of impurities, the greater is the scattering and shorter the mean free path. At low temperatures ($T << \theta_D$), both phonon-phonon and phonon-imperfection collisions become ineffective, because in the former case, there are only a few phonons present, and in the latter case, the few phonons which are excited at this temperature are associated with

long wavelengths. These are not effectively scattered by objects such as impurities, which are much smaller in size than the wavelength.

2.2.3 Thermal Diffusivity

Thermal diffusivity of a material is defined as "the ratio between the thermal conductivity to the volumetric heat capacity". Mathematically, it can be written as:

$$a = \frac{\lambda}{\rho.c_p} \tag{2.10}$$

where ρ is the density of the material and $\rho.c_p$ represents the volumetric heat capacity of the material. The S.I unit of thermal diffusivity is $m^2.s^{-1}$.

Thermal diffusivity of rocks/stones is a strong function of temperature and decreases with increasing temperature [15]. It varies in a same way as thermal conductivity but it is amplified/reduced by the temperature behavior of the heat capacity. According to Carslaw and Jaeger (1959), thermal diffusivity values for various rocks and soils range in between 0.2 and 1 $mm^2.s^{-1}$ [37].

2.2.4 Specific Heat Capacity

As name indicates, heat capacity (C) of a material is its ability to store thermal energy. It is an extensive property of material. A useful quantity is the specific heat capacity at constant pressure (c_p) that can be defined as, "the amount of heat required to raise the temperature of unit mass by one degree". The S.I unit of specific heat capacity is $J.kg^{-1}.K^{-1}$. Sometimes volumetric specific heat capacity term is also used. It is obtained by multiplying specific heat capacity (c_p) with density (ρ) and has units of $J.m^{-3}.K^{-1}$. The range of variation of specific heat capacity in solids and particularly in rocks/stones is much more narrow than that of thermal conductivity. Specific heat capacity of rocks varies from 400 to 2000 $J.kg^{-1}.K^{-1}$ and is usually higher than that of metals [17]. Specific heat capacity of a rock saturated with one or more fluids is dependent on the heat capacity and density of the saturating fluid, fractional porosity of the rock and the fractional saturation of the fluids. Specific heat capacity of rocks/stones also depends on temperature and increases with increasing temperature but only up to the extent of about 30 % over a wide temperature range [18].

2.2.4.1 Debye Approximation of Specific Heat Capacity

According to the classical statement (Dulong and Petit law), the specific heat capacity of a solid substance is equal to $3R$, where R is the universal gas constant.

Dulong-Petit law gives good prediction for the specific heat capacity of solids with relatively simple crystal structure at high temperatures ($T >> \theta_D$). However, it fails at room temperatures. In low (cryogenic) temperatures, this law completely fails for all substances. This classical theory for the specific heat capacity of solids does not explain the decrease of specific heat capacity at low temperatures. The physical models of the specific heat capacity as given by Einstein and subsequently modified by Debye, agree well with the experiments. In Debye approximation, specific heat capacity is represented by the following expression:

$$c_v\left(T\right) = 9R\left(\frac{T}{\theta_D}\right)^3 \int_0^{\theta_D/T} \frac{e^x x^4}{(e^x-1)^2} dx \tag{2.11}$$

where $x = \frac{\hbar\omega}{kT}$ is the Einstein temperature and $k = 1.38065 \times 10^{-23}$ J.K^{-1} is the Boltzmann constant.

2.2.4.2 High Temperature Limit

For high temperatures, when $T >> \theta_D$, the value of θ_D/T becomes very small. By using the approximation, $e^x = 1 + x$, equation 2.11 becomes as:

$$c_v = 3R = 3Nk. \tag{2.12}$$

This means, at higher temperatures the Debye approximation of specific heat capacity (equation 2.11) fulfills the classical Dulong-Petit law.

2.2.4.3 Low Temperature Limit

At low temperatures, when $T << \theta_D$, specific heat capacity tends to zero. This decrease is some times referred to the freezing of the degrees of freedom of the system. We may approximate $\theta_D/T = \infty$ and therefore the integral on the right-hand-side of the equation 2.11 becomes as:

$$\int_0^\infty \frac{x^4 e^x}{\left(e^x-1\right)^2} = \frac{4}{15}\pi^4. \tag{2.13}$$

By inserting above approximation in equation 2.11, we get:

$$c_v = \frac{12\pi^4 R T^3}{5\theta_D^3} \cong 324R\frac{T^3}{\theta_D^3}. \tag{2.14}$$

Equation 2.14 shows that, at low temperatures specific heat capacity varies as T^3 temperature dependence.

Chapter 3

Experimental Methods to Measure Thermophysical Properties

There exists a large variation in the thermal transport properties (thermal conductivity, thermal diffusivity and specific heat) of materials, consequently there are numerous experimental methods for the measurement of these thermal properties. Each of these methods is suitable for a limited group of materials depending on the thermal and physical properties as well as on the temperature field. All of these methods can be classified into two major groups namely,
(i) Steady-state methods,
(ii) Transient methods.
Measurement techniques in which temperature field and heat fluxes across the sample are kept constant are called steady-state methods. Whereas, in transient methods, heat is generated inside (except Laser Flash method) the material and temperature rise of the heating source is measured with time. In principle, these two methods can be classified on the basis of temperature field inside the sample. This temperature field can be described by its change in space (i.e., dT/dx) and its change in time (i.e., dT/dt).

3.1 Steady-state Methods

In steady-state methods temperature field across the sample does not change with time. Therefore, $dT/dt = 0$. But to measure thermal conductivity of the material a temperature difference across the sample is necessary. Therefore, in steady-state methods $dT/dx \neq 0$. Steady-state methods apply Fourier's law of heat conduction to determine the thermal conductivity. An example of a most widely used steady-state

method is guarded-hot plate method that is explained in below section.

3.1.1 Guarded Hot-plate Method

The GHP method was standardized in 1945 and is designated as ASTM test method C-177 [19]. This method is used for the determination of thermal conductivity of non-metals such as glasses, polymers, ceramics and thermal insulation materials. It can also be used for liquids and gases in a temperature range between 80 to 800 K [20]. A steady-state heat flow through the homogeneous material at constant temperature is a necessary condition in this method. A GHP apparatus has two types; namely, Single-sided Guarded Hot Plate (GHP-S) and Double-sided Guarded Hot Plate (GHP-D) apparatus. Both types of methods consist of a cold plate, a hot plate, guard heaters, samples and insulation. However, GHP-D consists of two cold plates. Hot plate is surrounded by guard heaters and by thermal insulation to make sure that the heat released in the hot plate is passed only from the sample. In this way, heat loses from the hot side may be minimized and accuracy in the results may be increased. In GHP method, there are two main sources of errors, (1) heat flux loses, and (2) temperature difference determination. The main role to the heat flux errors is due to the heat loses from the heater and the sample to the surroundings. Two-sided GHP apparatus is more accurate because of the fact that, heat loses can be controlled more effectively due to symmetric specimen arrangement.

A sketch diagram of a single plate guarded hot plate method (GHP-S) developed at Physikalisch Technische Bundesanstalt (PTB) Braunschweig, Germany, is shown in figure 3.1. It can measure thermal conductivity of solids in a range between 0.01 to 6 $W.m^{-1}.K^{-1}$ as a function of temperature between -80 to 200 °C. This GHP-S apparatus [21; 22] is designed as a stack and is fitted in a casing (G) that can be evacuated. Sample (A) is prepared in the form of a cylindrical disc and is placed between the upper hot plate (B) and the lower cold plate (C) and is insulated from its lateral faces (F). A constant electric current is passed through the electric heater inside the hot plate that generates thermal energy due to joule heating effect. To ensure one dimensional heat flow; two guard heaters, guard plate (D) and guard ring (E) are mounted above the sample. Push rod (H) helps in establishing good thermal contacts between the sample and the heater/sink. Heat flows from hot-plate side to cold-plate side and establishes a temperature difference ΔT across the sample after some time. The thermal conductivity (λ) of the sample can be determined by knowing the heat flux through the specimen and the temperature difference across its two faces using following formula,

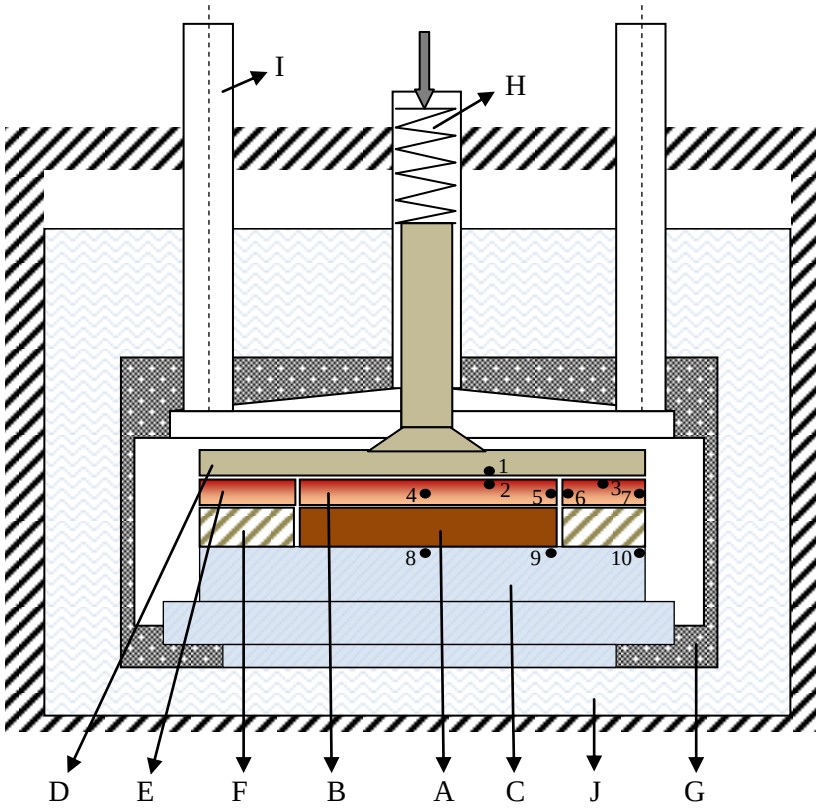

Figure 3.1: Schematic diagram of Guarded Hot Plate apparatus (GHP-S), A, specimen; B, hot plate; C, cold plate; D, guard plate; E, guard ring; F, edge insulation; G, casing; H, push rods; I, ducts; J, thermostatic bath; 1-10, thermocouples [21].

$$\lambda = \frac{Q.d}{A.(T_2 - T_1)} = \frac{q.d}{T_2 - T_1} \tag{3.1}$$

Where, q is the heat flux through the sample, d is the thickness of the sample, A is the cross-sectional area of the sample, T_2 is the temperature of the hot side of the sample and T_1 is the temperature of the cold-side of the sample. Heat flux (q) is determined by measuring the input electric power (Q) and dividing it by the cross-sectional area (A) of the sample. Temperature difference across the sample is measured using several thermocouples at different positions above and below the sample as shown in figure 3.1. To report thermal conductivity values, mean temperature $T_m = (T_1 + T_2)/2$ of the hot and cold-plate is used.

Steady-state methods [23; 24] are suitable for dry porous materials but not suitable for moist porous materials. This is because of the fact, that these methods need long measuring times and allow redistribution of fluids in porous medium due to temperature difference. Thus, the information obtained is far away from the real values needed. Due to these shortcomings of steady-state methods, we can not use these for moist porous materials.

On the other hand, transient techniques have advantage over the steady-state techniques in two ways, first, a significantly lower temperature difference of at most 2 K and second, very short measuring time (some minutes). Hence, the amount of moisture transferred during a run remains negligible, thus, the measurement of the effective thermal conductivity is nearly unperturbed.

3.1.2 Adiabatic Calorimetry

Adiabatic calorimetry is one of the most accurate thermal methods with an uncertainty of less than 1 % for heat capacity measurements [20]. A typical adiabatic calorimeter can be divided into three parts: a cylindrical inner part, an adiabatic shield and a furnace as shown in figure 3.2. The inner part consists of a heater, thermometer, sample holder and inner radiation shields. The fundamental principle of an adiabatic calorimeter is the measurement of the temperature rise in a specimen with a given known amount of heat. Specific heat capacity of a material is determined using following formula,

$$c_p = \frac{Q}{m.\Delta T} \tag{3.2}$$

Where m is the mass of the material. Sample is kept in a vacuum tight vessel and is heated by applying a precisely known amount of heat. During the measurement process there are also small heat losses. To get rid of these heat losses, measurements on the empty vessel are done. For this purpose, in the first run, heat capacity of

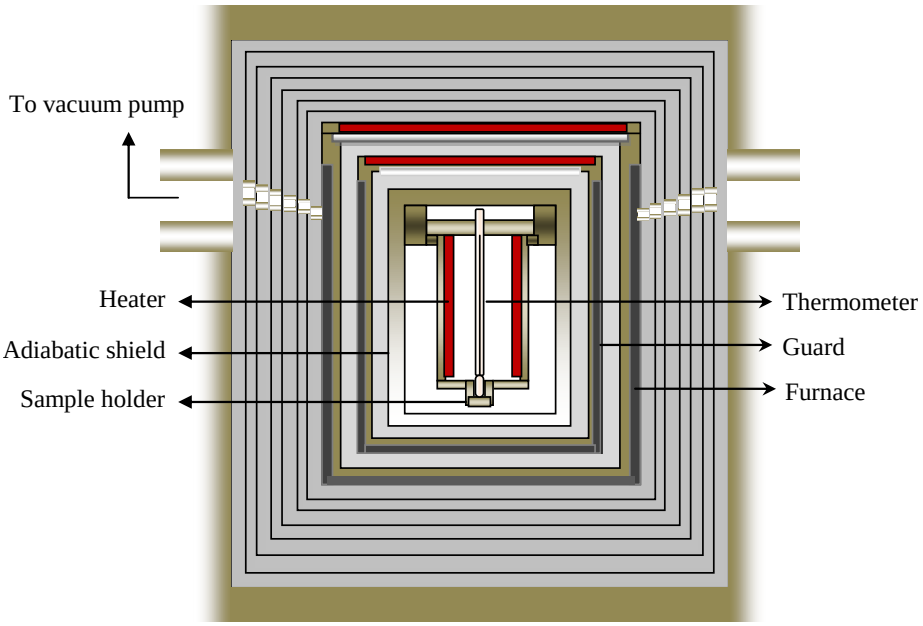

Figure 3.2: Sketch diagram of an adiabatic calorimeter [20].

the calorimeter is measured without a sample. Since, in an adiabatic calorimeter, heat loses in an empty and filled state are nearly equal. Therefore, we can calculate accurate heat capacity of the sample by subtracting the empty state heat capacity (c_{empty}) from the filled state heat capacity (c_{total}).

$$c_p = c_{total} - c_{empty} \tag{3.3}$$

Temperature measurements are usually done using a Platinum Resistance Thermometer with an accuracy of about 0.1 mK. Adiabatic calorimeters can be used in a temperature range from 1 K to 1000 K for heat capacity measurements.

3.2 Transient Methods

In transient or non-steady-state type methods, both temperature field in space (across the sample) and temperature field in time changes. Mathematically we can write that for a transient measurement, $dT/dx \neq 0$ and $dT/dt \neq 0$. Practically, the temperature field inside the sample is produced by passing an electrical current through a line or plane electrical resistance embedded in the sample or by a non-contact method through electromagnetic waves (i.e., laser flash method). A thermometer, that can be unified with the heat source or can be placed apart from the heat source, measures the temperature change caused by the heat source. In many transient techniques, the heating source also serves as a resistance thermometer. Transient methods work

in the following way:

→ First, the temperature of the sample and the heating source (sensor) are stabilized with the surrounding temperature.

→ Second, a small disturbance in temperature is applied by applying a heat pulse (i.e., by passing a small current through the sensor for a short time).

→ Third, from the change in the temperature of the heating source (sensor) itself, the thermal properties of the surrounding sample can be calculated according to the type (theoretical model) of the sensor used.

Normally, the temperature difference is kept less than 2 K and the sample size depends on the size and the theoretical model of the sensor used. The theory of the transient methods is based on an ideal model. An ideal model approximates that an infinite line/plane heat source of zero heat capacity is embedded in an infinitely extended (in all x, y and z-directions) isotropic medium. Since in practice an infinite medium and sensor are not possible, therefore by applying boundary conditions to the ideal model a semi-infinite ($x > 0$, $-\infty < y < \infty$, $-\infty < z < \infty$) medium is considered. The working equation of the heat source depends on its shape. More details on the working of a transient method, particularly transient line heat source, are given in below sections and in the appendix B.

Now a days, transient methods [25; 26; 28; 29] are becoming more and more popular with the availability of fast data acquisition and measuring computer systems. Transient methods are advantageous over steady-state methods not only due to their fast measuring time interval but also due to their ability to measure multiple thermal properties in a single run. There are a number of transient techniques; some of these are discussed in the following sections. We shall discuss only transient hot-wire method in details because the method used in this work (Transient hot-bridge method) is based on the theory of a line heat source.

3.3 Working Principle of Transient Techniques

Different transient methods determine thermal conductivity and thermal diffusivity in different ways depending on the shape and working theory of the sensor. In this work THB sensor is used to measure thermal properties and THB sensor is based on the working principle of THW method. In the following section, it is explained how thermal conductivity and thermal diffusivity of a material are calculated from a single run.

The general idea behind the transient techniques is to create an inhomogeneous temperature field inside the specimen by constant heating and then monitoring the corresponding temperature rise of the sensor. The temperature rise is measured

in terms of voltage. For instance, the working equation[2] of the transient hot wire technique is [25]:

$$\Delta V(t) = V(t) - V_0 \approx \frac{\alpha (V_0)^2 I}{4\pi\lambda L}\left(\ln(t) + \ln\left(\frac{4a}{Cr^2}\right)\right) \tag{3.4}$$

We can write the output voltage of the sensor in terms of slope and intercept. Equation 3.4 is linear with logarithm of time between t_{min} to t_{max} with slope m and intercept n as shown in figure 3.3.

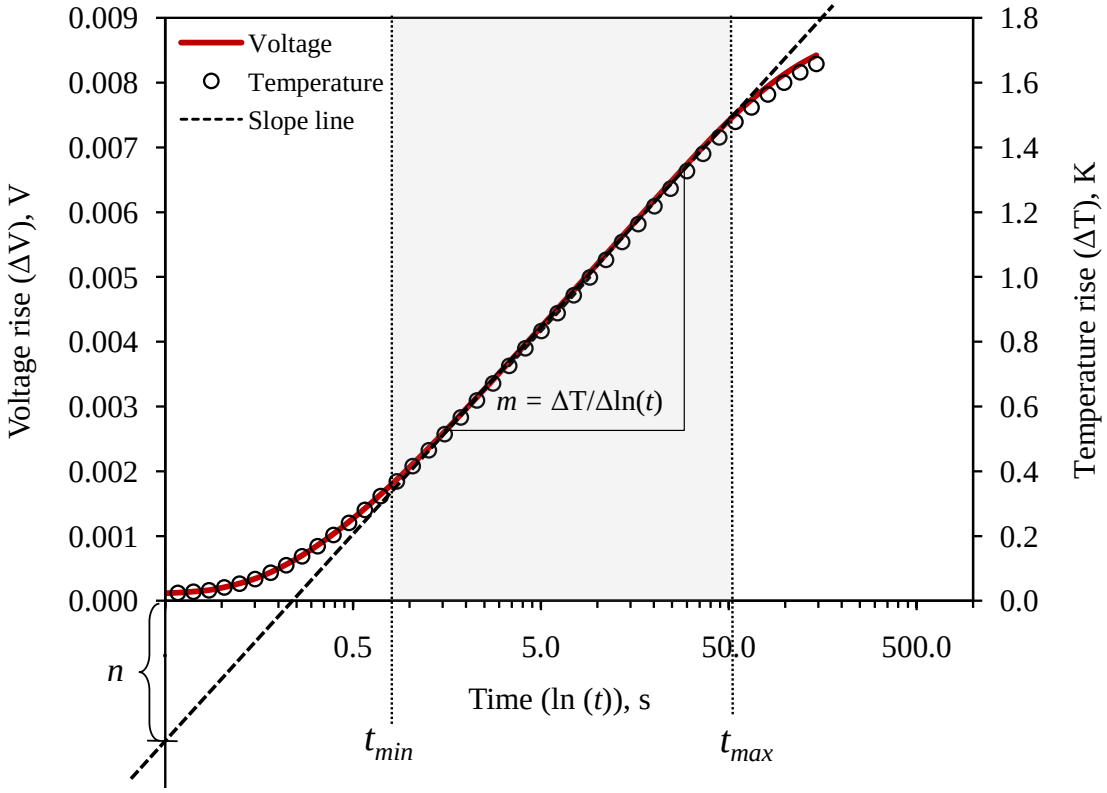

Figure 3.3: A typical transient hot-wire output signal.

$$\Delta V(t) = m\ln(t) + n \tag{3.5}$$

Where, slope of the output signal is,

$$m = \frac{\alpha (V_0)^2 I}{4\pi\lambda L} \tag{3.6}$$

and intercept is;

$$n = m\ln\left(\frac{4a}{Cr^2}\right) \tag{3.7}$$

[2]Further details on derivation of equation 3.4 are given in Appendix C.

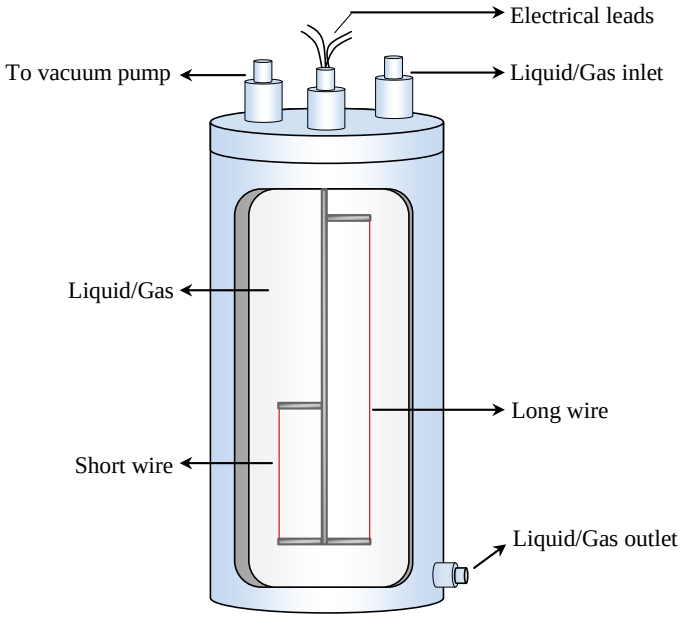

Figure 3.4: A typical transient hot-wire cell [30].

Where $C = \exp(\gamma) = 1.781$. From equations 3.6 and 3.7, both thermal conductivity and thermal diffusivity can be calculated respectively, within a single run:

$$\lambda = \frac{\alpha (V_0)^2 I}{4\pi m L} \tag{3.8}$$

$$a = \frac{r^2}{2.25} \exp\left(\frac{n}{m}\right) \tag{3.9}$$

3.3.1 Transient Hot-wire Method (THW)

Transient hot-wire method is probably the most widely used technique to measure the thermal conductivity of liquids, powders and gases. It can also be used for solids and pastes. In case of solid materials, hot-wire is embedded in a groove between two equally sized sample halves. Despite taking a great care in the preparation and fixing hot-wire in solid samples, there is always a problem of thermal contact resistance. Therefore, it is usually preferred to use some other methods like transient hot-strip [33] for the measurements on solid samples. On the other hand, THW method is considered as the best one for the thermal conductivity measurements on wetting fluids and on gases because of the negligible contact resistance. A typical transient hot-wire cell used for the thermal conductivity measurement of liquids/gases is shown in figure 3.4.

In its typical setup, a nickel or platinum wire is used as a heat source and as a

thermometer simultaneously. To compensate heat loses (end effects) from the hot wire, two wires of similar radius having short and long lengths are used in series. In the beginning, transient cell is in temperature equilibrium with the surrounding liquid specimen and the environment. An electric current is applied to heat the wires, which liberate constant heat per unit length through the entire length of the wire. A negligible part of the output heat is used in self heating of the wire due to its non-vanishing heat capacity, whereas most of the rest heat is conducted away from the wire into the sample. Due to self-heating of the wire, there is always a delay in temperature rise. Change in the wire temperature with time depends on the thermal conductivity of the surrounding medium (specimen). Temperature of the wire increases rapidly in case of low thermal conductivity surrounded medium. Whereas, temperature rise with time is low in case, if the wire is surrounded by a high thermal conductivity medium.

Thermal conductivity of the sample can be determined from the slope of the temperature rise versus time curve. Supply of electric current continues until the temperature of the wire reaches to its quasi stable higher value and convection currents starts in the liquid. The theory of the transient hot-wire starts with an ideal model in which we assume an infinitely long, vertical, line heat source possessing zero heat capacity and infinite thermal conductivity. Line source is immersed in an infinite (in all directions) isotropic fluid at same initial temperature. We assume only conductive heat transfer mode during dissipation of thermal energy from the line source. By applying initial and boundary conditions on a cylindrical shaped thin wire, the temperature rise ΔT (K) in the fluid at some distance r from the heat source is,

$$\Delta T(r,t) = T(r,t) - T_0 = -\frac{q}{4.\pi.\lambda}\mathrm{Ei}\left(\frac{-r^2}{4at}\right) \tag{3.10}$$

Where T_0 is the equilibrium temperature of the fluid with its surroundings and $Ei(-x)$ is the exponential integral function defined as

$$\mathrm{Ei}(-x) = \int_x^\infty \frac{e^{-u}}{u}du = \gamma + \ln(x) - x + \frac{1}{4}x^2 + \cdots \tag{3.11}$$

Wire acts as a heat source and produces a time-dependent temperature field within the test specimen. The approximated temperature rise at a radial distance r from the hot-wire is given by equation 3.12 [30; 31].

$$\Delta T(r,t) = \frac{q}{4.\pi.\lambda}\ln\left(\frac{4at}{r_w^2 C}\right) \tag{3.12}$$

Where $C = \exp(\gamma)$ and $\gamma = 0.5772$ is Euler's constant. Actual temperature

measurements are done by taking an average temperature along the whole length of the wire. A Complete derivation of equation 3.12 is given in appendix B. Thermal conductivity of the test specimen can be determined by choosing a linear part of the temperature rise versus logarithmic time curve using following equation [32]:

$$\lambda = \frac{q}{4.\pi}\left(\frac{\ln(t_2/t_1)}{T_2 - T_1}\right) \tag{3.13}$$

In reality, a quasi-linear relation between temperature rise and logarithmic time can be found in between times t_1 and t_2. For very short and long time intervals, systematic deviations may occur. The relative uncertainties for 95 % confidence level for THW method are calculated by U. Hammerschmidt (2000), these are 5.8 % for thermal conductivity and 30 % for thermal diffusivity. THW method is best suitable for the thermal conductivity measurement of liquids because of its better thermal contact with the specimen. Unfortunately, for the measurement of solid and especially of porous materials, this method offers much higher thermal contact resistance that ultimately destroys reliable thermal property values. Therefore, in order to get reliable thermal values on porous materials, we have to reject this method and search for some other one which is best suitable for moist porous materials.

3.3.2 Transient Hot-strip Method (THS)

Transient hot-strip method can be used for the simultaneous measurement of thermal conductivity and thermal diffusivity of both liquids and solids. The ideal model of a THS is based on a metal strip of infinite length and infinitesimal thickness embedded in an isotropic and homogeneous medium [29]. Strip is assumed to have its center at the origin of the coordinate system with a width of $2d$ in y-axis direction, infinitesimal thickness ($x = 0$) in x-axis direction and length is extended to infinity in z-axis direction. It is clamped between two rectangular cuboids as shown in figure 3.5 along with its zoom view.

Whole setup is assumed to be at equilibrium temperature T_0 before applying a heating current to the strip. When a constant electric current is passed through the strip, it serves as a continuous heat source and a resistive thermometer simultaneously. The output signal is obtained in the form of a voltage drop across the two ends of the sensor. This signal is the measure of the thermal conductivity and thermal diffusivity of the specimen. The temperature distribution in the metal strip due to the heat flux produced per unit area is given by equation 3.14 [29].

$$T(y,t) = \frac{q}{4a\sqrt{\pi}}\int_0^{\sigma}\left[\operatorname{erfc}\left(\frac{y-d}{\sigma}\right) - \operatorname{erfc}\left(\frac{y+d}{\sigma}\right)\right]d\sigma \tag{3.14}$$

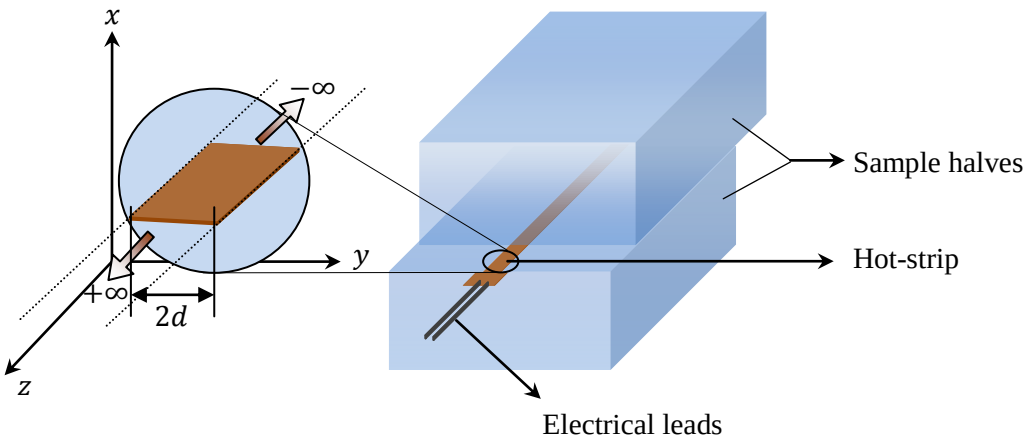

Figure 3.5: A typical setup of a transient hot-strip sensor.

Where d is the half width of the strip (heat source) and $\sigma = 2\sqrt{at}$. Since, temperature of the strip is not uniform throughout the sensor; therefore, the response due to heat supplied into the strip is measured as a change in its electrical resistance, which is directly related to the averaged temperature of the strip. Total resistance of the strip then, can be represented as a function of temperature,

$$R(T) = R_0(1 + \frac{\alpha}{2d}\int_{-d}^{d} T(y,t)dy) \tag{3.15}$$

Where R_0 is the electrical resistance of the strip at 0 °C and α is the temperature coefficient of resistance of the metal strip. Average temperature of the strip can be obtained by integrating equation 3.14 over the width. This yields the working equation of THS technique:

$$\overline{T} = \frac{q}{4\pi\lambda}\left[3 + \ln(t) + \ln(\frac{a}{e^{\gamma}d^2})\right] = m\ln(t) + n \tag{3.16}$$

Where m and n are the slope and intercept of this linear function, respectively. Thermal conductivity and thermal diffusivity of the test specimen can be calculated from the slope m and intercept n respectively as follows:

$$\lambda = \frac{q}{4\pi m} \tag{3.17}$$

and

$$a = d^2 e^{(\frac{n}{m} - 3 + \gamma)} \tag{3.18}$$

The relative uncertainties for 95 % confidence level for THS method are calculated by U. Hammerschmidt (2000) [33], these are 5 % for thermal conductivity and 22 %

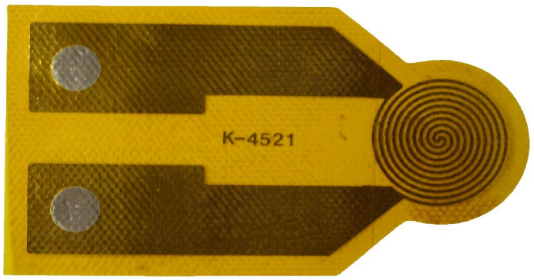

Figure 3.6: Transient plane source sensor (TPS).

for thermal diffusivity. Since, a transient hot-strip sensor uses a thin metal strip as a heat source that not only ensures a better thermal contact to the specimen than a transient hot-wire method but also liberates its heat at a smaller flow density [29; 34]. Nevertheless, due to its very small electrical resistance, the output signal of a strip is very low, i.e., the signal-to-noise ratio is rather poor. Furthermore, the so-called end-effect (the non-uniform temperature profile along a heated strip or wire), increases the uncertainty of the results. Therefore, due to high values of uncertainty in the results, this method is not a better choice for porous materials.

3.3.3 Transient Plane Source Method (TPS)

In 1991, S. E. Gustafsson [35] introduced a new transient plane source technique for the measurement of thermal conductivity and thermal diffusivity for a wide range of materials. It is also known as Gustafsson's probe. The shape of the TPS sensor is made in the form of a 10 μm thick Nickel spiral covered on both sides with a 25 μm thick insulating Kapton layer. The sensor acts as a heat source and a temperature sensor simultaneously. It is shown in figure 3.6. An electric pulse is applied to heat the sensor for a short time. The resistance of the sensor changes with time, which can be calculated with:

$$R = R_0 \left(1 + \alpha \left(\overline{\Delta T}\left(\tau\right)\right)\right) \tag{3.19}$$

Where R_0 is the initial resistance of the TPS sensor before applying current, α is the temperature coefficient of the resistance and $(\overline{\Delta T}(\tau))$ is the average value of the time-dependent temperature rise of the sensor. Generally, temperature rise of the TPS sensor depends mainly on three factors namely: output power of the sensor, thermal conductivity and thermal diffusivity of the surrounded test material and the design parameters of the sensor. Instead of all these three parameters, average temperature $(\overline{\Delta T}(\tau))$ can also be expressed as a function of only one variable "τ". Where, τ is a dimensionless parameter which can be defined as [29],

$$\tau = \sqrt{\frac{ta}{r^2}} \tag{3.20}$$

Where r is the radius of the sensor, a is the thermal diffusivity of the test specimen and t is the time. The temperature response of the TPS sensor as a function of dimensionless parameter τ is given by the following equation,

$$T(\tau) = \frac{P_0}{\sqrt{\pi^3} r \lambda} D(\tau) \tag{3.21}$$

Here, P_0 is the total output power and $D(\tau)$ is the characteristic time-dependent function and is defined as,

$$D\left(\tau\right) = \frac{1}{\left[m(m+1)\right]^2} \int_0^\tau \frac{1}{s^2} ds \left[\sum_{n=1}^{m} n \sum_{k=1}^{m} k \, \exp\left\{ -\frac{n^2+k^2}{4m^2 s^2} \right\} I_0 \left(\frac{nk}{2m^2 s^2} \right) \right] \tag{3.22}$$

Where m is the number of concentric circles in the sensor. Equation 3.22 shows a conductive pattern of a disk shaped sensor. However, the actual sensor consists of concentric circles. Therefore, there is a difference in the output of the experimental and theoretical curves. This difference can be removed, if the number concentric circles m are larger than 10, the value of dimensionless parameter τ is greater than 0.1 and small time correction is applied.

TPS may be a good choice to measure thermal properties of porous materials but because of its nonlinear implicit output temperature response, it is hard to find the best linear part of the curve and ultimately, to find the best value of the thermal conductivity and thermal diffusivity.

3.3.4 Pulse Transient Method (PT)

The pulse transient technique employs a simple experimental method for determining the temperature field of the test sample [36]. It is based on the determination of maximum temperature rise in a sample at a specific distance from the heat source. The working principle of the technique is shown in figure 3.7. Sample is divided into three parts. A planar heat source is sandwiched between sample I and II. Planar heat source (sensor) is heated by passing an electric pulse. A thermometer is located in between parts II and III of the sample, and records the temperature response due to the applied heat pulse. Theoretical model of the pulse transient method assumes a planar heat source with infinitesimal thickness embedded in an infinite body. The temperature response at point x (simplified to one directional case) after a time t can be represented as [37],

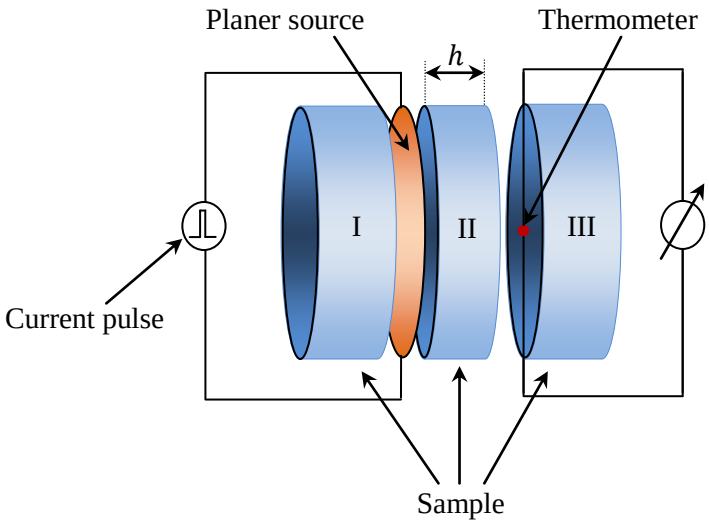

Figure 3.7: Pulse transient technique setup.

$$T(x,t) = \frac{Q}{c\rho\sqrt{\pi at}}\exp\left(-\frac{x^2}{4at}\right) \tag{3.23}$$

To reduce the thermal contact resistance between the samples, thermal paste and a very thin thermocouple is used. To calculate thermal properties from the temperature response, a fitting procedure is applied in an appropriate time window. From maximum of the function (equation 3.23) at a point $x = h$ (see figure 3.7), we can derive relations for thermal diffusivity (a) and specific heat capacity (c) as,

$$a = \frac{h^2}{2t_m} \tag{3.24}$$

$$c = \frac{Q}{\sqrt{2\pi\exp(1)}\rho h T_m} \tag{3.25}$$

Where h is the thickness of the sample, $\exp(1) = 2.718282...$, ρ is the density of the sample, Q is the applied pulse energy and t_m is the time at which temperature response reaches its maximum value (T_m). The third parameter, thermal conductivity, can be calculated from standard equation:

$$\lambda = \rho a c = \frac{hQ}{2\sqrt{2\pi e}t_m T_m} \tag{3.26}$$

L. Kubicar (1990) discusses measurement uncertainties of the pulse transient methods [36]. The uncertainty values for the thermal diffusivity, heat capacity and thermal conductivity lies in between 3 to 10 %, 3 to 5 % and 6 to 15 % respectively.

The disadvantages of pulse transient method is that, it needs a high pulse input,

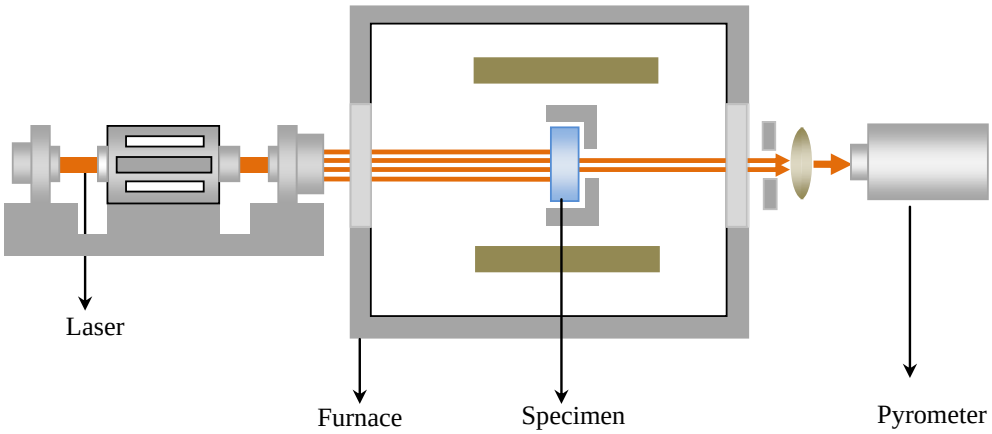

Figure 3.8: Working principle of laser flash technique.

which establishes a large temperature difference at the two measuring ends of the sample. Due to this high temperature pulse, not only the moisture inside a moist sample starts evaporating but also due to the dependence of thermal conductivity itself on temperature, we can not get reliable values.

3.3.5 Laser Flash Method (LF)

Laser flash is probably the most widely and frequently used method for the determination of thermal diffusivities of a wide range of materials including polymers, glasses, ceramics and metals. The key reason is that, it can be used for wide temperature (-100 to 3000 °C) and thermal diffusivity (1×10^{-7} to 1×10^{-3} $m^2.s^{-1}$) ranges [38]. Although, the method was primarily designed for characterizing homogeneous and isotropic materials, but it can be successfully used for inhomogeneous and anisotropic materials.

The principle of the laser flash method is based on the heating of a specimen from one side (front) using a laser pulse and measuring the temperature response at the other side (rear). The sample is in the form of a disc having a diameter of about 6 to 25.2 mm and thickness of about 2 mm. A sketch diagram of laser flash method is shown in figure 3.8. If the sample is kept at adiabatic conditions and a short laser pulse is applied then, the thermal diffusivity can be calculated using following formula [38],

$$a = 0.1388 \frac{d^2}{t_{1/2}} \tag{3.27}$$

Where d is the thickness of the sample and $t_{1/2}$ is the time when temperature of the rear face of the sample reaches half of it maximum value.

The main sources of error in laser flash method are the finite resolution of the data acquisition system and the heat capacity of the pyrometer itself. If the experiments

are repeated at each temperature and mean values of the measurements are taken, then, the total error can be kept below 2 % [39]. The benefit of laser flash method is that, it can measure thermal diffusivity without having any physical contact of the heat source with the sample. Therefore, there is no worry about contact resistance probleme. Thermal diffusivity measurements are carried out only by knowing relative temperature change as a function of time. That is why relative measurement uncertainties lie in a range of 2 to 5 % even at higher temperatures [40]. Laser flash method is suitable to measure only thermal diffusivity. To measure other two thermal parameters (thermal conductivity and heat capacity) we still require some other methods, which makes the process time consuming and costly. While, for the measurements of fluid-saturated or moist porous materials we want to have three thermal parameters to be measured at the same time. Therefore, we still need some state of the art instrument that can measure three thermal parameters simultaneously with reasonable accuracy.

3.4 Transient Hot-bridge Method (THB)

3.4.1 Theory

The THB sensor is made-up of a 7.5 μm thin printed circuit foil of Nickel which is sandwiched between two polyimide sheets each having thickness of 27.5 μm (figure 3.9). It has an overall size of $120 \times 60 \times 0.062$ mm^3 to fit in between two sample halves of $100 \times 60 \times 20$ mm^3 each. The layout of the sensor consists of four parallel tandem strips. Each tandem strip consists of a short and a long segment having lengths $L_S =$ 14 mm and $L_L = 64$ mm respectively. Its effective length is $L_{eff} = L_L - L_S = 50$ mm, and the associated effective electrical resistance is R_{eff} with temperature coefficient α. The effective middle segment is free from the end effects during measurement time t_m. As long as the sample temperature is uniform, the bridge is inherently balanced. An electric current establishes a predefined inhomogeneous temperature profile that turns the bridge into an unbalanced condition. The eight segments of the four strips are connected in the Wheatstone-bridge against each other so that each of the voltage drops of a long segment is reduced by that of a short one. The output signal (V_{THB}) of the sensor is then obtained by taking a difference of temperature rises between inner and outer strips.

$$\Delta T = T_{inn} - T_{out} \tag{3.28}$$

Where, the temperature rise on the inner and outer strips is the sum of the self heating and the heat produces by the neighbouring strips with distance D_i, where,

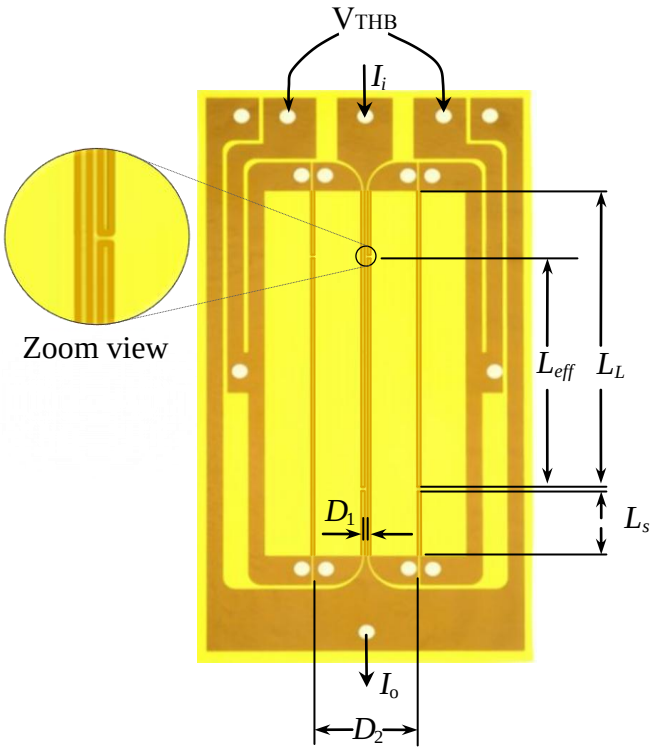

Figure 3.9: Top view of THB sensor

i= 1, 2, 3, 4. D_i are the distances between the sensor strips from each other as shown in figure 3.10.

$$T_{inn} = T(D_0) + T(D_1) + T(D_3) + T(D_4) \tag{3.29}$$

$$T_{out} = T(D_0) + T(D_2) + T(D_3) + T(D_4) \tag{3.30}$$

By subtracting equation 3.30 from equation 3.29 we get,

$$\Delta T = T(D_1) - T(D_2) \tag{3.31}$$

The output signal of the THB sensor is proportional to ΔT through a thermometric equation:

$$V_{THB} = \frac{R_{eff} I_B \alpha \Delta T}{2} \tag{3.32}$$

where, α is the temperature coefficient of electrical resistance, R_{eff} is the electrical resistance and I_B is the applied current to the bridge circuit.

The mean temperature rise of a line heat source as a function of dimensionless time (τ) is obtained as [26]:

$$\overline{T}(\tau) = \frac{q}{\sqrt{4\pi} L \lambda} f(\tau) \tag{3.33}$$

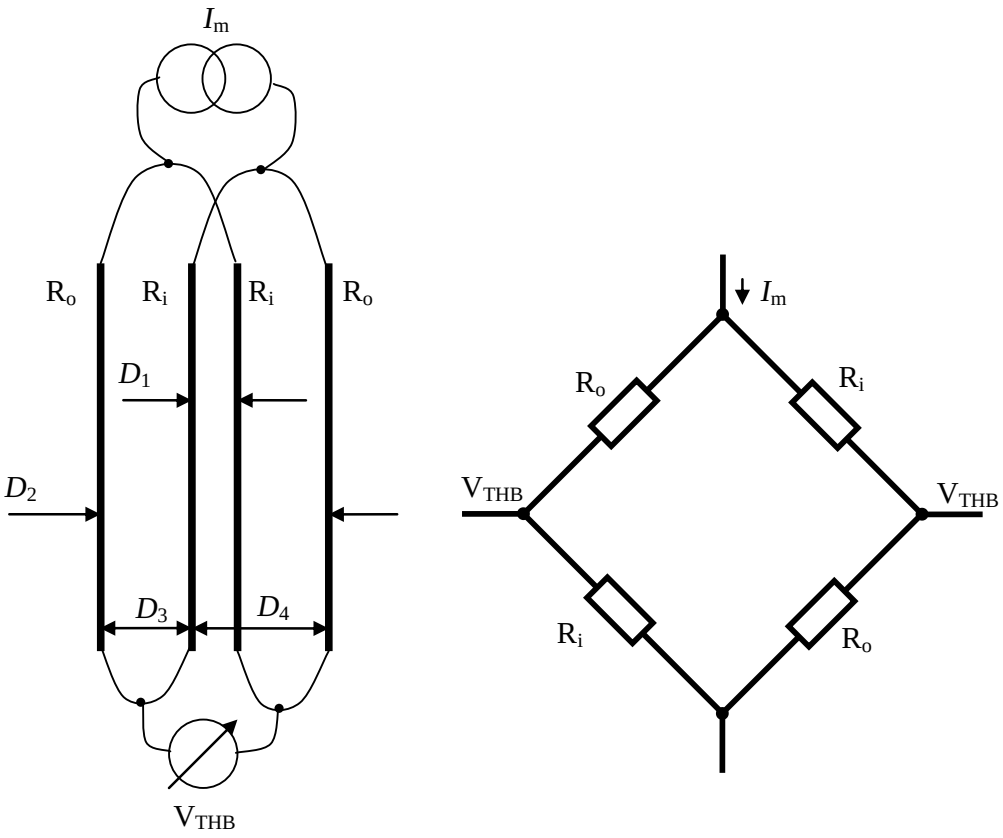

Figure 3.10: Sketch diagram (left) and circuit diagram (right) of THB sensor.

where

$$f(\tau) = \tau \text{erf}(\tau^{-1}) - \frac{\tau^2}{\sqrt{4\pi}}\left(1 - \exp(-\tau^{-2})\right) - \frac{1}{\sqrt{4\pi}}\text{Ei}(-\tau^{-2}) \tag{3.34}$$

and

$$\tau = \frac{\sqrt{4at}}{D} \tag{3.35}$$

Here, $q = I_B^2 R_{eff}/L$ (W.m^{-1}) is the heat flux per unit length of the embedded heat source strips, a represents thermal diffusivity, D is the width of the heating strip and -Ei($-x$)" is the exponential integral.

The characteristic time τ is defined separately for each inner and outer strips. For inner strip it is $\tau_{inn} = \frac{\sqrt{4at}}{2D}$ and for the outer strip it is $\tau_{out} = \frac{\sqrt{4at}}{D}$. The mean temperatures of both inner and outer strips can be evaluated separately and their difference can be written as:

$$\Delta T = \overline{T}_{inn}(\tau) - \overline{T}_{out}(\tau) = \frac{q}{\sqrt{4\pi}L\lambda}\left(f_{inn}(\tau) - f_{out}(\tau)\right) \tag{3.36}$$

By putting value of ΔT into equation 3.32, we can get the output voltage signal of the THB sensor.

$$V_{THB} = \frac{R_{eff} I_B \alpha}{2} \frac{q}{\sqrt{4\pi} L\lambda} \left(f_{inn}(\tau) - f_{out}(\tau) \right) \tag{3.37}$$

Equation 3.37 is the fundamental relation for the basic operation of the THB sensor and represents the output signal well. However, it is nonlinear and implicit, therefore, thermal properties need to be estimated.

After applying first order approximations to equation 3.34, the mean temperature of the inner and outer strips can be obtained as following [34]:

$$\overline{T}_{out}(t) = \frac{q}{4\pi L\lambda} \ln\left(\frac{45at}{D^2}\right) \tag{3.38}$$

$$\overline{T}_{inn}(t) = \frac{2q}{4\pi L\lambda} \ln\left(\frac{45at}{4D^2}\right) \tag{3.39}$$

The net temperature rise of the sensor can be obtained by subtracting equation 3.38 from equation 3.39.

$$\Delta T(t) = \overline{T}_{inn}(t) - \overline{T}_{out}(t) \tag{3.40}$$

The final output signal of the sensor is then calculated by combining the electrical and thermal modes:

$$V_{THB} = \frac{\alpha R_{eff}^2 I_B^3}{8\pi L\lambda} \left[\ln(t) + \ln\left(\frac{45a}{16D^2}\right) \right] \tag{3.41}$$

Equation 3.41 is linear with logarithm of time. When we plot V_{THB} against $\ln(t)$ then, a straight line with slope m and intercept n is obtained. From the slope of this curve, thermal conductivity of the sample can be determined.

$$\lambda = \frac{\alpha R_{eff}^2 I_B^3}{8\pi L m} \tag{3.42}$$

From slope and intercept both, the thermal diffusivity can be calculated as given below [34]:

$$a = 2.82 \exp\left(\frac{n}{m}\right) \tag{3.43}$$

A typical output curve of THB sensor taken on Borosilicate glass (BK-7) sample is shown in figure 3.11.

3.4.2 Measurement Uncertainty

The relative uncertainty in the values of thermal conductivity and thermal diffusivity can be calculated from equations 3.42 and 3.43 respectively as,

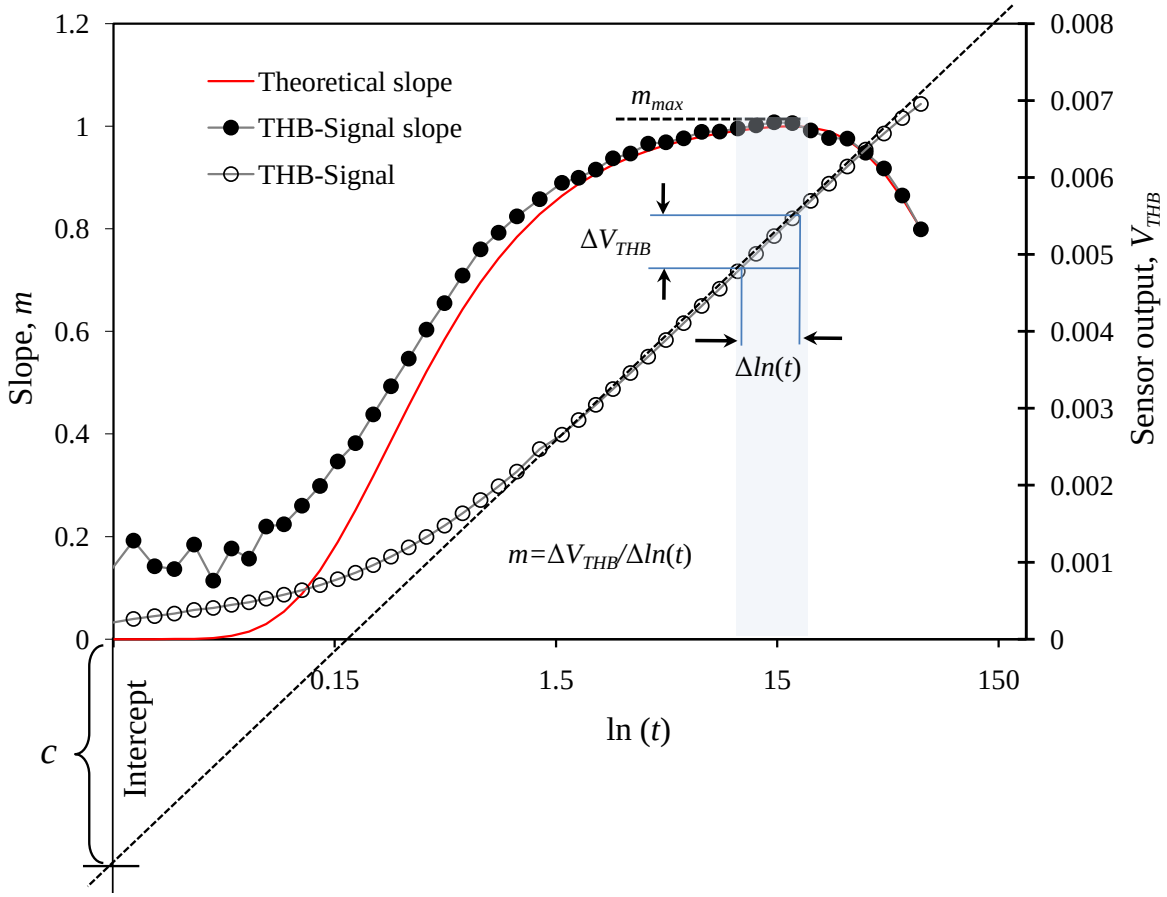

Figure 3.11: A Typical THB output-signal obtained from a run on the optical glass (BK7) at a sensor current I_m= 400 mA. The maximum of the signal corresponds to a rise in relevant temperature of $\Delta T = 1$ °C.

$$\frac{\delta\lambda}{\lambda} = \sqrt{\left(\frac{\delta\alpha}{\alpha}\right)^2 + \left(2 \cdot \frac{\delta R_{eff}}{R_{eff}}\right)^2 + \left(3 \cdot \frac{\delta I_m}{I_m}\right)^2 + \left(\frac{\delta L_{eff}}{L_{eff}}\right)^2 + \left(\frac{\delta m_{max}}{m_{max}}\right)^2} \quad (3.44)$$

$$\frac{\delta a}{a} = \sqrt{\left(\frac{\delta n}{n}\right)^2 + \left(\frac{\delta m}{m}\right)^2} \quad (3.45)$$

Where, $(\delta\alpha/\alpha)$= 0.5 %, $\delta R_{eff}/R_{eff}$ = 0.5 % by temperature rise (change) <1 K; $\delta I_m/I_m$ = 0.3 %, $\delta L_{eff}/L_{eff}$ = 0.5 %. The slope as well as intercpt of the signal is affected by the ambient temperature drift, heat capacity of the strips, thermal contact resistance between the sensor and the sample and the outer boundary conditions. Therefore the total relative uncertainty for the slope determination is relatively higher and is $\delta m/m \leq 3$ %. Therefore, equation 3.44 and 3.45 gives us $\delta\lambda/\lambda \approx 3$ % and $\delta a/a \approx 9$ % respectively. Apart from instrument type uncertainties, there may be additional systematic uncertainties like contact resistance and inhomogeniety of the sample. Effect of systematic uncertainties on output data are studied by using FEM analysis.

3.4.3 Validation of the THB Sensor

Before the THB sensor is used for measurements, it is validated using few standard reference materials. The results on thermal conductivity and thermal diffusivity values of THB sensor in comparison with the reference values are given in table 3.1.

	THB Sensor		Literature value	
	λ	a	λ	a
Material	($W.m^{-1}.K^{-1}$)	($mm^2.s^{-1}$)	($W.m^{-1}.K^{-1}$)	($mm^2.s^{-1}$)
Polystyrene foam	0.032 ± 3 %	0.60 ± 10 %	0.031	0.650
Plexiglas (PMMA)	0.196 ± 3 %	0.12 ± 10 %	0.195	0.118
Glycerol	0.285 ± 3 %	0.10 ± 10 %	0.286	0.095
Water	0.610 ± 3 %	0.14 ± 10 %	0.605	0.140
Glass BK7	1.090 ± 3 %	0.56 ± 10 %	1.090	0.550
Stainless steel (1.4301)	14.30 ± 8 %	3.80 ± 10 %	14.70	3.750

Measurements uncertainty is evaluated according to the GUM [27] rules with coverage factor k = 2.

Table 3.1: Calibration of THB sensor using reference materials.

3.4.4 Comparison of the Measurement Methods

The main problem for all experimental methods to measure thermal properties of any material is that there exists no ideal heat source or heat sink. Therefore, each method for the measurement of thermal properties is restricted to a special class of materials and temperature ranges. Table 3.2 gives a comparison between few important thermal property measuring techniques discussed in the above sections.

3.4.5 Choice of the Measurement Method

As mentioned before, there exists a broad variety of thermal property measurement techniques depending on different types of materials and temperature ranges. From a number of these techniques we have discussed six important methods in the above sections. First step of choosing an appropriate measurement method from the list of above given techniques was to sort out only those methods which are suitable for moist and porous materials. In the second step, we needed to choose those methods, which can measure three thermophysical parameters (thermal conductivity, thermal diffusivity and heat capacity). Third, we had to choose those methods that have lowest uncertainty in the measurements. By taking a closer look on the list of methods, we came to the end to choose Transient hot-bridge (THB) method because of its following qualities.

1. Time required for a measurement is very short (1 to 2 minutes)
2. Maximum temperature rise is 2 K
3. Constant penetration depth of heat for different samples[3]
4. Low uncertainty range (3 % for thermal conductivity and 10 % thermal diffusivity)

The newly developed transient hot-bridge method (THB) preserves all advantages of the transient-based techniques and avoids their major drawbacks [26]. The benefit of using THB sensor is that its unique design compensates the end-effect and minimizes the contact resistance problem.

[3]Penetration depth of THB sensor remains the same because of the fact that the thermal conductivity and thermal diffusivity values are calculated through a dimensionless slope function. For low thermal diffusivity materials THB sensor needs long measurement time and for higher thermal diffusivity materials it needs short measurement time, therefore the over all penetration depth of the heat waves remains the same for different kinds of materials. This dimensionless function depends on the geometry of the sensor.

Method	Temperature range	Uncertainty	Materials	Merits	Demerits
Guarded Hot-plate	80 to 800 K	2 %	Insulation materials, plastic and glasses	High accuracy	Long measurement time, Large specimen size, Low conductivity materials, Not suitable for moist materials
Adiabatic calorimeter	1 to 1900 K	0.05 to 2 %	Solids, liquids and gases	High accuracy	Long measurement time, expensive
Transient hot-wire Transient hot-strip	20 to 2000 K	3 to 5 %	Liquids, gases and low conductivity solids	High temperature range, Fast and accurate	Limited to low conductivity materials
Transient plane source	77 to 1073 K	2 to 5 %	Metals, ceramics, polymers, liquids and powders	Wide variety of materials, In-situ measurements	Unable to measure low viscosity liquids due to convective effects, Effect of heat loses
Pulse transient	—	3 to 10 %	Both homogeneous and heterogeneous materials	Suitable for moist materials	Contact resistance, Effect of heat loses
Laser Flash	173 to 3273 K	3 to 5 %	Solids and liquids	High temperature range, Most solids, liquids and powders, Small specimen, fast	Expansive, Not suitable for insulation materials, No direct measurement of thermal conductivity
Transient hot-bridge	173 to 573 K	3 to 5 %	Solids, viscous liquids, ceramics, polymers and powders	Wide variety of materials, In-situ measurements, Suitable for moist porous materials	Unable to measure low viscosity liquids due to convective effects

Table 3.2: Comparison of different thermal property measuring techniques.

Chapter 4

Validation of THB Sensor Using Finite Element Simulation (FEM)

Many thermal processes such as heat conduction, thermal waste, diffusion phenomena etc., are described by partial differential equations that, for more complicated situations, are only solvable by numerical analysis such as Finite Element Methods (FEM) [41]. In this work, COMSOL Multiphysics version 3.4 is used to describe the complete geometry of the THB sensor, i.e., Nickel strips, Kapton foil, contact resistance (air gap) and sandstone sample. The COMSOL 3.4 package allows precise modeling of the THB sensor, resulting in a good agreement with the experimental data. In this chapter, operation of the THB sensor is modeled numerically and is subsequently confirmed by direct observation.

4.1 Geometry of a 2D FEM Model

In the case of THB sensor, a three dimensional heat conduction model is limited to a two dimensional one because of the absence of the axial heat flux from the middle and outer strips. In addition, due to the symmetrical setup, only a quarter of the 2D geometry is considered. Geometry for FEM model is taken according to the real experimental setup; however, because of the negligible deviation in the output data, the meander structure of the strips was replaced with a single strip of width 0.8 mm. A Kapton foil of thickness 27.5 μm covers both (inner and outer) strips. A schematic diagram of the FEM model and its 2D sketch setup are shown in figure 4.1 and figure 4.2 respectively. All outer boundaries are fixed at constant temperature (isothermal) of 298 K and symmetry axes are considered as adiabatic. Sander sandstone has a pore radius range between 0.001 to 100 μm, so it is quite possible to introduce an air gap of an average pore radius between the sensor and the sample to realize the FEM

geometry setup close to real conditions. Starting from an initial thermal equilibrium condition at temperature $T = 298$ (K), a heat pulse Q (W.m^{-3}) is applied for 1000 s. The transient signal is then obtained as a time-dependent temperature profile. Table 4.1 shows all geometrical and thermal parameters used in the model.

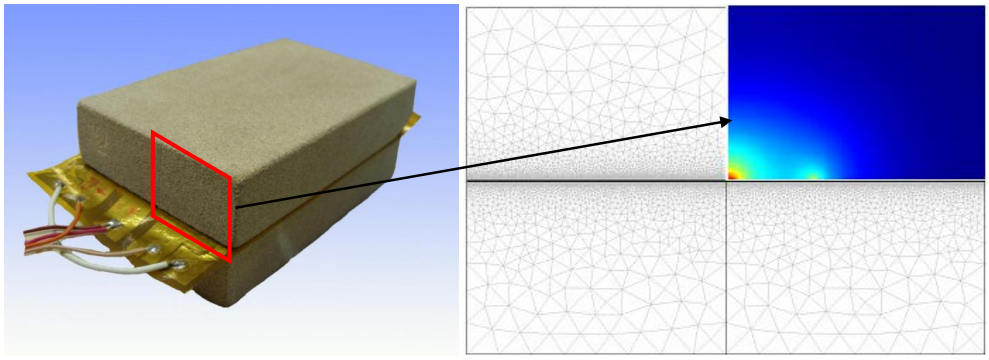

Figure 4.1: 2D FEM model of THB sensor.

	2D geometry blocks					
	Width (mm)	Height (mm)	Thermal conductivity (W.m^{-1}.K^{-1})	Thermal diffusivity (mm^2.s^{-1})	Heat capacity (J.kg^{-1}.K^{-1})	Density (kg.m^{-3})
Dry Sandstone	25	20.00	1.671	1.0	800	2132
Air gap	25	0.040	0.026	18.5	1005	1.20
Kapton foil	25	0.025	0.140	0.1	1200	1200
Nickel strips	0.8	0.0037	90.00	18	8900	444

Table 4.1: Geometry blocks of FEM model and their thermophysical properties.

FEM simulations are performed in four ways, using (1) perfect thermal contact between heat source (including Kapton foil) and the sample, (2) introducing a 25 μm thick air gap (which acts as a thermal contact resistance) between sensor and the specimen, (3) 40 μm thick air gap and (4) 50 μm air gap. FEM results, in which contact resistance is not taken into account, show lower values of temperature rise, because heat is directly transmitted to sandstone without any thermal resistance, which is not possible in real cases. Distribution of the temperature profile through the sample can be seen from an output window of the FEM model. It is shown in figure 4.3.

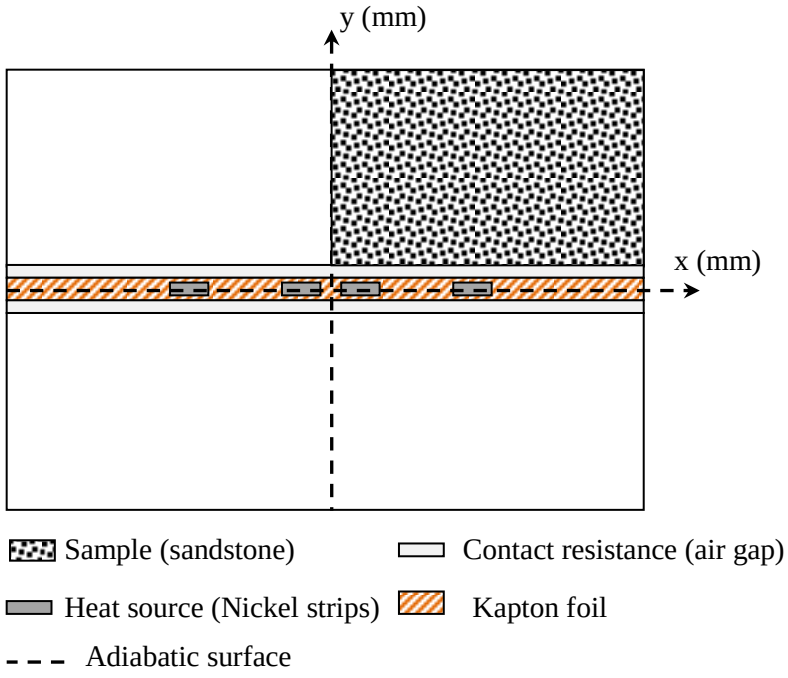

Figure 4.2: Exaggerated schematic diagram of a 2D FEM geometry.

4.2 Simulation Results

FEM results are compared with the experimental values; both are in good agreement with a maximum deviation of 3 %. However, deviation in the values is more for time window of less than 0.5 s. The temperature of the strips increases more rapidly if we include a contact resistance i.e., air gap. This is because of the fact that very low thermal conductivity ($\lambda = 0.026$ W.m^{-1}.K^{-1}) of the air as compared to sandstone ($\lambda = 1.67$ W.m^{-1}.K^{-1}) prevents penetration of the heat into the sample. Therefore, at very short initial times, heat accumulates on the strip and results a time-delayed curve in the end. The temperature rise of each strip for different time intervals is shown in figure 4.4. Both temperature profiles (experimental and FEM) and the effect of contact resistance are shown in figure 4.5.

It can be seen from figure 4.5 (upper right corner), that, there is a difference of about 0.1 K between the experimental and the simulated values at long time intervals (in case if we do not consider contact resistance). This is due to the entirely different slopes of conduction profile at the beginning. To remove this difference we introduce different thicknesses of air gaps. After few simulation runs it was noticed that, this difference could be removed by adding a 40 μm air gap between sensor and the specimen. However, this thickness may be different for different materials depending on the roughness of the specimen surface and the quality of the contact between

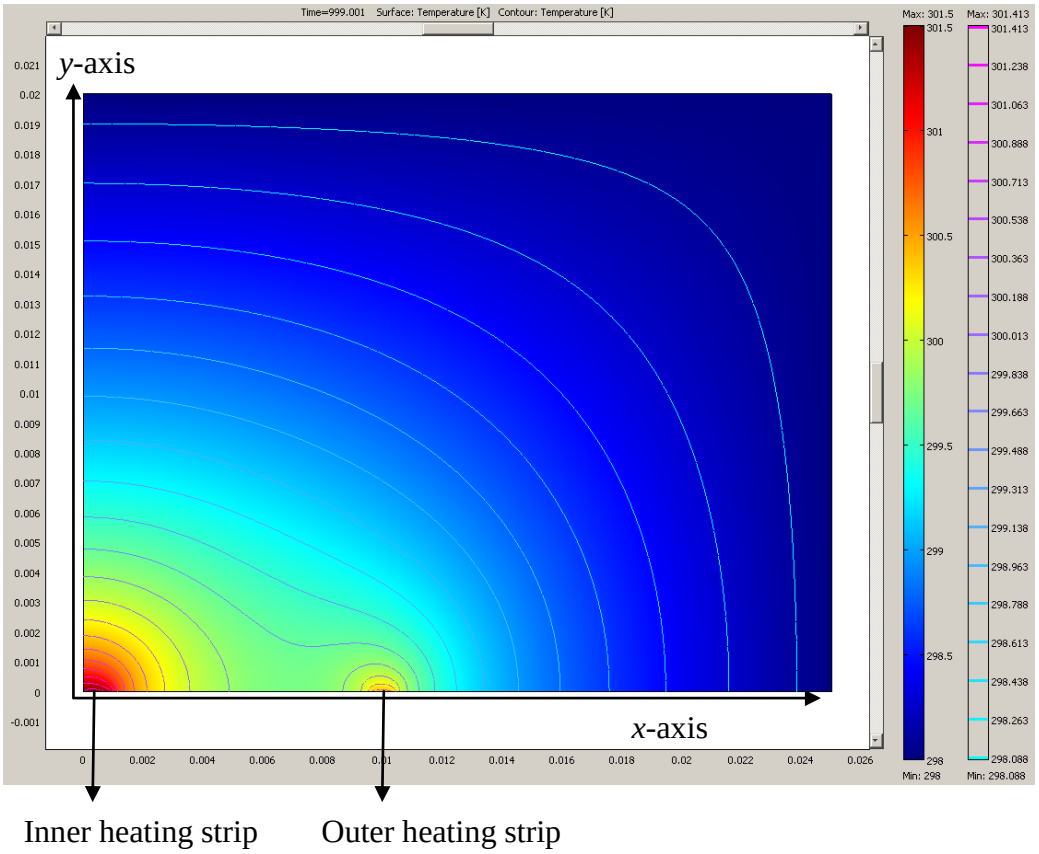

Figure 4.3: Output window of COMSOL (FEM) model.

sensor and the specimen.

Figure 4.6 shows the temperature rise of inner and outer heating strips of the THB sensor independent of each other. The two temperatures end up with a difference of about 1 K. Different slopes in different time windows shows different thermal properties of the materials. As heat is generated by the source, it has to pass through three sheets of different materials (Kapton sheet, air gap and finally through the sandstone) until it flows out of the last sheet. Conduction of heat through each sheet shows different slopes depending on the thermal properties of each material (sheet). Since, thermal conductivity of a material is inversely proportional to the slope of the temperature rise versus logarithm time curve; therefore, higher slopes indicate low thermal conductivity values while lower slope values correspond to higher thermal conductivity values. First part of the curve in figure 4.6 explains the properties of Kapton foil for a time slot of 1 to 10 ms, second part of the curve explains the properties of the contact resistance (i.e., air gap for instance) that spans from 0.01 to 0.3 s and the third part corresponds to the properties of Sander sandstone sample for a time window of 0.3 to 200 s. The average temperature rise (ΔT) of the sensor is calculated by taking a difference between temperature rises at the center of the inner and outer strips.

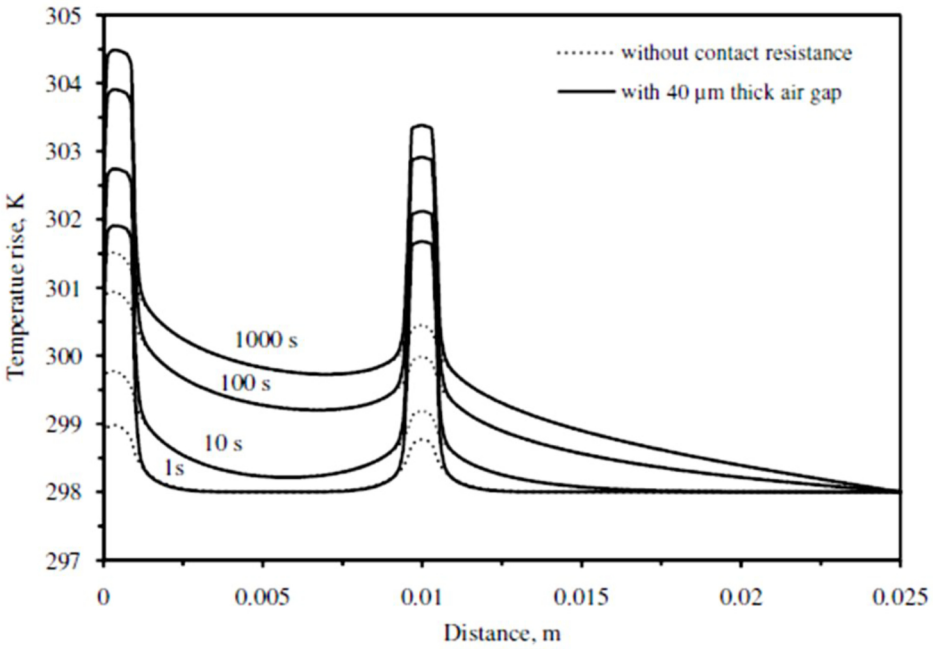

Figure 4.4: Temperature rise of the Nickel strips along x-axis of the symmetry axis at different time intervals.

4.3 Effect of Clamping Force

In order to analyze the disturbing effect of thermal contact resistance between the sensor and the specimen halves, two types of experiments were performed at ambient temperature. For the first series of runs, the sensor was sandwiched between the sample halves without any additional clamping force, and then carried out a few runs. For the second series, successive loads of 1 kg were put on top of the upper sample half to make a better thermal contact between sensor and the sample halves. Again, in order to minimize the random errors, the measurements were repeated three times and mean values were calculated. Figure 4.7 shows the output signals of the THB sensor plotted against logarithmic time scales. It is clear from the figure that, the slopes of almost all the runs (with load or without load) are similar. This represents that, THB sensor measures thermal conductivity very well even if there is a problem of contact resistance between the sensor and the sample. However, thermal diffusivity values are different because of different intercept values of each curve. Therefore, THB sensor may not the best choice for measurement of thermal diffusivity in such cases where contact resistance is much higher. Nevertheless, thermal contact resistance may be reduced by using thermal pasts.

All the experimental thermal conductivity results on brick samples are listed in table 4.2. The mean value of the thermal conductivity obtained from the first series of experiments on dry samples is $\lambda = 0.528 \pm 0.006$ W.m^{-1}.K^{-1}. The second series furnishes a mean thermal conductivity of $\lambda = 0.519 \pm 0.004$ W.m^{-1}.K^{-1}. The mutual

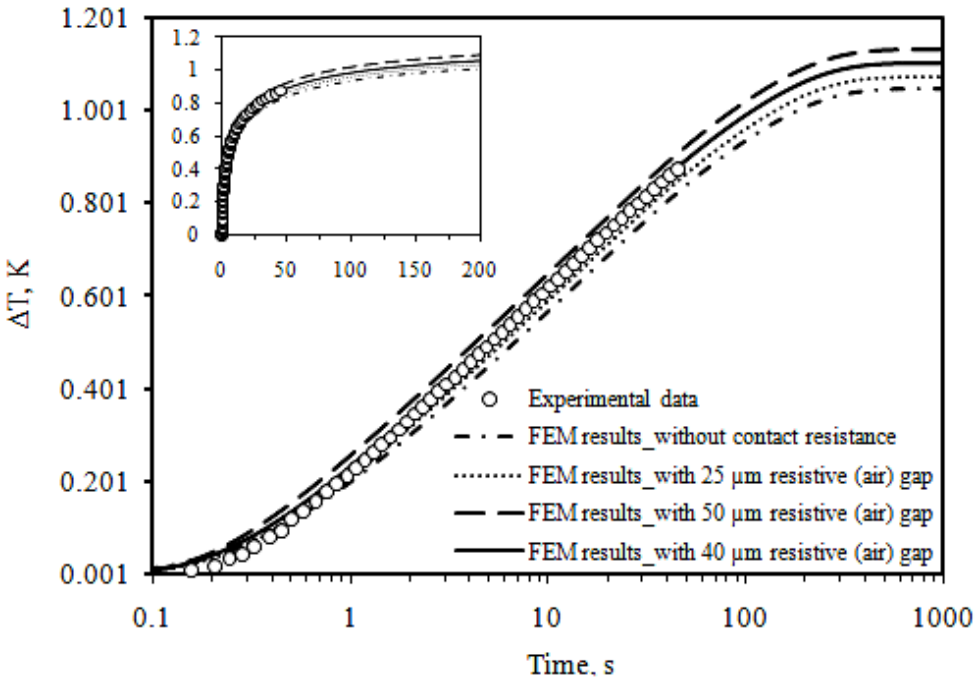

Figure 4.5: Experimental and simulated results of temperature rise in Sander sandstone.

difference in these two results is 1.7 % that agrees very well with the uncertainty range of ±6.8 % at an expansion factor of K= 2. Hence, a significant load effect could not be ascertained beyond doubt. That is, the weight of the upper sample half of the brick under test meets the load requirements.

	Dry without load	Dry with load	Water-saturated with load
Thermal conductivity values ($W.m^{-1}.K^{-1}$)	0.526	0.518	1.006
	0.524	0.520	1.011
	0.535	0.520	1.012
Mean value	0.528	0.519	1.010
Uncertainty ($2.57\times\sigma$)	0.006 (1.1 %)	0.004 (0.8 %)	0.008 (0.8 %)

Table 4.2: Potential effect of load (clamping force) on the results of thermal conductivity measurement on bricks at 25 °C.

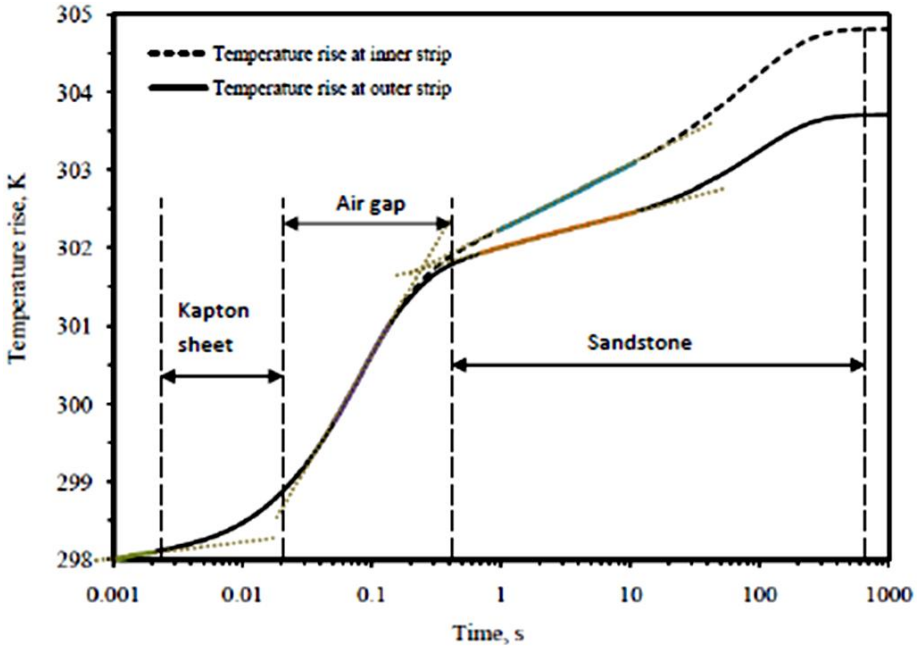

Figure 4.6: FEM (COMSOL Multiphysics) simulated temperature rises calculated at the center of the inner and outer strips of THB sensor as a function of logarithmic time for dry Sander sandstone at 25 °C.

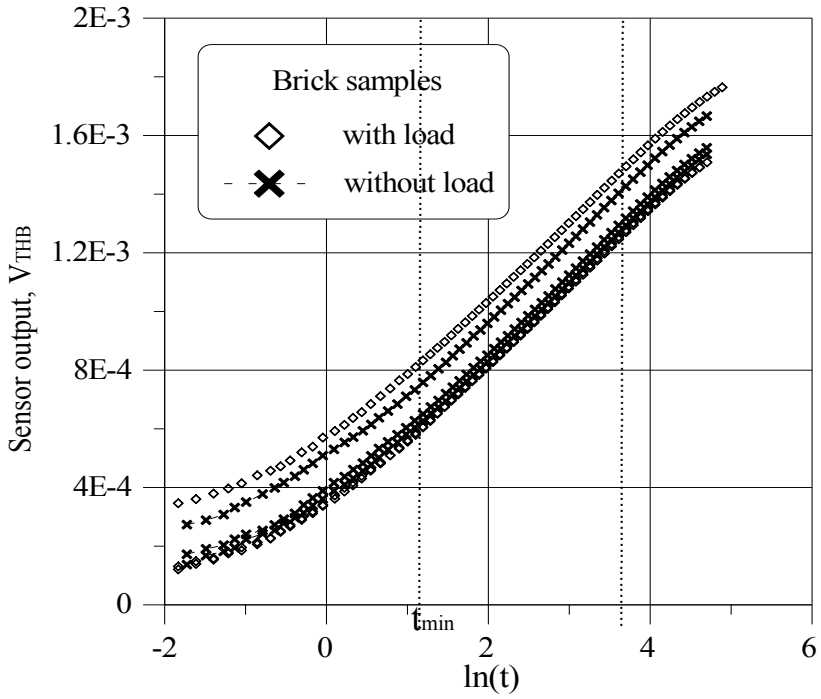

Figure 4.7: Effect of clamping force on the sensor output signal for a dry brick sample plotted on logarithmic time scale.

Chapter 5

Physical Characterization of Sander Sandstone

To understand the mechanism of heat transfer in porous sandstone properly, it is important to know the physical characteristics of the stone. The investigated specimen is taken from the place Sander Schilfsandsteinbruch "Hermannsberg (Sand am Main)", Haßberge, Germany. This sample is selected because of its special porous uniqueness discussed in chapter 1. Two sample halves were cut from a bulky piece of sandstone and both sample halves were prepared in the form of two rectangular blocks of dimensions $100\times60\times20$ mm^3 each. First, a conventional oven-drying method is used to dry the samples. Both sample halves were put in a temperature-controlled oven, (MEMMERT UE-400), and dried at 105 °C for at least 24 hours[4]. The water-saturated state is reached by immersing the dry specimen into deionized water for 96 hours followed by reweighing until the mass change between two consecutive weighing is less than 0.3 %. Free saturation porosity is determined using Archimedes principle by the mass change between dry and water-saturated specimens. Porosity of a porous material can also be calculated by density method, if density of the bulk stone and the densities of the mineral components of the stone are known [42]. The porosity value obtained by free saturation method is always lower than the porosity values obtained by true density method. This difference is because of the fact that, not all the pores can be filled using free saturation method. Density and porosity values of Sander sandstone calculated using different methods are given in table 5.1.

[4]According to the standards of DIN EN 18125.

Bulk density (kg.m^{-3})		Porosity (%)			
Dry	Water-saturated	Calculated[a] free porosity	Calculated by MIP[c]	Published [43]	$\phi^b = 1 - \rho_r/\rho_0$
2132	2303	17	19	17.80	19.32

[a]Porosity is calculated using formula $\phi=(V_p/V_b)\times100$, where V_b is the total volume of the porous material and V_p is the volume contained by the pores

[b]ϕ is the total porosity calculated from raw bulk density (ρ_b) of the whole specimen and the true density (ρ_{matrix}) of all mineral components in the specimen

[c]Mercury Intrusion Porosimetry

Table 5.1: Porosity and density data of Sander sandstone at ambient temperature and pressure.

5.1 Mineral Composition of Sander Sandstone

Sandstone is a sedimentary rock formed from a combination of many minerals settled down at higher pressures. The major mineral component in almost all types of sandstones is quartz. It is important to study the complete mineral composition in sandstone. Once we have thermal data of each mineral component, we can estimate the matrix thermal properties, which are free from the pore effect. Sander sandstone is a special type of sandstone, which contains a high portion of binding minerals (32 % rock binding fragments) in all different kinds of sandstones. Its colour is olive-green and contains fine mineral grains homogeneously distributed throughout the stone. Mineral composition is determined using XRD (X-ray Diffraction) method. Results of this test show that Sander sandstone contains about 54 % quartz. Therefore, thermophysical properties of this stone largely depend on the properties of quartz. Quartz is a very hard and chemically stable mineral. Second largest mineral portion found is of binding minerals (stone fragments), which is about 32 %. Binding minerals are mainly hornblende and calcite. There are some more binding minerals but their portion is very low therefore, these can be ignored. Table 5.2 shows a list of all mineral components in Sander sandstone and their thermophysical properties. Matrix thermal conductivity (λ_{matrix}, prtial product of thermal conductivities of all mineral constituents) can also be calculated using thermal conductivity values of each minerals by using following equation [44].

$$\lambda_{matrix} = \prod_{i=1}^{n} \lambda_i^{vol_i} \tag{5.1}$$

Where n is the total number of mineral constituents in stone, λ_i and vol_i are the thermal conductivity and volume fraction of the ith mineral constituent, respectively. In order to apply this formula, it is necessary to know the actual values of thermal con-

ductivities of each mineral component. For example, the matrix thermal conductivity for Sander sandstone is calculated as following,

$$\lambda_{matrix} = (7.69)^{0.54} \times (2.05)^{0.02} \times (2.37)^{0.03} \times (1.87)^{0.07} \times (5.12)^{0.01} \times (4.29)^{0.01} \times (3.59)^{0.16} \times (2.54)^{0.16} = 4.81 \quad (5.2)$$

Specific heat capacity values of the Sander sandstone can also be calculated using Kopp's law [45]. This method is based on the mineral summation method and uses the weighted sum of heat capacities of all mineral components in a particular rock/stone.

$$c_{matrix} = \sum_{i=1}^{n} x_i c_{m_i} \quad (5.3)$$

Where, the variables x_i and c_{m_i} are the weight fraction and the heat capacity of a particular mineral: and n, is the total number of minerals in the stone. Thermal conductivity and heat capacity values shown in table 5.2 are taken from reference K. Horai et al., 1969 [46].

Minerals	Volume Fraction (%)	Thermal properties			Density ($kg.m^{-3}$) [45; 47]
		Thermal conductivity ($W.m^{-1}.K^{-1}$) [45; 17]	Heat capacity ($J.kg^{-1}.K^{-1}$) [46]	Thermal diffusivity ($mm^2.s^{-1}$) (equation 2.10)	
Quartz	0.54	7.690	740	3.930	2648
Mica (Muscovite)	0.02	2.050	770	0.932	2855
Alkali Feldspar	0.03	2.370	700	1.316	2572
Plagioclase	0.07	1.870	750	0.933	2676
Rutile	0.01	5.120	800	1.508	4244
Tourmaline	0.01	4.290	850	1.583	3187
Calcite	0.16	3.589	830	1.589	2721
Hornblende	0.16	2.540	817	0.955	3254
Volumetric sum	1	4.810	768	2.260	2770

Table 5.2: Mineralogical composition of Sander sandstone and thermophysical properties of minerals at ambient temperature and pressure.

5.2 Scanning Electron Microscopy (SEM)

Grain sizes, grain shape and grain contacts may control the pore size, pore shape and ultimately the ability of the stone to absorb and to store fluids through capillaries. A high resolution scanning electron microscope (HRSEM JSM-6700F NT), is used for getting scanned images of the sample. Each image shown in figure 5.1 is taken by 150 times optical zoom. Figure 5.1(a) and figure 5.1(b) are taken from the outer surface of the sample. In these images, we can see that most of the pores (especially small pores) are filled with sandstone dust particles. This is because of the cutting process used to shape the samples in rectangular blocks. In order to view the pore sizes, shapes and their distributions inside sandstone, SEM images are also taken from the inner part of the sample by breaking it. Figure 5.1(c) and figure 5.1(d) clearly shows a microscopic porous system inside Sander sandstone and different types of pores can be seen easily. Few pores are captured in between grains and have no connectivity to other pores. Such pores are called blind pores. Estimated average grain size is 180 μm and pore sizes lie in the range of 1 μm to 100 μm.

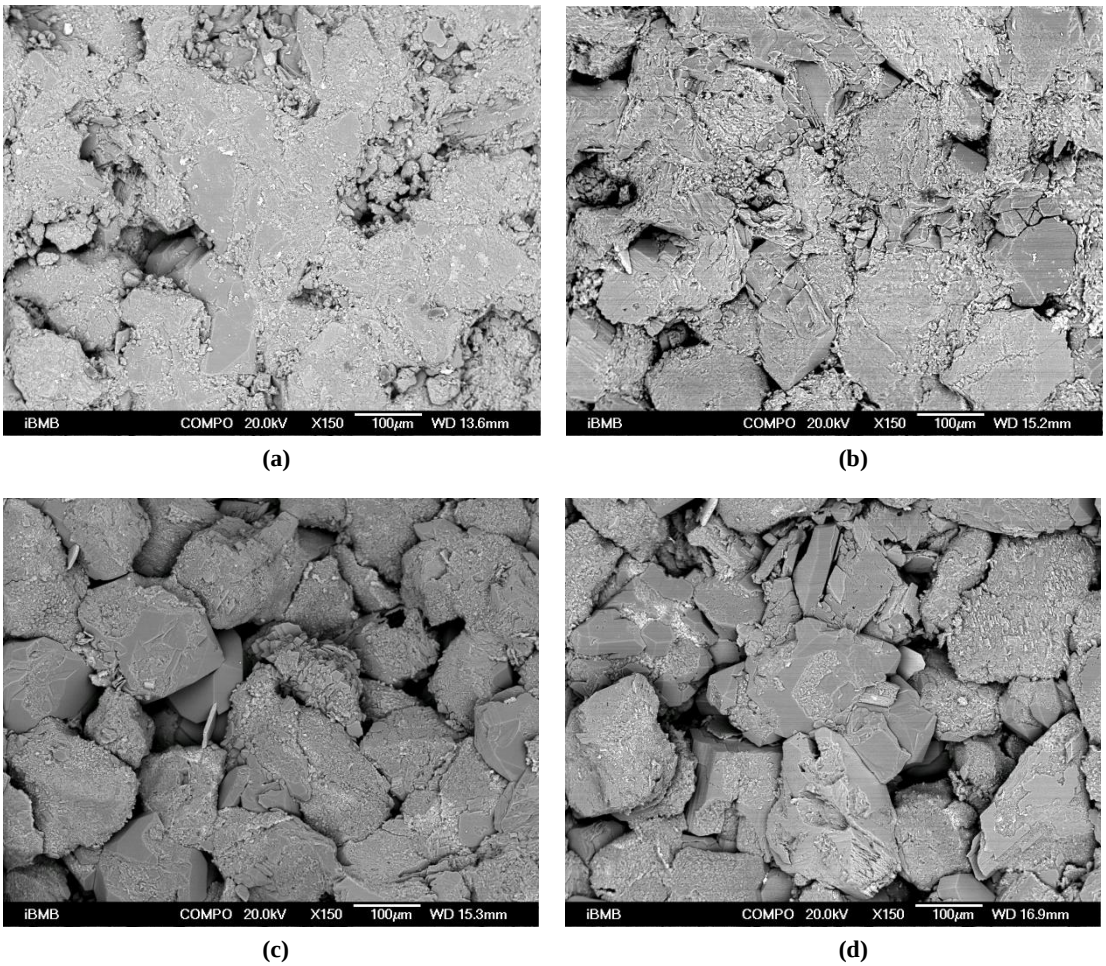

Figure 5.1: Scanning Electron Microscopic images of Sander sandstone.

5.3 Pore Size Distribution

To investigate the pore sizes and their distribution we used Mercury Intrusion Porosimetry (MIP) method. In this work, Porosimeter Pascal 240 from the company Thermo Electron Corporation was used. Porosity values of Sander sandstone as determined by this method are 19.54 % and 18.63 % for dry and wetted stone, respectively [48]. Whereas, porosity of the sample as determined through water saturation method is 17 %. A difference of 11 % is observed in the porosity values due to two different measuring techniques. It is obvious that, during free saturation process only open pore can be filled while, closed pores remain unsaturated. Due to this reason, we obtained less porosity values as compared to MIP method. In porosimetry method, a pressure of 350 kPa is used to intrude mercury inside sandstone, which fills almost all pores, hence giving higher porosity values as compared to free saturation method. At any pressure, the pores into which mercury has intruded have radius greater than r_p (Washburn equation).

$$r_p = \frac{-2\sigma \cos\theta}{P} \tag{5.4}$$

Where P is the applied pressure, σ is the surface tension of the intrusion fluid (mercury) and θ is the contact angle formed by the intrusion fluid (mercury) with the sample surface. Generally, the surface tension of mercury is equal to 0.48 J.m^2 and the contact angle is assumed to 140° [49]. Pore size distribution curve shows two prominent peaks. Results in figure 5.2 shows that, most of the pores (60 % of the total pore volume) have a pore radius size in between 1 to 10 μm which indicates a strong network of macro-porosity (radius $\geq$ 0.025 μm) inside the dry as well as in wetted sandstone. A complete range of pore sizes for dry as well as wetted sandstone is given in table 5.3 and few additional important parameters are given in table 5.4.

	Relative volume (%)	
Pore radius ranges (μm)	Dry sandstone	Wetted sandstone
100 - 10	3.15	6.05
10 - 1	59.57	58.54
1 - 0.1	13.90	13.66
0.1 - 0.01	19.95	18.96
0.01 - 0.001	3.43	2.78

Table 5.3: Pore size distribution in dry and wetted Sander sandstone.

Parameters	Dry sandstone	Wetted sandstone
Total cumulative volume ($mm^3.g^{-1}$)	92.12	88.11
Total specific surface area ($m^2.g^{-1}$)	2.432	2.032
Average pore radius (μm)	3.320	3.682
Total porosity (%)	19.54	18.63
Bulk density ($g.cm^{-3}$)	2.121	2.114
Apparent density ($g.cm^{-3}$)	2.636	2.598

Table 5.4: Important characteristic parameters of Sander sandstone.

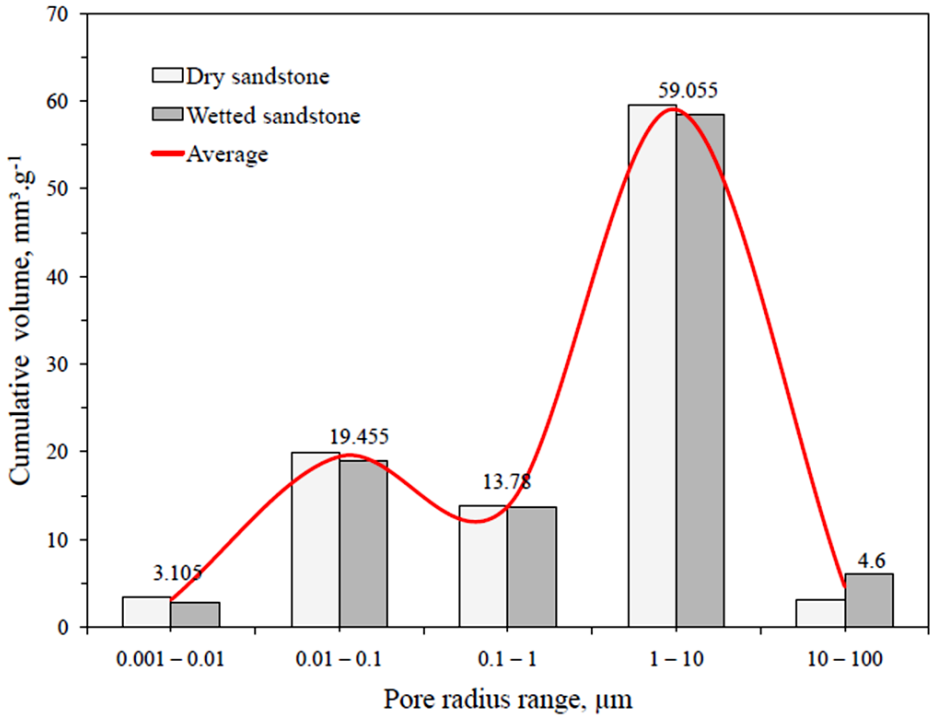

Figure 5.2: Pore size distribution curve in Sander sandstone.

Chapter 6

Temperature Dependent Thermophysical Properties of Sander Sandstone Using THB Technique

Thermal properties of porous masonry materials may drastically change when the pore structure fills with moisture from the ambient surroundings. The magnitude of these changes depends on the moisture content and on the temperature. In water saturation (free-saturation) case, there is a considerable additional transport of heat carried by water vapor. Therefore, any reliable thermal characterization of porous materials must include measurements on the effect of moisture and temperature on thermal properties. This situation occurs mostly during heavy rainy seasons when stone-made building walls absorb much amount of water due to continuous rainfall. This simultaneous effect of temperature and water absorption deteriorate the effectiveness of insulations during application. This is especially true for low temperatures when freezing and thawing occurs as well [43; 50]. In this chapter, temperature dependent thermophysical properties of Sander sandstone are presented using THB sensor within a temperature range of -20 to +40 °C. To obtain more details on the simultaneous transport of heat and matter inside sandstone, measurements are performed in dry, alcohol, toluene, alcohol-water and water-saturated states of the samples. Purpose of saturating sandstone with different fluids is to analyze the effect of these fluids on overall effective thermal

conductivity (ETC)[5] of the sandstone. Freeze-thaw process is analyzed using slow cooling rate between the temperature range of 0 to -5 °C. A general equation to estimate the temperature dependent ETC of Sander sandstone is also proposed [51].

6.1 Experimental Setup

The experimental setup of the THB sensor in combination with a Keithley 2602 system-source meter (which works as a current source and voltmeter simultaneously) is shown in figure 6.1. To obtain measurements on dry sandstone, samples were kept in an air-tight box[6] to prevent them from sudden changes in ambient conditions e.g., influence of moisture and sudden temperature fluctuations.

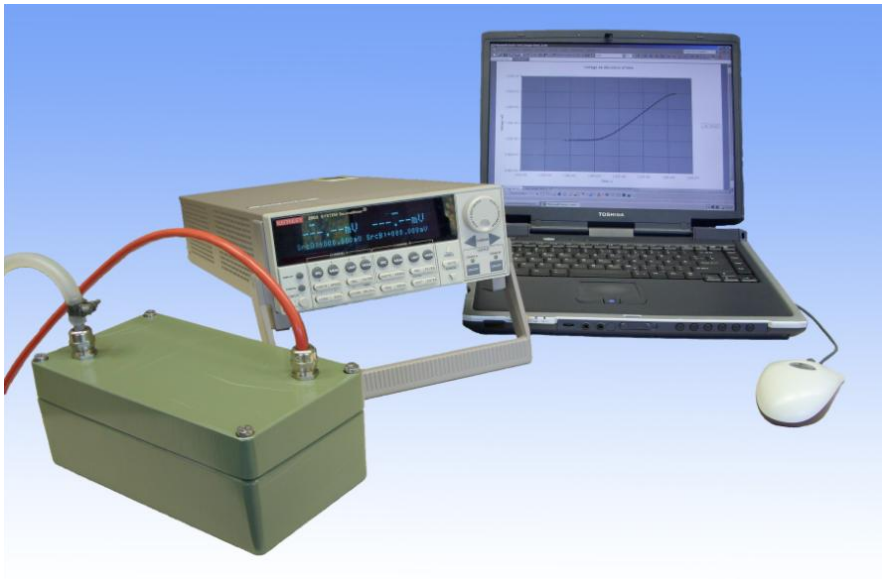

Figure 6.1: Experimental setup of THB sensor.

In order to perform measurements at different working temperatures, the box is placed in a temperature and air-tight climate chamber (Heraeus Vötsch, model VUK 04/500). The samples are prepared in the form of two rectangular blocks of dimensions 100×60×20 mm^3 and dried at 105 °C for 24 hours before starting the measurements. To perform a run, the sensor is sandwiched between two samples (here referred as two similar sample halves), and heated by applying a constant current using a programmable source meter (Keithley 2602). Figure 6.2 shows a sketch diagram of the entire experimental arrangement. Output data is obtained in the form of voltage drop versus time as shown in figure 6.3. This setup is able

[5]Thermal conductivity obtained through mutual effects of convection, conduction and radiation.
[6]Box can be opened during measurements at different humidities.

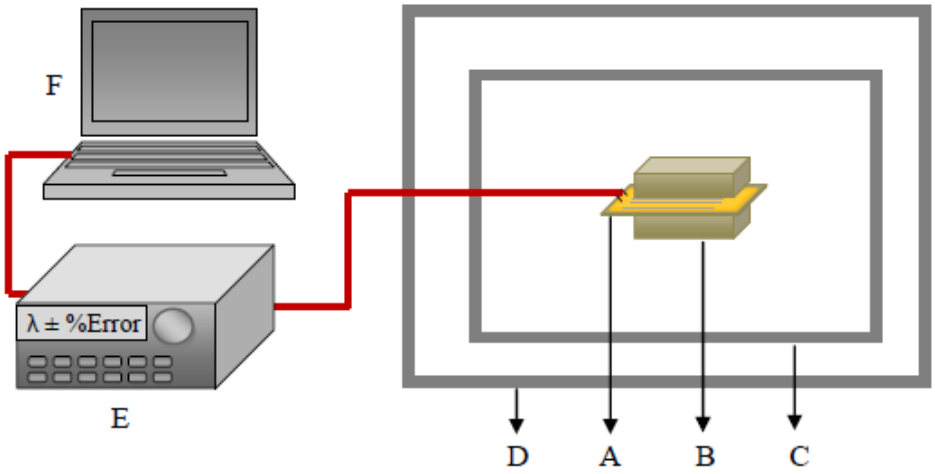

Figure 6.2: Sketch diagram of the experimental setup for thermophysical analysis of Sander sandstone using transient hot-bridge sensor: (A) THB sensor, (B) Sample half, (C) Air-tight box, (D) Climate chamber, (E) Keithley 2602 programmable source meter, (F) Data acquisition system.

to measure thermal conductivity and thermal diffusivity simultaneously in a single run. The instrument has a capability for a wide range of measurements from 0.02 to 100 $W.m^{-1}.K^{-1}$ for thermal conductivity and from 0.05 to 10 $mm^2.s^{-1}$ for thermal diffusivity.

6.1.1 Trial of the Sensor

Before using the sensor for the first time, it has to be tested using some reference materials. For this purpose, a Borosilicate Crown Glass (type BK-7) supplied by Physikalisch-Technische Bundesanstalt (PTB), Braunschweig was used. The thermal conductivity of the reference material (BK-7) was measured at ambient temperature (25 °C) by applying a current of 200 mA. The output signal of the sensor is plotted against time and is shown in figure 6.4. If we plot the output signal against logarithmic time scale then we will get a curve as shown in figure 6.5.

By taking slope of the linear part of the curve shown in figure 6.5, and by putting this slope into the equation 3.42, thermal conductivity of the sample can be calculated. To minimize the random errors, the measurements are repeated three times and a mean value is calculated. The experimental value of the thermal conductivity of the reference material (BK-7) is $\lambda = 1.098 \pm 0.018$ $W.m^{-1}.K^{-1}$. The deviation from the reference value ($\lambda = 1.1$ $W.m^{-1}.K^{-1}$) is equal to 0.8 %.

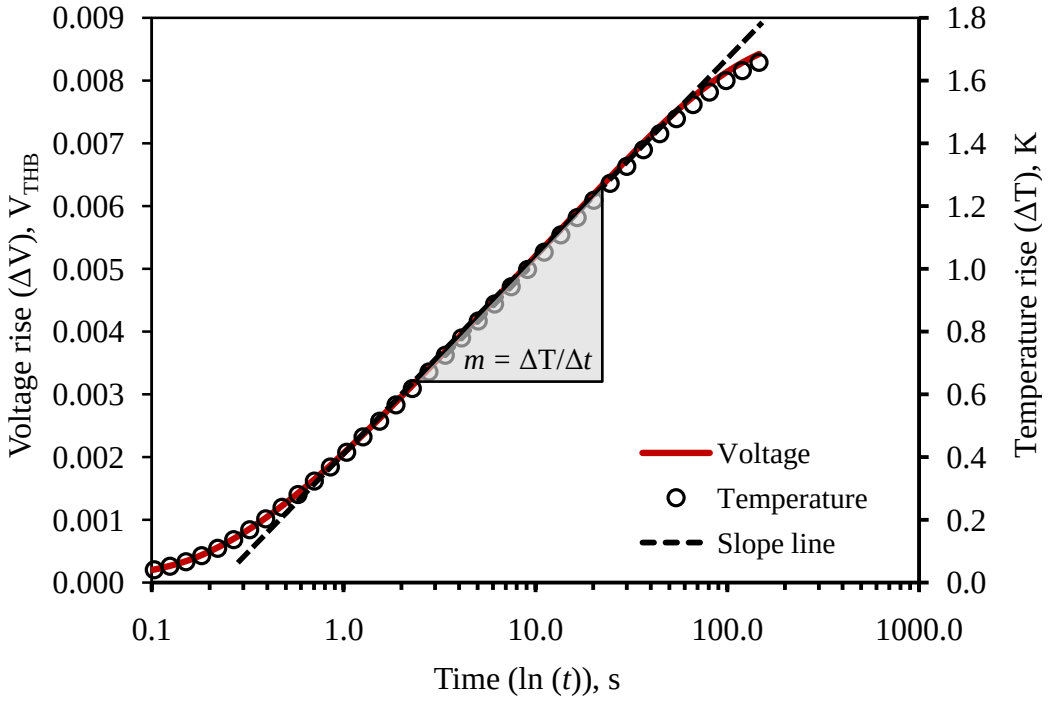

Figure 6.3: Typical THB sensor output signal and corresponding temperature rise (calculated using equation 3.42) in dry sandstone as a function of logarithmic time.

6.2 Experimental Results and Discussion

The temperature dependence of three major thermophysical parameters namely, thermal conductivity, thermal diffusivity and specific heat capacity of Sander sandstone is studied in before mentioned saturated states using THB sensor. Temperature range is restricted from -20 to +40 °C due to weathering temperature range in Europe. Results show that, the values of the thermal conductivity and thermal diffusivity decreases with increasing temperature in all saturated states of sandstone. Anomalies in thermophysical parameters are found for water-saturated sandstone between temperature ranges of -1 °C to -3 °C. This discontinuity in thermal parameters is because of the phase change of water into ice. On contrary, no anomaly is found in the case of dry, aqueous alcohol and alcohol-saturated sandstone. Figure 6.6 to figure 6.8 depicts experimentally determined values of thermophysical properties of Sander sandstone. It is observed that, thermophysical properties are highly dependent on temperature and moisture content. Table 6.2 shows the overall difference in thermal properties of the dry, water-saturated and alcohol-saturated sandstone at 5 °C, when water in the pores is in a fluid state, and at -10 °C when water in the pores is frozen i.e., ice. On the other hand, Alcohol has very low freezing point (-114 °C) therefore, we do not observed any change of phase of alcohol at -20 °C and consequently no sudden change in the thermal properties. In this way, we can see a clear difference in the thermal

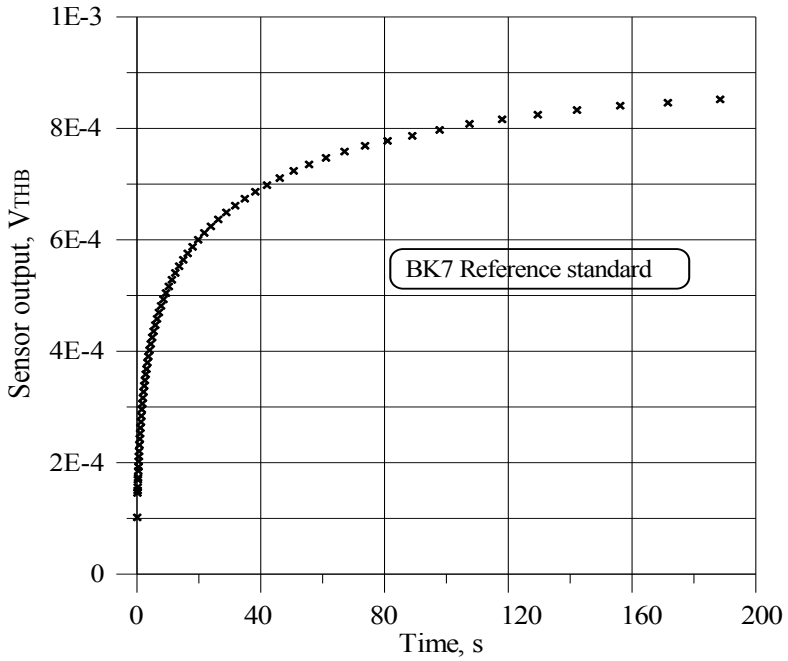

Figure 6.4: THB Sensor output-signal on a BK-7 standard reference plotted against real time scale.

properties between a solid filled (ice) pores and liquid filled pores (ethanol) at same low temperature. A large difference is observed in the values of thermal conductivity and thermal diffusivity of sandstone between dry and water-saturated state, while the effect of alcohol is less as compared to water. The difference in thermal conductivity of water-saturated sandstone before and after freezing point of water (+5 to -10 °C) is 12 %, whereas in case of alcohol it is only 2 % as shown in figure 6.6. A large shift of 48 % is observed in the values of thermal diffusivity of water-saturated sandstone (as compared to its dry state) and no change in case of alcohol-saturated sandstone as shown in figure 6.7. A significant large difference of 24 % also exists in the values of specific heat capacity for water-saturated case (same difference is reported in [43]) and 3 % for alcohol-saturated stone as shown in figure 6.8. The thermal conductivity and thermal diffusivity data are obtained directly from the experiment while specific heat capacity (c_p) is calculated by applying equation 2.10 with an additional knowledge of density. Experimentally, thermal conductivity is not measurable in a material volume when a phase transition is taking place in it. It is because of the fact, that the temperature gradient vanishes. Therefore, well-defined clear values of the thermal conductivity and thermal diffusivity can be established only below and above the phase transition of water in sandstone pores. Combined heat and mass transfer can occur in porous structures when temperature and mass gradients are well-established throughout the material under test. However, there is a significant difference between the classic steady-state methods and the transient hot bridge (THB) method as men-

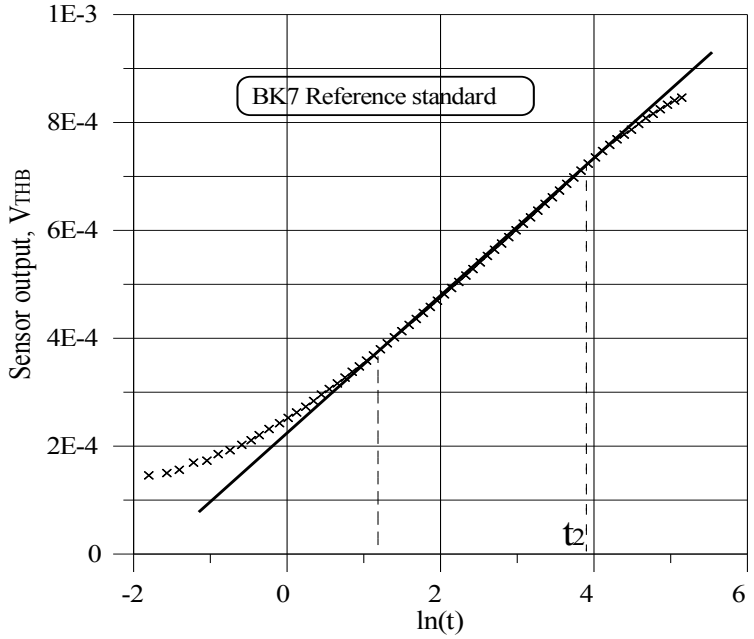

Figure 6.5: THB Sensor output-signal on a BK-7 standard reference plotted against logarithmic time scale.

tioned in chapter 2. Thermal conductivity values of dry as well as water-saturated sandstone are also calculated by Guarded Hot-plate method. Values of both methods are plotted in figure 6.6. By using THB method, the measuring process can be completed within one minute. Thermal diffusivity values obtained by the THB method are also compared with the values obtained by laser flash technique. Our results lie in between the dry and water-saturated values obtained by laser flash method as shown in figure 6.7. This indicates the reliability of THB sensor for measurements of thermal diffusivity of porous materials like sandstone. When water changes its phase to ice, it releases energy to form ice crystals. During this change, thermal properties are hard to find because of the unsteady temperature distribution within the material. Due to this reason, we get a sharp peak in the output data of thermal diffusivity for a temperature range of -1 to -3 °C. Since, thermal diffusivity and specific heat capacity are inversely correlated according to equation 2.10; therefore, this peak appears inversely for heat capacity values as shown in figure 6.8. Sander sandstone consist of a large number of pores (connected through capillary paths) which are filled with water (in water-saturated case). During freezing process, it takes more time to freeze in these pores as compared to the normal water. Therefore, we observe a peak at higher lower temperature and not at 0 °C. Thermal conductivity and thermal diffusivity of crystalline rocks decrease with increasing temperature [17]. This effect is more prominent in stones that have high contents of quartz mineral. Since, quartz is the main mineral component in sedimentary rocks and has the highest values of

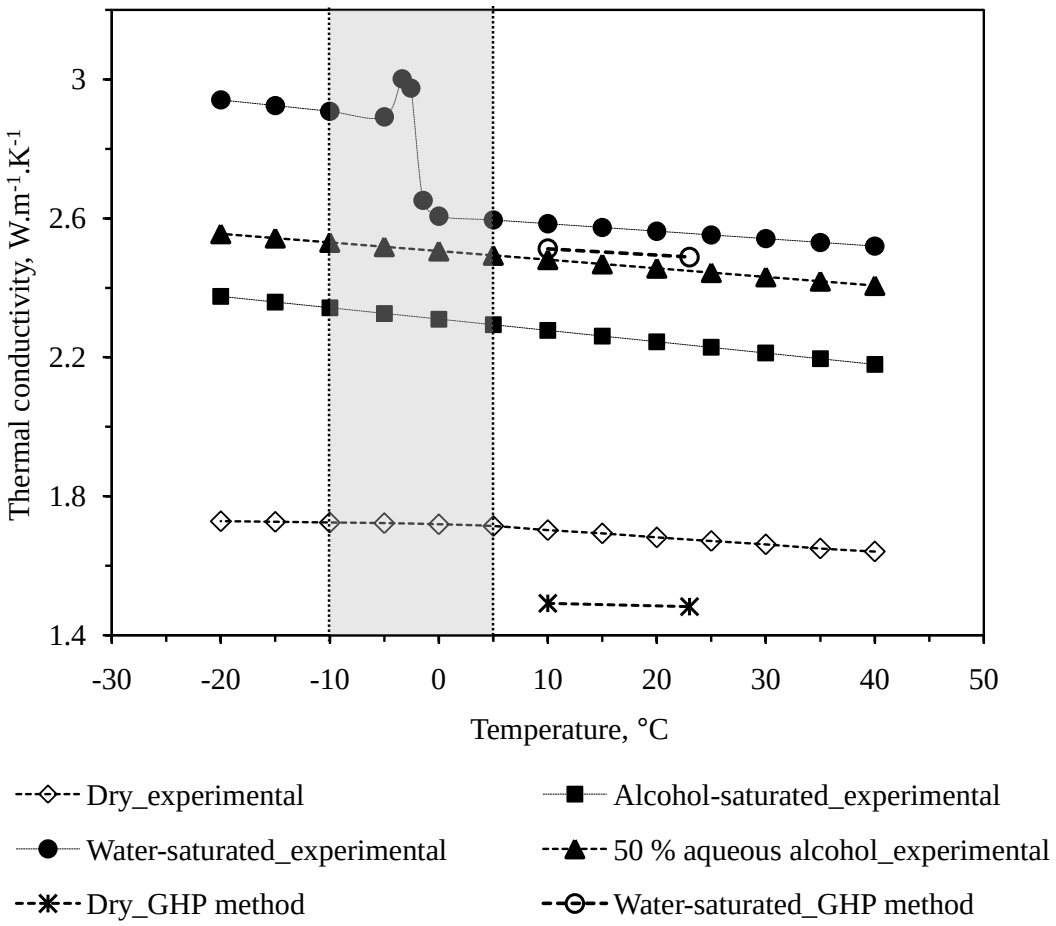

Figure 6.6: Temperature dependent thermal conductivity of Sander sandstone.

thermal conductivity in all rock forming mineral components; therefore, quartz-rich rocks show high values of thermal conductivity and diffusivity with a high negative gradient with temperature. Investigated sandstone (Sander) contains 54 % quartz content that is one of the main reasons of decreasing the thermal conductivity and thermal diffusivity with temperature. Dependence of thermal diffusivity seems to be stronger on temperature as compared to the thermal conductivity. However, in case of mixed or highly disordered crystal rocks, rate of decrease of thermal conductivity with increasing temperature is very less or even opposite. Table 6.1 shows percentage decrease (negative sign) or increase (positive sign) in thermal properties within a temperature range of -20 to +40 °C.

Unlike thermal conductivity and thermal diffusivity, specific heat capacity of sandstone increases with increasing temperature. Maximum increase in the heat capacity is 54 % in the case of water-saturated sandstone. This difference is because of the fact that, heat capacity of water is more than 5 times the heat capacity of rock forming minerals, which increases the overall heat capacity of the stone[7]. The differences in

[7]Average heat capacity of rock forming minerals in Sander sandstone is 768 $J.kg^{-1}.K^{-1}$, while

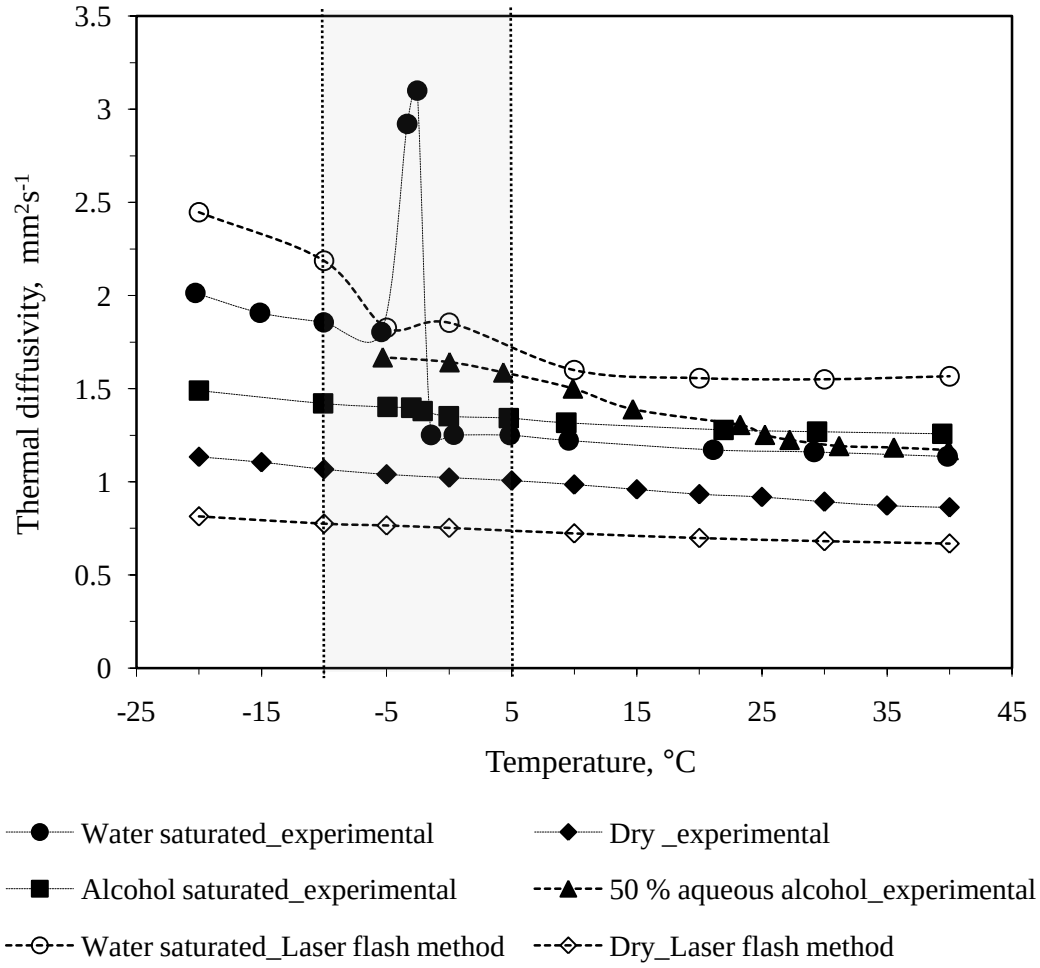

Figure 6.7: Thermal diffusivity of Sander sandstone as a function of temperature.

thermophysical properties of Sander sandstone before and after freezing temperature of water for dry, water-saturated and alcohol-saturated states are given in table 6.1.

6.3 A General Empirical Relation for $\lambda(T)$

In this section, an empirical relation for the estimation of the temperature dependent thermal conductivity of sandstone is given. In the past, many authors [52; 53; 54] tried to correlate the effective thermal conductivity of rocks/stone with temperature. The proposed correlation is derived after some modifications in the previously published correlations and using the experimental data obtain from this work specifically suitable for Sander sandstone. This empirical relation is suitable to obtain temperature dependent effective thermal conductivity of multi-fluid saturated Sander sandstone for a temperature range of -20 to +40 °C. Dependence of the effective thermal conductivity of Sander sandstone on measurement temperature and the room temperature

heat capacity of water is 4180 J.kg^{-1}.K^{-1} at ambient conditions.

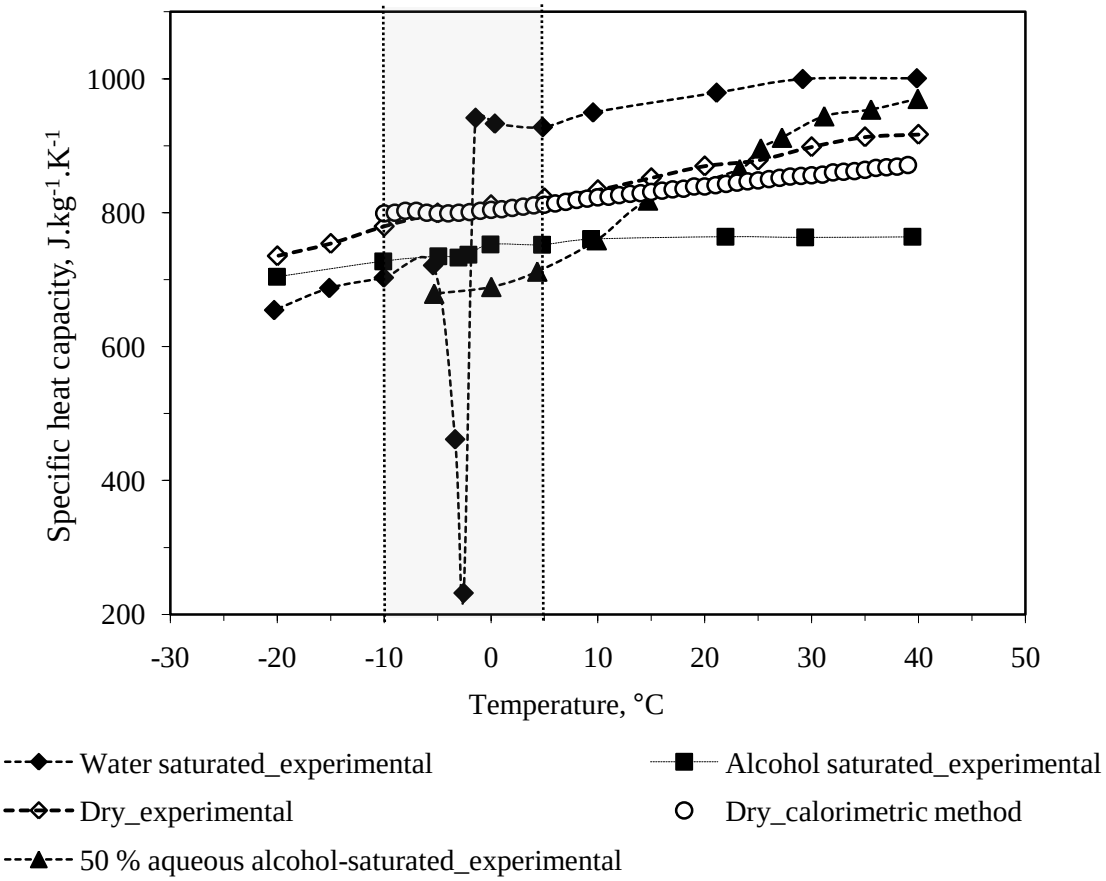

Figure 6.8: Heat capacity of Sander sandstone as a function of temperature.

thermal conductivity of saturated stone can be described by following proposed relation,

$$\lambda_{eff} = \left[\frac{(1.08\lambda_{25} - 0.15)^2}{\lambda_{25}\,(1.09 + 0.0033T) - 0.009T - 0.149}\right] - 0.0048T + 0.065 \qquad (6.1)$$

Where, λ_{eff} is in W.m^{-1}.K^{-1}, T is in °C and λ_{25} is the room temperature (25 °C) thermal conductivity of sandstone. However, in the case of ice saturation, λ_{25} is taken by extrapolating the experimental values to 0 °C. Experimental values of the thermal conductivity are compared with the proposed empirical equation 6.1. The maximum deviation between the experimental values and those derived from empirical relation is ± 1.99 % in the case of 50 % weight mixture of water and alcohol. The ranges of deviations between experimental and predicted values are shown in table 6.3. Based on the experimental values of the thermal conductivity of sandstone, an inverse linear relation between λ_{eff} and T is found. The thermal conductivity values are found to increase by decreasing temperature in all saturation states of sandstone. However, the rate of increase of the thermal conductivity by decreasing temperature is more

% Change in properties	Sandstone state				
	Dry	Water-saturated	Alcohol-saturated	Aqueous-alcohol-saturated	Ice-saturated
Thermal conductivity ($\Delta\lambda$), W.m^{-1}.K^{-1}	-5.3 %	-3.4 %	-9 %	-6.2 %	-1.7 %
Thermal diffusivity (Δa), mm^2.s^{-1}	-31 %	-10 %	-18.5 %	-42.5 %	-11.6 %
Specific heat capacity (Δc_p), J.kg^{-1}.K^{-1}	+19.7 %	+54 %	+7.8 %	+30 %	+9 %

Table 6.1: Percent increase/decrease of thermophysical properties of Sander sandstone in a temperature range of -20 to +40 °C.

in the case of higher thermal conductivity saturating fluids. Experimental and fitted values (according to equation 6.1) are plotted in figure 6.9.

Thermophysical properties	5°C					-10°C				
	Dry	Water-saturated	Alcohol-saturated	Diff. in dry- and water-saturated	Diff. in dry and alcohol-saturated	Dry	Water-saturated	Alcohol-saturated	Diff. in dry- and water-saturated	Diff. in dry- and alcohol-saturated
Thermal conductivity, $W.m^{-1}.K^{-1}$	1.71	2.58	2.29	51 %	34 %	1.72	2.90	2.34	69 %	36 %
Thermal diffusivity, $mm^2.s^{-1}$	1.03	1.17	1.28	14 %	24 %	1.07	1.62	1.42	51 %	33 %
Specific heat capacity, $J.kg^{-1}.K^{-1}$	795	980	832	23 %	5 %	776	796	767	2.6 %	-1 %

Table 6.2: Difference in thermophysical properties of Sander sandstone before and after freezing temperature of water for dry, water-saturated and alcohol-saturated states.

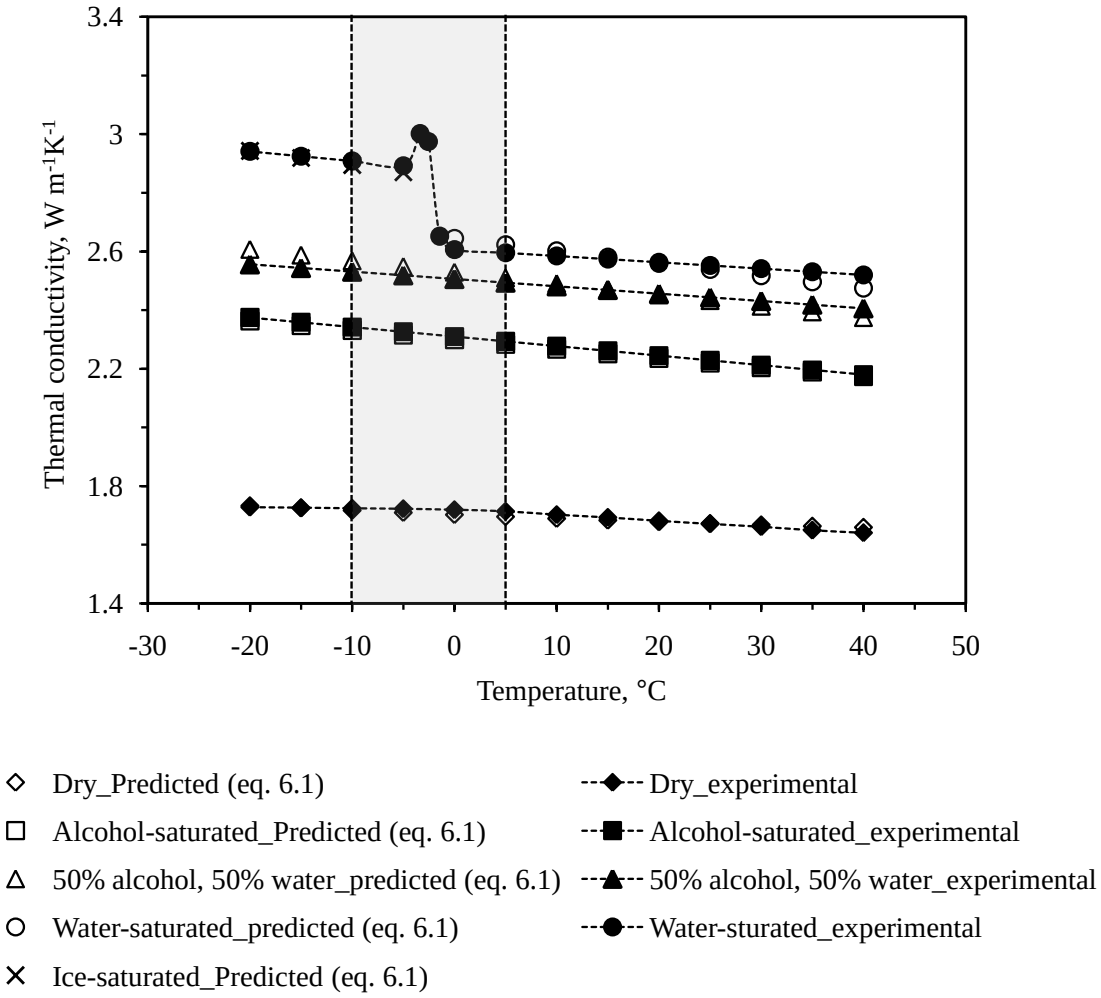

Figure 6.9: Comparision of experimental and predicted values of the thermal conductivity of sandstone.

Saturating fluid	Error ($\Delta\lambda^a$) in percent
Air (dry sandstone)	-1.10 $\leq \Delta\lambda \leq$ 1.09
Alcohol	0.30 $\leq \Delta\lambda \leq$ 0.51
50 % alcohol, 50 % water	-1.99 $\leq \Delta\lambda \leq$ 1.33
Water	-1.45 $\leq \Delta\lambda \leq$ 1.80
Ice	-0.06 $\leq \Delta\lambda \leq$ 0.76

$^a\Delta\lambda = [(\lambda_{exp} - \lambda_{fit})/\lambda_{fit}] \times 100.$

Table 6.3: Deviation (%) between experimental and predicted values (eq. 6.1) of the thermal conductivity of Sander sandstone as a function of temperature (-20 to +40 °C).

Chapter 7

Thermophysical Properties of Fluid-saturated Sander Sandstone

As mentioned before, study of thermophysical properties of stones/rocks plays a vital role in buildings where moisture can affect the thermal performance of building made from stones. Thermal properties of such porous materials significantly changes when the pore structure is filled with some fluid (e.g., water, alcohol, oil, air, moisture etc) and the magnitude of these changes depends on the moisture content and thermal properties of the saturating fluids [51]. In addition, thermophysical data on stones/rocks are required at different pressure, saturating fluid and temperature in several geothermal applications. In chapter 5, we discussed thermal properties of Sander sandstone depending on temperature. In this chapter, the dependence of thermal properties of multi-fluid-saturated sandstone are presented using the same transient hot-bridge technique at ambient conditions. The aim is to observe the change in overall thermal conductivity of the stone depending on the thermal conductivity of the pore filling fluid. Measurements are carried out by filling the porous sandstone structure first, with six different fluids of different thermal conductivities and next with six different gases also having different thermal conductivities. Variations in the thermal properties due to liquid and gas saturations are discussed. Furthermore, effects of the applied gas pressure and moisture (relative humidity of air) on thermal properties are also discussed in this chapter.

7.1 Experimental Setup

The experimental arrangement to measure thermal properties of sandstone as a function of different saturating gases and different pressures is shown in figure 7.1. Sensor is sandwiched between two sample halves and clamped to ensure better thermal contact. Experiments on liquid saturated sandstone are performed at room temperature and room pressure. Whereas, to perform experiments at different pressures, THB sensor together with sample halves are put in a vacuum chamber. The used vacuum pump is able to create a vacuum down to 1 μbar. The vacuum chamber (along with the sample halves) is evacuated each time before filling different gases. A full sketch diagram of the complete experimental setup is clear from figure 7.2.

Figure 7.1: Experimental setup used to measure thermal properties of gas-saturated sandstone at different pressures.

7.2 Experimental Results and Discussion

One of the important questions regarding thermal conductivity of liquid or gas-saturated sandstone is the relationship between the total effective thermal conductivity of the porous sample and the thermal conductivity of the pore filling material. Do we get similar values of the effective thermal conductivity by filling the porous structure with a liquid and gas while both having same thermal conductivity? To find out the answer of this question, measurements are done by filling the porous sandstone structure first, with six different fluids of different thermal conductivities

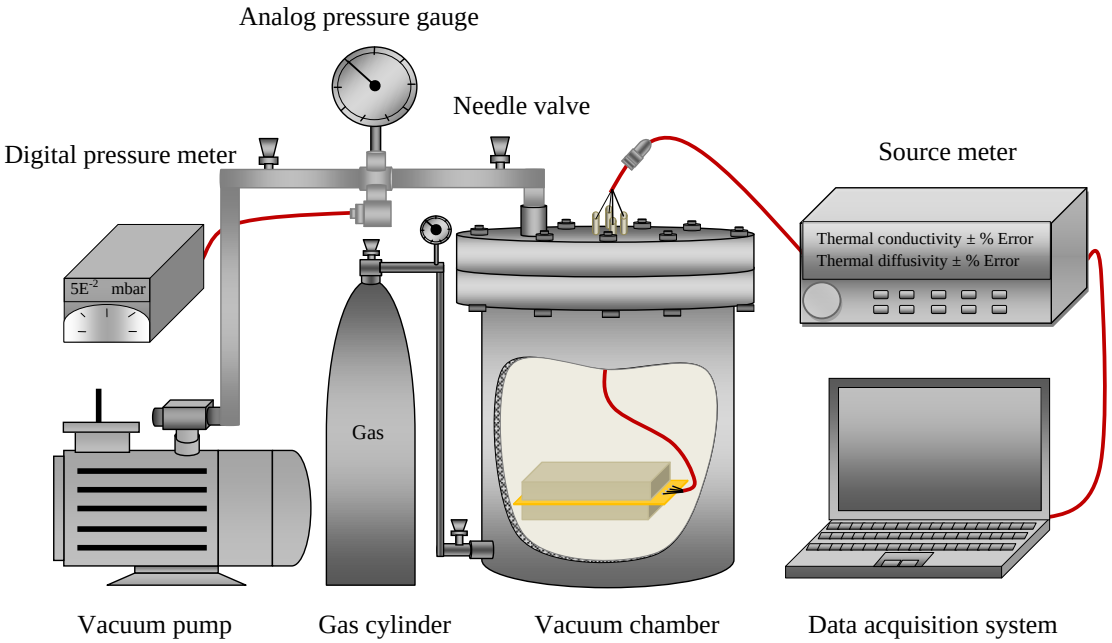

Figure 7.2: Sketch diagram of the complete experimental setup for thermophysical analysis of Sander sandstone using transient hot-bridge sensor.

namely; toluene, alcohol, a mixture of 75 % alcohol and 25 % water, a mixture of 50 % alcohol and 50 % water, a mixture of 25 % alcohol and 75 % water and pure water and in the next step, with six different gases having different thermal conductivities. The gases used are Argon, Nitrogen, a mixture of 50 % Nitrogen and 50 % Helium, a mixture of 20 % Nitrogen and 80 % Helium, Helium and Hydrogen. Investigated sandstone is 19 % porous and the pores are filled only with (above mentioned) removable fluids. Non-removable fluids (e.g., oil and glycerine) were avoided to fill in. Sample is dried each time before filling the pores with a different fluid.

In most porous materials, heat propagates by three processes (1) thermal conduction through the solid and fluid phase (2) radiation across the pores and (3) convection within the pores. All these three processes are responsible for overall thermal performance. It is generally known that the effect of radiative heat transfer mode is negligible at moderate temperatures (< 600 °C) [55]. Furthermore, for convection currents to form in the pore space, the diameter of the pore space should be more than 27 mm [56]. Whereas, the pore size in the investigated sandstone lies in between ranges of 0.01 to 100 μm, which is too small to produce significant convection currents. Thus, by neglecting convective and radiative parts of heat transfer we assume that the heat transfer is only due to conduction through the saturated fluid/gas and the solid part (matrix).

Figure 7.3 shows a sketch of an actual SEM image of the 19 % porous Sander sandstone sample. Pore sizes, their distribution and micro-crackes play an important

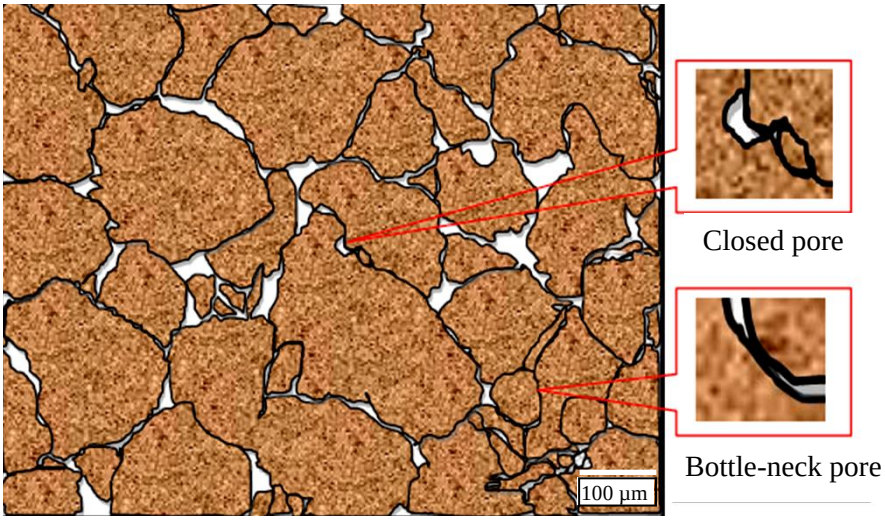

Figure 7.3: A sketch view of the porous system in Sander sandstone.

role in heat transfer because of their different contact thermal resistance and different surface areas. The flow of fluids is therefore expected through the interconnected void spaces and the capillary channels. Porous structure of this stone also consists of fractures in between two individual grains forming a bottleneck shape. If this bottleneck is dry, then it will act like a thermal resistor and prevents the flow of heat due to its lower thermal conductivity. Few pores are tightly closed in between two solid grains and cannot be filled with a saturating fluid; therefore, these pores only act like a thermal resistor. Results on thermal conductivity show that, the effective thermal

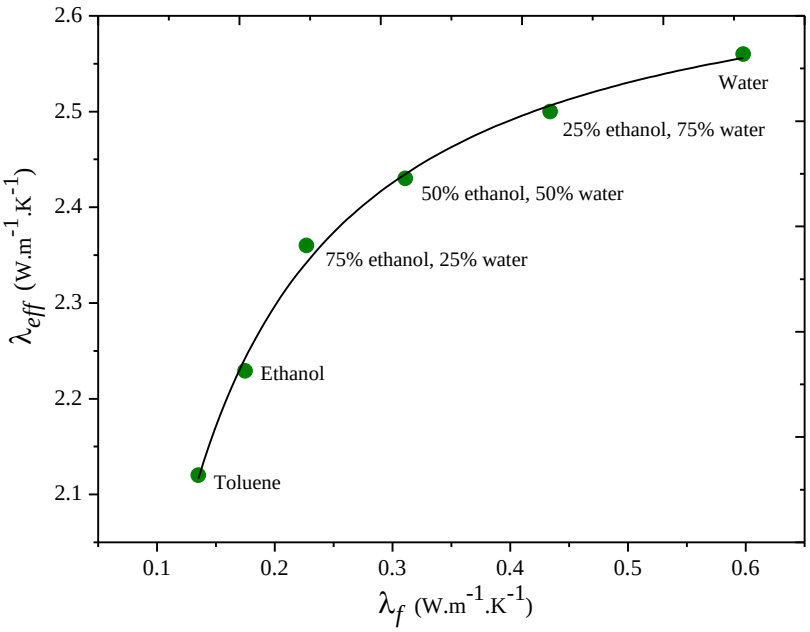

Figure 7.4: Effective thermal conductivity of Sander sandstone as a function of thermal conductivity of different liquids.

conductivity (λ_{eff})[8] of Sander sandstone increases nonlinearly by increasing the thermal conductivity of the pore filling fluid, λ_f (figure 7.4). Replacing a poor conducting pore space with a higher thermal conductivity fluid ensures a better thermal path for heat flow, thus increasing the overall thermal performance of the stone. It is noticed that, if we go on increasing pore filling thermal conductivities, the total effective thermal conductivity of the stone also goes on increasing but it tends to converge at some higher value and the trend of linearity no longer holds. Thermal behavior of gas-saturated sandstone is different from liquid-saturated sandstone. However, the trend of increasing of the effective thermal conductivity is similar (non-linear) as it is in the case of liquid-saturates. Figure 7.5 represents the dependence of the effective thermal conductivity on different saturating gases.

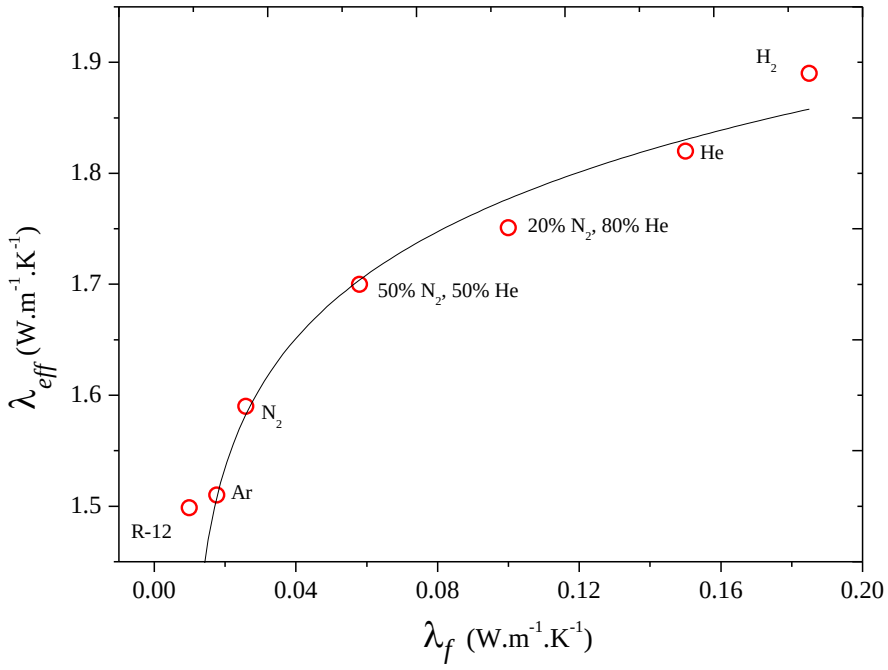

Figure 7.5: Effective thermal conductivity of Sander sandstone as a function of thermal conductivity of different gases.

Thermal conductivity of a gas-saturated sandstone deviates more and more from liquid saturants as we go towards higher thermal conductivity values of the gas fillings. This behavior is evident from figure 7.6. Thermal conductivity value of liquid toluene is similar to the thermal conductivity of helium gas but the difference in bulk thermal conductivity of the stone is 16 %. Similarly, the thermal conductivity value of liquid alcohol is similar to the thermal conductivity of the hydrogen gas but the difference in bulk thermal conductivity of the stone is 18 %. This difference seems to be increasing more and more from the trend lines along x-axis.

[8]We will use the term "effective thermal conductivity" in this text. However, the effects of radiation and convection are ignored.

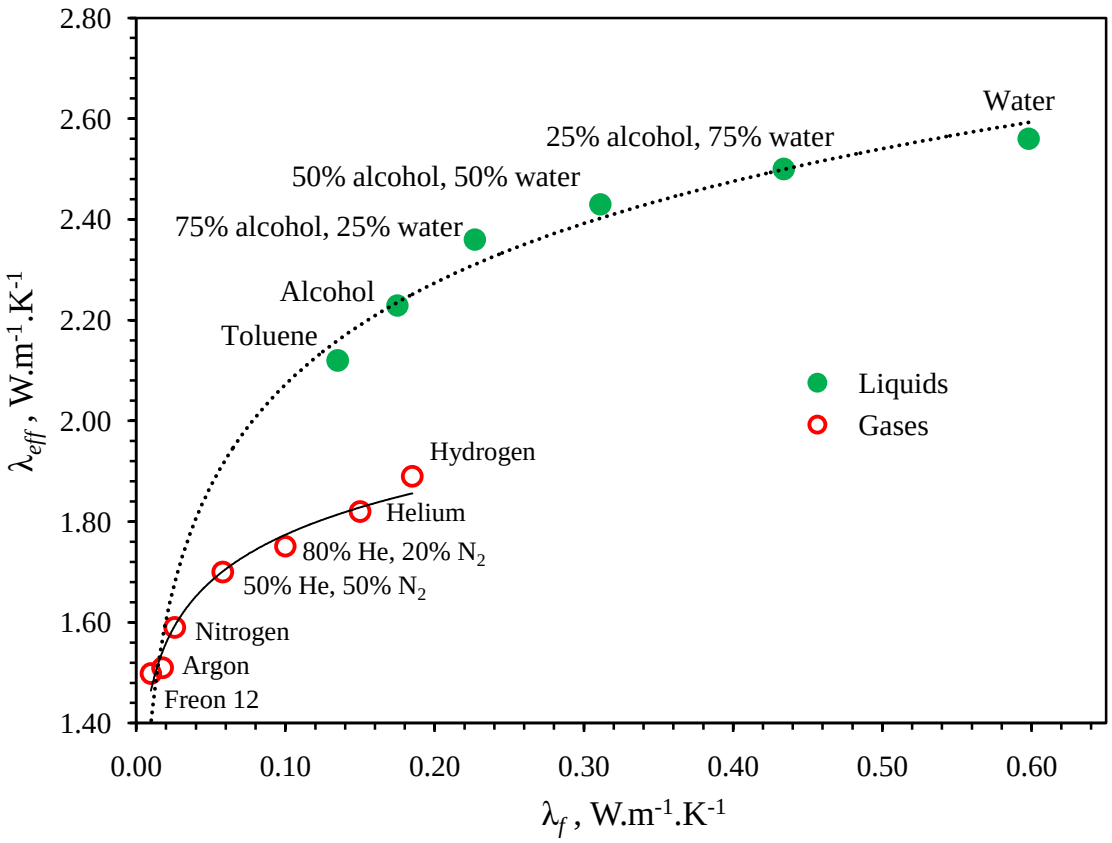

Figure 7.6: Comparison between thermal conductivities of a liquid and gas-saturated sandstone at ambient temperature and ambient pressure.

The major reasons of the difference between the two curves shown in figure 7.6 can be explained in terms of following five expected effects.

Knudsen Effect: In small pores (nano-scale pores), where mean free path of the gas molecules becomes equal to the average pore size, the thermal conductivity of the gas is reduced. This reduction is due to the exclusion of the elastic collisions between gas molecules in the pores and consequently reduction in the gas pressure. Thermal conductivity of helium is higher than nitrogen which yields an increase in the bulk thermal conductivity of the material. However, thermal conductivity of both gases decreases if we consider these gases in small pores and this decrease is much sharper in the case of helium gas [96]. Therefore, due to Knudsen effect in small pores, we get lower values of thermal conductivity for gas saturated sandstone as compared to its liquid saturation states. Low thermal conductivity values due to Knudsen effect are discussed in detail in section 7.3.

Effect Due to Contact Resistance: Thermal conductivity is strongly dependent on the contact resistance between the filled liquid/gas in the pores and the grain bound-

ary. In case of liquids, thermal contact is much better as compared to the case of gases. This is because of the fact that, liquid molecules can stick to walls of the pores that provides less resistance to the conduction of heat. On the other hand, this is not the case for gases.

Effect Due to Thermal Path: When we saturate a dry porous stone with a liquid, it absorbs liquid through capillary suction. As discussed above, absorption of liquid improves thermal contact between the pores and grain boundaries. Absorbed liquid molecules not only fill the vacant pore spaces but also swells the internal surface of the pore by residing in between tiny fragments of the binding minerals. As a cumulative result, swelling of many small pores enhances thermal path for conduction. On the other hand, gas particles can only collide with the fragments but cannot be absorbed. This may be the second reason of increased thermal conductivity in case of liquids as compared to gases.

Effect Due to Density of Fluid: Density of the saturating fluid may also be an important factor in increasing or decreasing the overall thermal conductivity of the stone. The denser is the pore filling material, the better is the overall thermal conduction (for the same filling material). By exploring figure 7.6, one finds that despite increasing thermal conductivity of gases to higher values, their density decreases which is an evidence of producing bad thermal path between the filled gas and pore boundary. This may be a reason for increasing the deviation between the two curves more and more along the x-axis.

Effect Due to Fluid Saturation: When we put a dry porous stone into a liquid, liquid is absorbed by the stone through strong capillary forces. This process is fast and can saturate the whole stone within few hours depending on its dimensions. On the other hand, gases may be filled in a porous stone after putting the stone into a high vacuum atmosphere and then filling the gas. During this study a maximum vacuum of 0.03 millibar is achieved which may not be sufficient to evacuate all the air particles from internal pores, especially blocked pores and thus only surfaces of the stone are properly filled with gas while air particles still reside in the internal pores. Due to partial-filling of gases we get lower values of thermal conductivity in case of gases as compared to liquids.

The above mentioned five proposed reasons are based only on the experimental results carried out on Sander sandstone. However, in few further experiments on

Borosilicate glass sieve samples, a reverse effect[9] has also been seen. Experimental results on Borosilicate glass sieve show that, thermal conductivity of the sieves depends strongly on the pore sizes. To reveal the hidden facts behind these effects, further experimentation is needed. There is no concrete theoretical evidences that can explain the actual reasons for the decrease/increase in overall thermal conductivity of sandstone/glass sieves filled with gases in comparison to liquids.

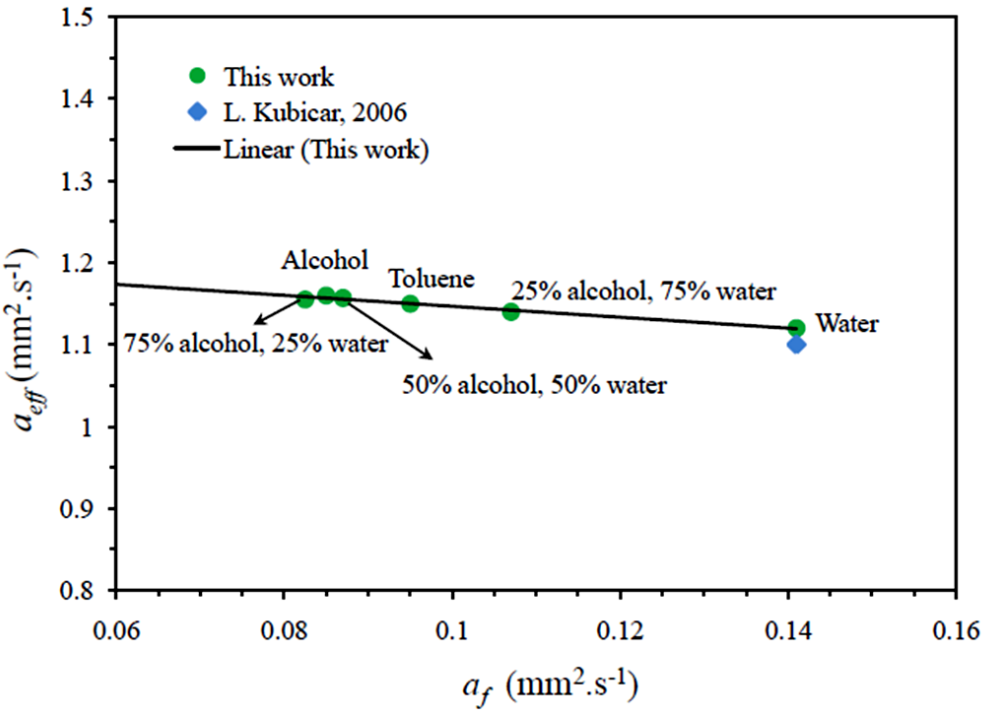

Figure 7.7: Thermal diffusivity of Sander sandstone as a function of thermal diffusivity of saturating fluids at room temperature (25 °C) and room pressure.

Figure 7.7 shows thermal diffusivity of Sander sandstone as a function of thermal diffusivity of the saturating fluids at ambient temperature and pressure. The values of the thermal diffusivity of Sander sandstone lie in between 1.11 to 1.17 mm^2.s^{-1} for all saturation cases and exhibit surprisingly a minute inverse effect with fluid-saturation. The data has been fitted with a linear trend line that makes an intercept with the y-axis at a thermal diffusivity value of 1.21 mm^2.s^{-1}. As mentioned before, thermal conductivity and thermal diffusivity data on Sander sandstone are obtained directly from the experiment while specific heat capacity can be calculated using interrelated formula $c_p = \lambda/a\rho$ with having an additional knowledge of the density of the stone.

Experimental values on specific heat capacity reveals that, the specific heat ca-

[9]Experiments show that thermal conductivity of Borosilicate glass sieves for a particular pore size is higher when filled with gases as compared to liquids at the same thermal conductivity of the filling fluid.

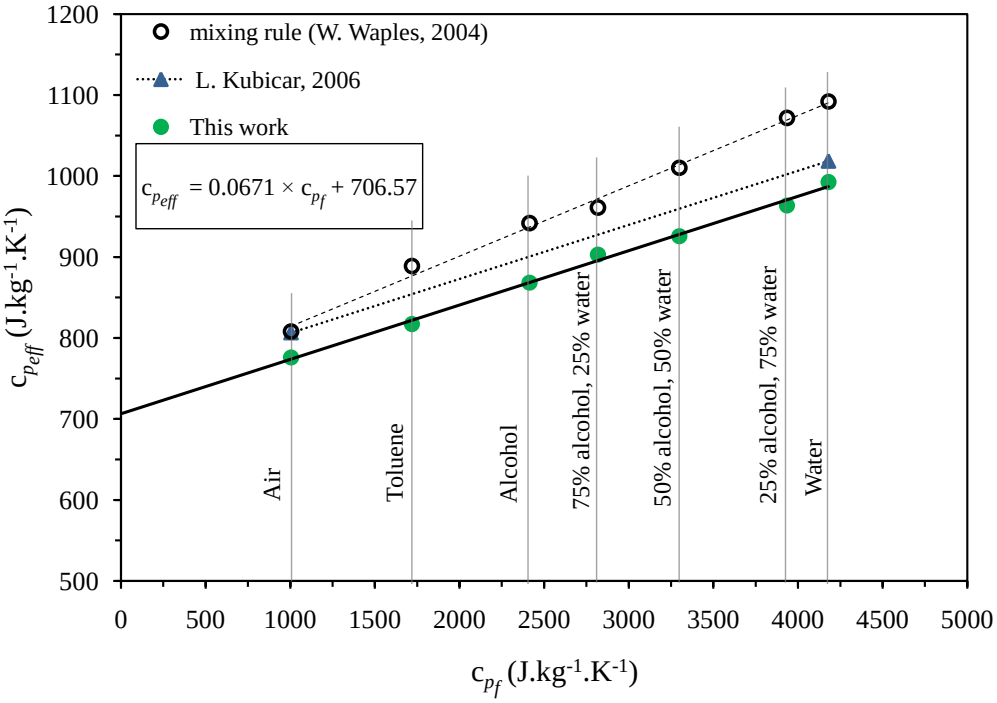

Figure 7.8: Specific heat capacity of Sander sandstone as a function of specific heat capacity of saturating fluids at ambient conditions.

pacity ($c_{p_{eff}}$, J.kg^{-1}.K^{-1}) of Sander sandstone increases linearly by increasing the specific heat capacity of pore filling fluids (c_{p_f}, J.kg^{-1}.K^{-1}) as shown in figure 7.8. By extrapolating the fitted line backwards to y-axis, we get a specific heat capacity value of 707 J.kg^{-1}.K^{-1}. This value of heat capacity is very close (with a difference of ≈ 9 %) to the heat capacity value obtained by mineral summation method[10].

In other words, if no fluid is filled in sandstone pores then the net specific heat capacity will be the sum of the volume fractional heat capacities of all constituents. Heat capacity of real rock/stones (that is, a mixture of solids and liquids) can also be calculated from the weighted average of the heat capacities of rock constituents [57; 58; 59]. Experimental data on specific heat capacity are compared with the heat capacity mixing law (equation 7.1) [18] and with the already published data [43] and are fitted linearly.

$$c_{p_{eff}} = \frac{\rho_{matrix} \times (c_{p_{matrix}}) \times (1-\phi) + \rho_{fluid} \times (c_{p_{fluid}}) \times (\phi)}{\rho_b} \tag{7.1}$$

Where ϕ is the fractional porosity, ρ_b is the density of the bulk material (sandstone), ρ_{matrix} and $c_{p_{matrix}}$ are the density and specific heat capacity of the solid

[10]Sum of the volume fraction heat capacities of each mineral component in the rock is calculated to be 768 J.kg^{-1}.K^{-1}.

matrix[11], ρ_{fluid} and $c_{p_{fluid}}$ are the density and specific heat capacity of the pore filling fluid respectively. Raw data used to calculate bulk heat capacity of the stone is given in table 7.1 and table 7.2.

7.3 Effect of Pressure and Pore Size on Thermal Conductivity

Vacuum can be used to lower the thermal conductivity of gases. Theoretically, gas thermal conductivity can approach to 0 $W.m^{-1}.K^{-1}$ in a perfect vacuum [92], although a perfect vacuum is purely theoretical. Thermal conductivity of a gas is not only a function of pressure but also depends on the size of pores and their distribution [93]. The smaller is the pore sizes in a material the lower is the thermal conductivity of the material even at atmospheric pressure if the pore size reaches a certain lower value [92]. When the pores of a porous material are filled with a gas, the gas (non-convective gas) conductivity remains unaffected until the mean free path of the gas molecules is less or equal to the size (diameter) of the biggest pore in the material. On reducing pressure, the mean free path of the gas molecules increases from the size of the pores and the gas molecules collide only with the surface of the pores and therefore, there is no energy transfer due to elastic collisions between the molecules. Thermal conduction of a gas in a porous material can be written as [94; 95]:

$$\lambda_g = \frac{\lambda_{g,0}}{1 + 2\beta K_n} \tag{7.2}$$

where,

$$K_n = \frac{l_{mean}}{\delta} \tag{7.3}$$

and

$$l_{mean} = \frac{K_B T}{\sqrt{2}\pi d_g^2 P_g} \tag{7.4}$$

Where K_n is called Knudsen number and it is a ratio between mean free path (l_{mean}) of the gas molecules to the size of the pores (δ), $\lambda_{g,0}$ is the thermal conductivity of the gas at ambient conditions, d_g is the diameter of the gas molecules, P_g is the gas pressure and β is a characteristic constant which shows the efficiency of energy transfer when gas molecules hit the solid structure of the material. It has values in between 1.5 and 2.0 and depends on the gas type, the temperature and the

[11] Solid matrix means the material which excludes the pore spaces. Therefore, ρ_{matrix} and $c_{p_{matrix}}$ are the density and specific heat capacity of the total sum of sandstone forming minerals.

Pore filling fluid	λ_f ($W.m^{-1}.K^{-1}$) [60; 61]	a_f ($mm^2.s^{-1}$) [60; 62]	c_{p_f} ($J.kg^{-1}.K^{-1}$) [60; 63]	λ_{eff} ($W.m^{-1}.K^{-1}$) (This work)	a_{eff} ($mm^2.s^{-1}$) (This work)	$c_{p_{eff}}$ ($J.kg^{-1}.K^{-1}$) (This work)	$c_{p_{eff}}$ ($J.kg^{-1}.K^{-1}$) (equation.1)	ρ_b ($kg.m^{-3}$) (This work)
Air	0.026	18.50	1005	1.67	1.010	776	808	2132
Toluene	0.135	0.095	1719	2.12	1.150	817	889	2256
Alcohol	0.175	0.085	2414	2.23	1.160	868	942	2213
75 % alcohol, 25 % water	0.227	0.082	2818	2.36	1.156	903	961	2263
50 % alcohol, 50 % water	0.311	0.087	3299	2.43	1.157	926	1010	2269
25 % alcohol, 75 % water	0.434	0.107	3935	2.50	1.140	964	1072	2276
Water	0.598	0.141	4180	2.56	1.120	992	1092	2303

Table 7.1: Thermal properties of different saturating liquids (except air) and their effect on overall thermophysical properties of sandstone at ambient conditions.

Gas	λ_f	λ_{eff}
Freon 12	0.010	1.50
Argon	0.018	1.51
Nitrogen	0.026	1.59
50 % N2, 50 % He	0.058	1.70
20 % N2, 80 % He	0.100	1.75
Helium	0.150	1.82
Hydrogen	0.185	1.89

Table 7.2: Thermal conductivity of gases and corresponding effective thermal conductivity of sandstone.

solid material. In highly porous materials (e.g insulation materials), the contribution of gas conductivity plays an important role in lowering the effective thermal conductivity. Free gas conduction ($\lambda_{g,0}$) is strongly reduced due to Knudsen effect if we consider the narrow pore size (nano-porous) material. Knudsen effect in small pores eliminates exchange of energy between gas molecules thus convective heat transfer is vanished and therefore overall thermal conductivity is reduced. Thermal conductivity of Sander sandstone as a function of gas pressure is shown in figure 7.9. This data is obtained after evacuating the chamber along with the sample halves up to 50 μbar and then performing measurements by slightly increasing the air pressure up to atmospheric pressure. Temperature is kept constant at 23 °C during the whole series of measurements. However, a slight change in temperature is observed due to changing pressure, which can be ignored.

Experiments are performed in two different ways, (1) filling the evacuated chamber with 45 % RH moist air and, (2) with dry Nitrogen gas. It is assumed that there is no chemical reaction inside the porous rock within the measured temperature and pressure range. Results show that, the thermal conductivity values are higher in case of moist air filling; furthermore, the difference in both curves increases as pressure increases and we end-up with a difference of 4 % at atmospheric pressure.

From equation 7.4, it is clear that if we decrease pressure, concentration of the gas molecules also decreases but at the same time mean free path of the gas molecules increases and we get no net change in thermal conductivity of gas. If we continue decreasing pressure, molecular mean free path increases and approaches the size of the enclosure (in sandstone it is equal to pore diameter). Then a stage comes when there is no effect on mean free path by further decreasing the pressure. Nevertheless, we still have a decrease in concentration of the gas molecules which results in overall

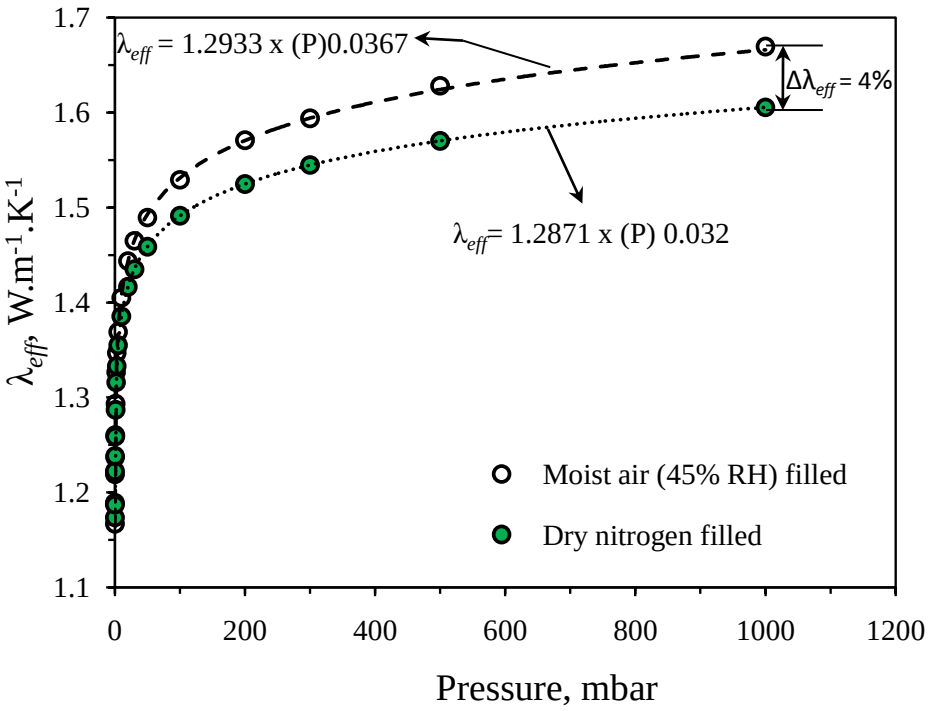

Figure 7.9: Thermal conductivity of Sander sandstone as a function of interstitial Nitrogen and moist air (45 % RH) pressure.

decrease in the thermal conductivity.

Not only the pressure but also the nano-scale small pores in sandstone contribute in lowering the overall thermal conductivity. Even at atmospheric pressure, gas (air) molecules which resides in the pores having diameters less than the normal mean free path[12] of air molecules are responsible for reduction in overall thermal conductivity. However, in investigated sandstone such small pores constitute a very small portion (see table 5.3).

7.4 Effect of Relative Humidity on Thermal Properties of Sander Sandstone

Old and historical buildings are mostly constructed with long-lasting stones. In Germany, there are thousands of historical buildings made from such stones (mostly used is sandstone) representing a well-built cultural and historical heritage of the country. Unfortunately, after the Second World War, most of these historical and monumental buildings were destroyed due to heavy bombardment and after that considerable financial funds were spent to restore these buildings (like castles, churches, monuments etc). For restoration, sandstone is extensively used because of its durability and its

[12]The mean free path of air molecules at standard temperature and pressure is 70 nm [94].

better mechanical properties. On one hand, this stone is very durable and long lasting but on the other hand; it may be appalling for thermal insulation purposes because of its moisture absorbing ability from the surroundings. Thermal conductivity of sandstone may increase or decrease depending on the relative humidity of the moist air. Relative humidity of air may change from time to time depending on the weather temperature and pressure, and may increase upto 90 % in summers. Therefore, to understand hygroscopic thermal performance of this stone, it is necessary to have knowledge on the thermal conductivity data depending on moisture content in the air. Mechanism of heat transfer through a porous materials is very complex. A sketch

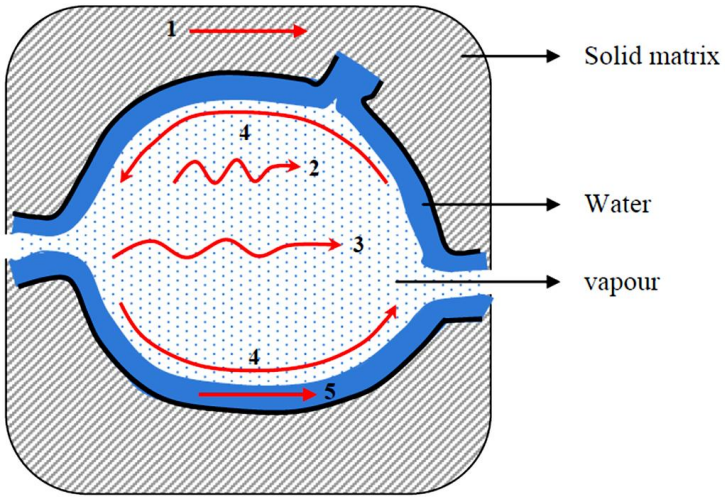

Figure 7.10: Heat transfer mechanism in the pores of a moist porous material.

diagram of the possible heat transfer paths through a moist porous structure is shown in figure 7.10. Heat flow through such porous stuffs may be caused by the following most important mechanisms [64].

1. Conduction of heat through solid body
2. Conduction of heat through saturated fluid (water vapors or gas) inside the pores
3. Radiation through the pore space
4. Convection currents within the pore space
5. Conduction through the bounded water to the pore walls

In this work, heat flow mechanism via radiation (process 3) and convection (process 4) are neglected due to before mentioned reasons.

In this section, measurement of the thermal conductivity of Sander sandstone at different humidity conditions (10 to 90 %) is presented. Before starting measurements

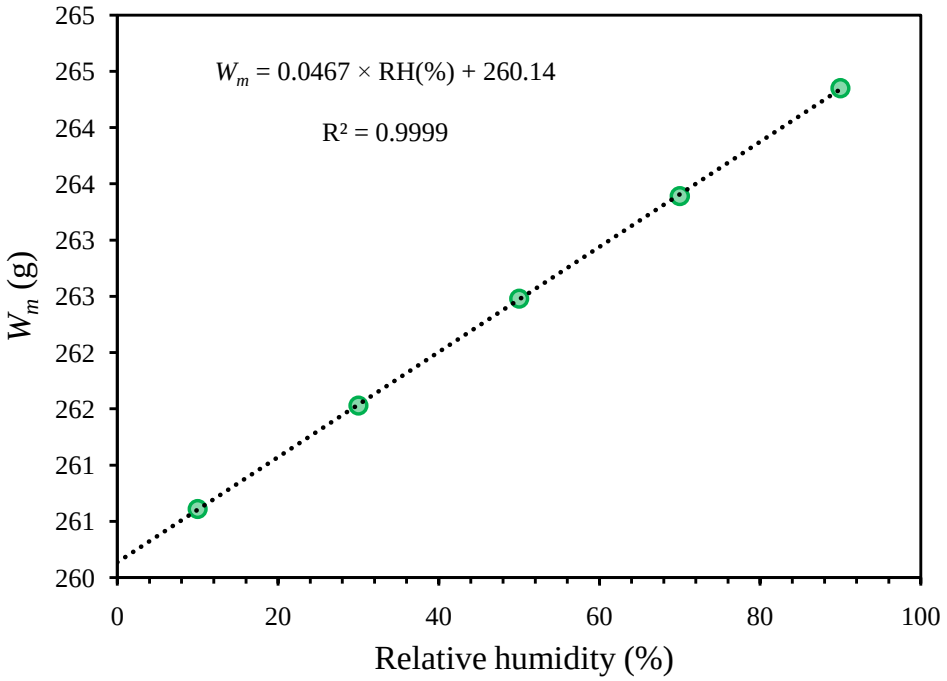

Figure 7.11: Linearly increasing weight of the sample with increasing relative humidity.

at different humidity conditions, sample was completely dried in an oven according to ASTM standards (ASTM D 2216-05) [65]. Calculated weight of the dry sample is $W_d = 260.14$ g. After that, sample is put in a humidity and temperature-controlled chamber (CTS-C70). Temperature during all measurements is kept constant at 25 °C. Weight of the sample is noted after constant intervals of time and a run for thermal conductivity is done when the weight seems to be stabilized. For each thermal conductivity value, five runs are performed and an average value is taken. Increase in the weight of the dry sample at different humidity conditions is given in table 7.3 and is plotted in figure 7.11.

RH (%)	W_m (g)	ΔW (g)	ΔW (%)	Saturated water content (kg.m^{-3})
Dry	260.14	0.00	0.000	0.00
10	260.61	0.47	0.181	3.92
30	261.53	1.39	0.534	11.6
50	262.48	2.34	0.900	19.5
70	263.39	3.25	1.249	27.1
90	264.35	4.21	1.618	35.1

Table 7.3: Change in weight of the sandstone with moisture content.

Where, W_m is the weight of the moist sample, ΔW is the difference in dry and moist weight. Surface of the sample in contact with water vapor molecules have the tendency to adsorb water molecules because of the polar molecular nature of water. As the sample is exposed to moist air for a long time, water vapor molecules continuously adsorb to the surface and increase the water content significantly. As the relative humidity increases, the moisture content of porous sandstone also increases because more water vapors adhere to the surfaces. As the relative humidity exceeds 80 % to 90 %, tiny liquid water droplets begin to form in the smallest pores and finally in the larger pores. Now, further moisture is stored in the pores due to capillary suction process (absorption). In this work, the tested sandstone is exposed to moist air (relative humidity range of 10 % to 90 %) for duration of one week for each humidity value. Figure 7.12 shows that the ETC of Sander sandstone increases as

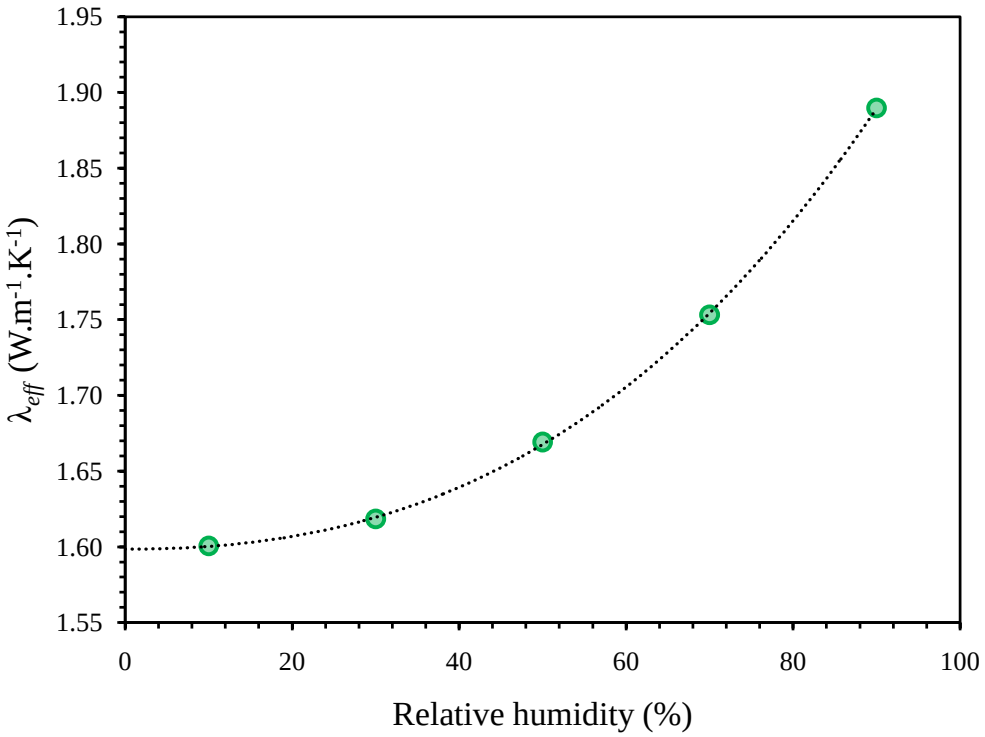

Figure 7.12: Effective thermal conductivity of Sander sandstone as a function of relative humidity of air.

the humidity value in the air increases. The trend of increasing ETC is non-linear and steeper at higher humidity values. At about 90 % RH, we obtain the value of thermal conductivity of 1.89 $W.m^{-1}.K^{-1}$, whereas; fully water-saturated sandstone has a thermal conductivity value of 2.56 $W.m^{-1}.K^{-1}$. There is a difference of about 26 % between 90 % (RH) humidified and fully water-saturated sandstone values. This difference is obviously because of two different saturation conditions and correspondingly two different heat transfer mechanisms inside the porous structure.

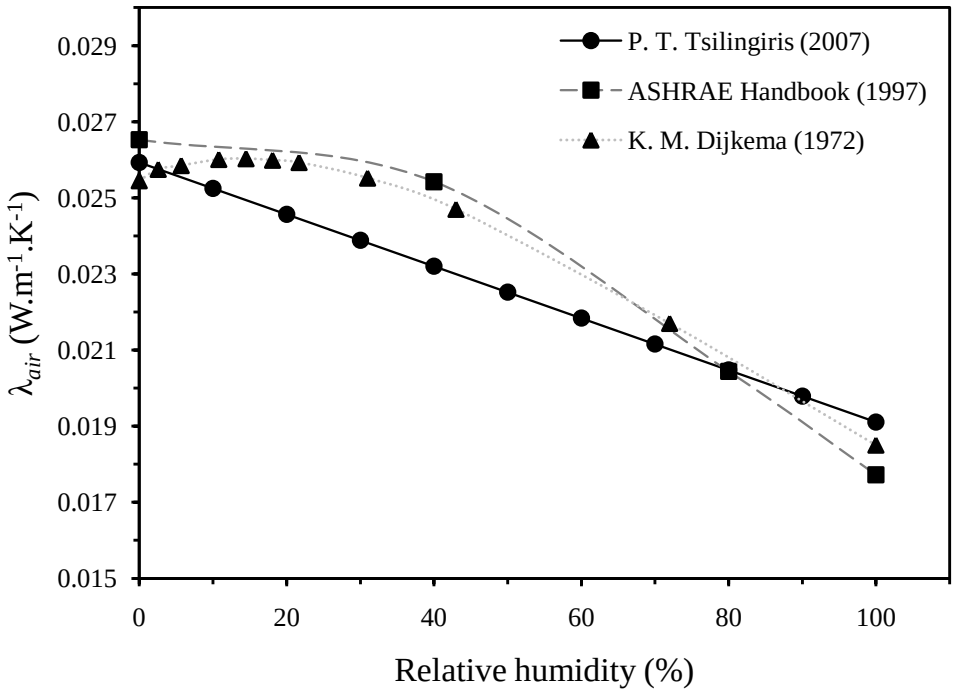

Figure 7.13: Reference data showing decrease in thermal conductivity of moist air with increasing moisture content in air.

After having a literature surveying [66; 67; 68; 69; 70], it is seen that thermal conductivity values of the air (dry) decreases as the relative humidity in air increases. Figure 7.13 shows three important reference data on the thermal conductivity of moist air at 25 °C. In figure 7.14, thermal conductivity of Sander sandstone is plotted against the thermal conductivity of moist air. With increasing humidity, thermal conductivity of the stone also increases but the thermal conductivity of the moisture itself decreases. Table 7.4 gives the experimentally determined thermal conductivity values of sandstone at different humidity values and the reference data on the thermal conductivity of the moisture itself. This effect is due to the fact which is discussed in the above paragraph. Moist air is less dense than dry air (http://www.theweatherprediction.com/habyhints/260/). Water vapor (H_2O) is a relatively light gas as compared to the diatomic Oxygen (O_2) or diatomic Nitrogen (N_2). As water vapor increases, the amount of O_2 and N_2 decreases per unit volume and ultimately density decreases because mass decreases. This decrease in density may be one cause of the decrease in the thermal conductivity of the vapor.

The obtained experimental data is also important from computational point of view because, it can be used as input parameter in simulations for the estimation of possible damage in buildings due to moisture. In addition, hygroscopic and thermal performance of historical buildings can also be predicted.

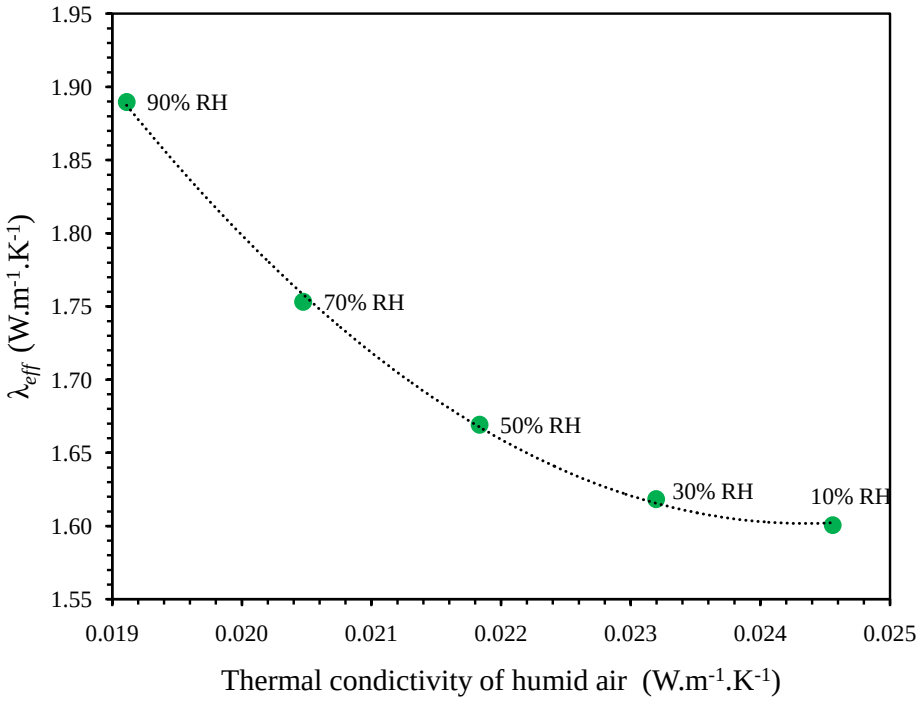

Figure 7.14: Effective thermal conductivity of Sander sandstone as a function of thermal conductivity of moist air at different moisture conditions at room temperature (25 °C) and pressure.

RH (%)	λ_{air} (W.m^{-1}.K^{-1})	λ_{eff} (W.m^{-1}.K^{-1})
10	0.0252	1.601
30	0.0239	1.618
50	0.0225	1.669
70	0.0212	1.753
90	0.0198	1.890

Table 7.4: Dependence of the thermal conductivity of sandstone on the thermal conductivity of the relative humidity in air at room temperature and room pressure.

Chapter 8

Thermal Conductivity of Unconsolidated Sander Sandstone, Bricks and Cellular Concrete

In the above chapters we have discussed thermal properties of Sander sandstone in its consolidated (compact) form because of its extensive use in buildings. However, sandstone is also present in its unconsolidated (powder) form in the upper part of the earth crust. Most underground thermal energy storage (UTES) systems are accomplished in the upper part of the earth crust which is formed by a combination of unconsolidated and consolidated form of different rocks. For example, in Germany, groundwater is pumped for heating at an average temperature of 10 °C from aquifer and cooled down to typically 5 °C via heat pump [71]. According to L. Wolf et al. (2010), the concept of supplying heat energy to a single households with open loop systems is well established in Germany and there are currently more than 700 officially registered groundwater heat pumps only in the State of Baden-Württemberg (35 Mio.km^2). This concept of using energy from renewable energy sources is growing even more due to rising costs of energy. In order to complete such type of projects, there are a number of factors which has to be taken into account before their start. One of the most important factor is to find out the thermal properties of the ground. In this chapter, we will discuss thermophysical properties of three completely different materials having different pore structure from each other. The chosen material are, powder (unconsolidated) form of Sander sandstone, commonly used bricks and cellular concrete.

8.1 Thermophysical Properties of Unconsolidated (Powder) Sander Sandstone

At low underground depths, sandstone is found in the form of powder due to low overburden pressure of the strata. Many building applications like, the buried hot and cold water pipes, electrical wires, gas and oil pipe lines etc, are kept in the range of approximately 1 to 8 meters down the ground. It is important to know the thermal properties of the surrounding soil. Need on the information of thermal data increases when rainy water penetrates easily up to this depth and can destroy the thermal insulation of the pipes. This section is based on the thermal properties of the unconsolidated (powdered) form of Sander sandstone.

Figure 8.1: Different forms of sandstone powder, (a) dry powder, (b) water-saturated powder, (c) dried form (compact) after wetted-state.

8.1.1 Results on Thermophysical Properties of Powder Sander Sandstone

A consolidated Sander sandstone sample is taken and it is broken into small pieces. These pieces are grinded to form a powder as shown in figure 8.1(a). Experiments are carried out using three forms of pre-treated sandstone, namely: dried powder, water-saturated powder and dried form of water-saturated state. Experimental results of powdered sandstone show that the presence of water has a strong influence on the thermal properties. Thermal conductivity value of a water-saturated powder increases 7 times more as compared to its dry state values as shown in figure 8.2. However, there is very small effect of compactness on the overall thermal conductivity values. Thermal diffusivity of the powdered sample also increases with water saturation as it can be seen from figure 8.3. It means that, the insulation of underground buried pipes is affected badly if the pipe is surrounded by wetted soil and heat loses may be up to 7 times higher as compared to its dry states.

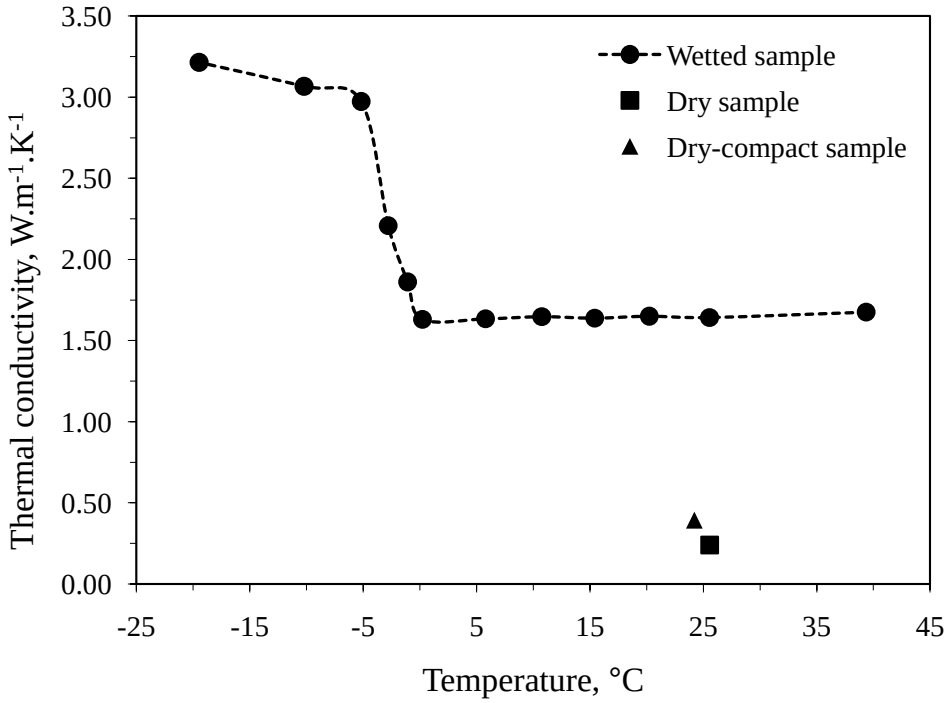

Figure 8.2: Thermal conductivity of powder Sander sandstone in three different states.

8.2 Thermophysical Properties of Bricks

Bricks are commonly used in our building constructions therefore, the knowledge of accurate heat transfer (thermal conductivity) in dry as well as in water-saturated state of bricks is of much importance in such buildings. In the following section, thermal conductivity of dry and water-saturated bricks in the temperature range of -20 °C to +25 °C using the transient hot-bridge method are presented.

8.2.1 Experimental Setup

The experimental setup used to measure the thermal conductivity of bricks is shown in figure 8.4 [72].

8.2.2 Effect of Water-saturation on Thermal Conductivity of Bricks

Water-saturated brick samples are obtained by immersing the dry samples in a distilled water-filled vessel for 24 hours. Their masses after full water-saturation are 109.06 g and 111.47 g, showing an increase of 20.1 % and 22.7 % respectively as compared to their dry weight. Figure 8.5 and figure 8.6 show sensor output-signals for dry and water-saturated brick samples as measured against normal and logarithmic time

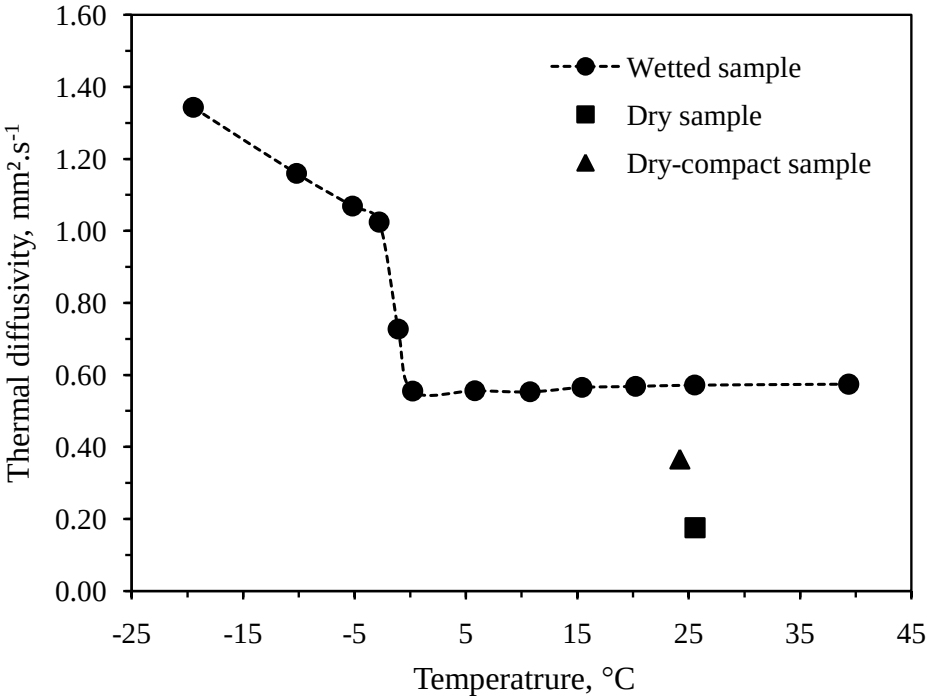

Figure 8.3: Thermal diffusivity of powder Sander sandstone in three different states.

scales respectively. Please note, that for the water-saturated samples, the output curves lie closer to each other than for the dry samples. However, their uncertainty is higher. The mean value of thermal conductivity for water-saturated brick is $\lambda = 1.010 \pm 0.008$ W.m^{-1}.K^{-1}.

8.2.3 Analysis of Temperature Dependent Thermal Conductivity

Thermal conductivity measurements conducted on dry and water-saturated samples as a function of temperature are shown in figure 8.7. We can see that, the thermal conductivity of the dry brick is 0.523 W.m^{-1}.K^{-1} at 26 °C. There is a slight decline with decreasing temperature down to 0.503 W.m^{-1}.K^{-1} at -14 °C. The thermal conductivity of brick remarkably increases from 0.523 W.m^{-1}.K^{-1} to 1.01 W.m^{-1}.K^{-1} at 26 °C after the uptake of water. The temperature dependent decrease is greater than for the dry brick. The thermal conductivity attains 0.923 W.m^{-1}.K^{-1} at -7 °C. Within the temperature interval between -7 °C and -10 °C, the thermal conductivity abruptly changes from 0.923 ± 0.0002 W.m^{-1}.K^{-1} to 1.160 ± 0.003 W.m^{-1}.K^{-1}. This 'jump' is certainly due to a phase transition (freezing/thawing) of water [72]. For temperatures below -10 °C, the thermal conductivity of the fully water-saturated brick rises to 1.298 ± 0.003 W.m^{-1}.K^{-1} at -20 °C. This effect is caused by the fact that the temperature dependent decrease in thermal conductivity of the bulk mate-

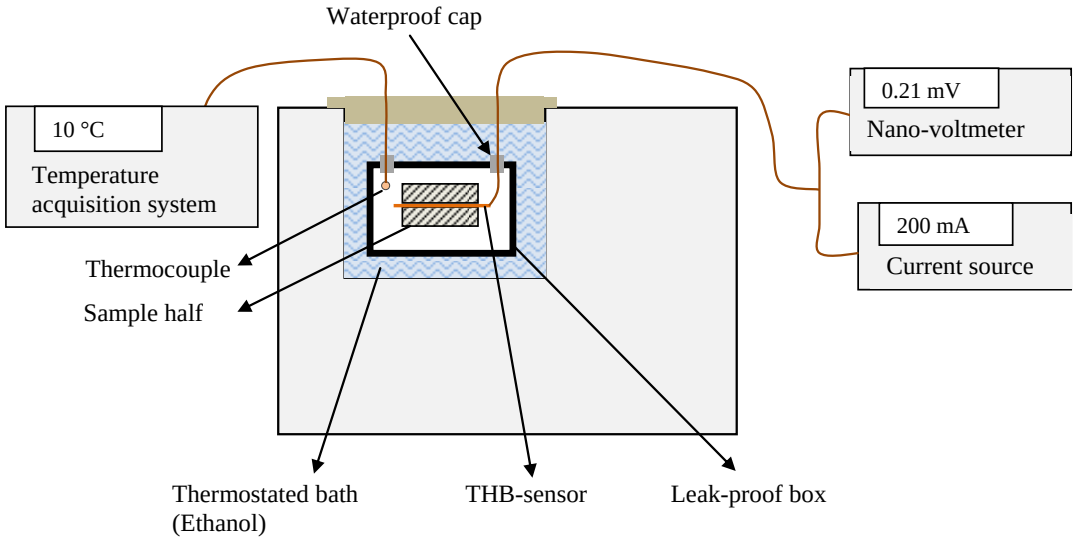

Figure 8.4: A sketch diagram of the used experimental setup.

rial is over-compensated by the increase in thermal conductivity of the ice inside the pores [73; 74].

8.3 Thermophysical Properties of Cellular Concrete

In before mentioned chapters, we have discussed thermal properties of such porous materials in which pores are connected to each other through capillary tubes of very small radius. In the following section, we will discuss the thermal properties of cellular concrete. Cellular concrete or foam concrete is a light-weight building material used in the construction of light-weight buildings for the purposes of high thermal insulation and fire protection. It can significantly reduce heating or cooling costs due to its low thermal conductivity. There are different types of cellular concrete depending on their density and porosity values. Investigated cellular concrete has very low density (306 kg.m^{-3}). It has very different pore structure as compared to the bricks or sandstone in the sense that its pores are closed and isolated from each other as shown in figure 8.8. For comparison reasons, it is very important to have thermal data of such type of materials. Few basic physical properties of the investigated cellular concrete are given in table 8.1. The investigated cellar concrete is 70 % porous, which is comparatively very high to the porosity of sandstone (porosity value of 20 %). It has low water absorption coefficient because of its closed pores. That is why its free saturation porosity is calculated to be 30 % which is much lower as compared to its actual porosity value. In this section, measurements are done on the

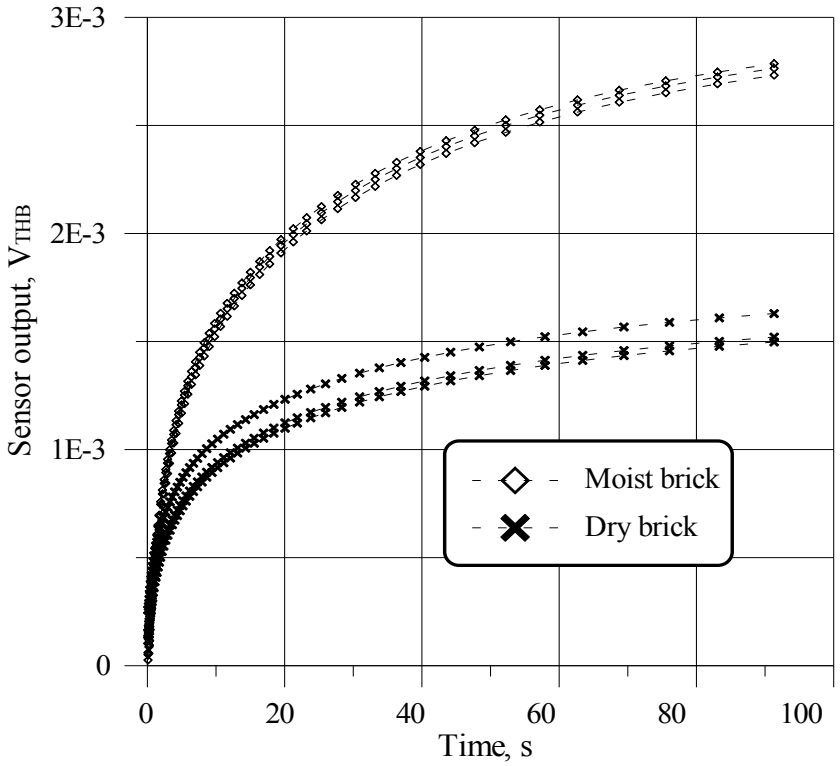

Figure 8.5: Sensor output signals for dry and water-saturated brick samples against real time scale.

thermal conductivity of dry as well as water-saturated foam concrete. It has very low thermal conductivity values (about 0.1 $W.m^{-1}.K^{-1}$) as compared to the normal concrete (about 1.7 $W.m^{-1}.K^{-1}$).

Dry weight (g)		Wet weight (g)		Density ($kg.m^{-3}$)		Porosity (%)
Sample half 1	Sample half 2	Sample half 1	Sample half 2	Dry	Wet	Free-saturation
245	238	483	478	306	600	30

Table 8.1: Density and porosity values of cellular concrete.

Results on thermal conductivity, thermal diffusivity and specific heat capacity of cellular concrete are given in figure 8.9, figure 8.10 and figure 8.11 respectively.

It is observed that for dry concrete sample the values of three thermal parameters remain almost unchanged during the whole temperature range of -20 to +40 °C. However, thermal conductivity and thermal diffusivity values of water-saturated cellular concrete increase sharply after the formation of ice in pores. Heat capacity values of water-saturated cellular concrete increases linearly with temperature as shown in figure 8.11.

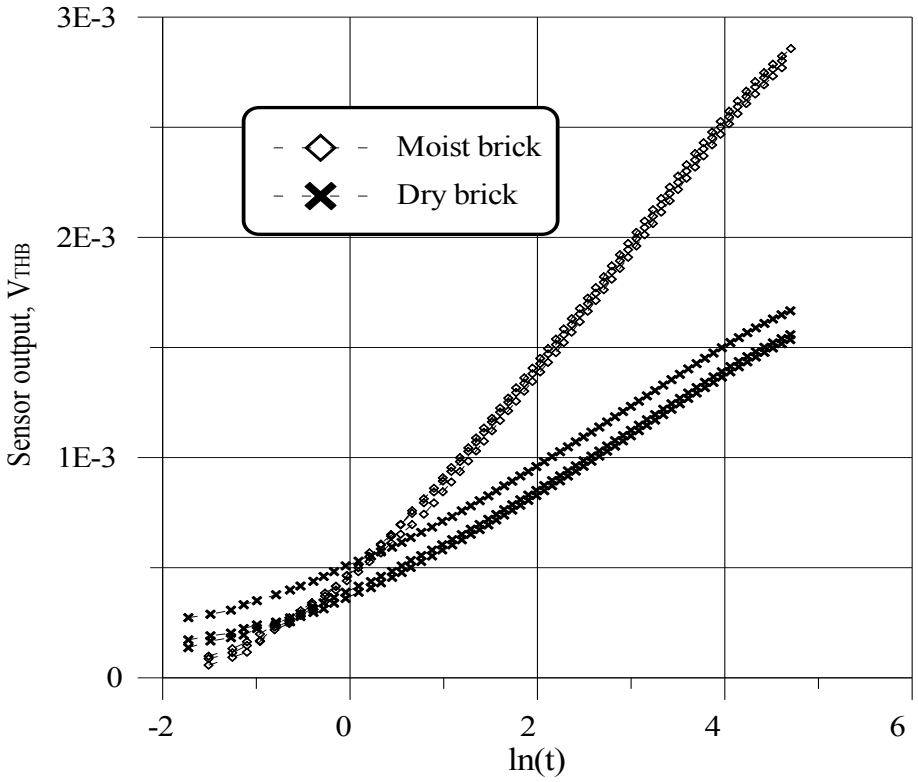

Figure 8.6: Sensor output signals for dry and water-saturated brick samples against logarithmic time scale.

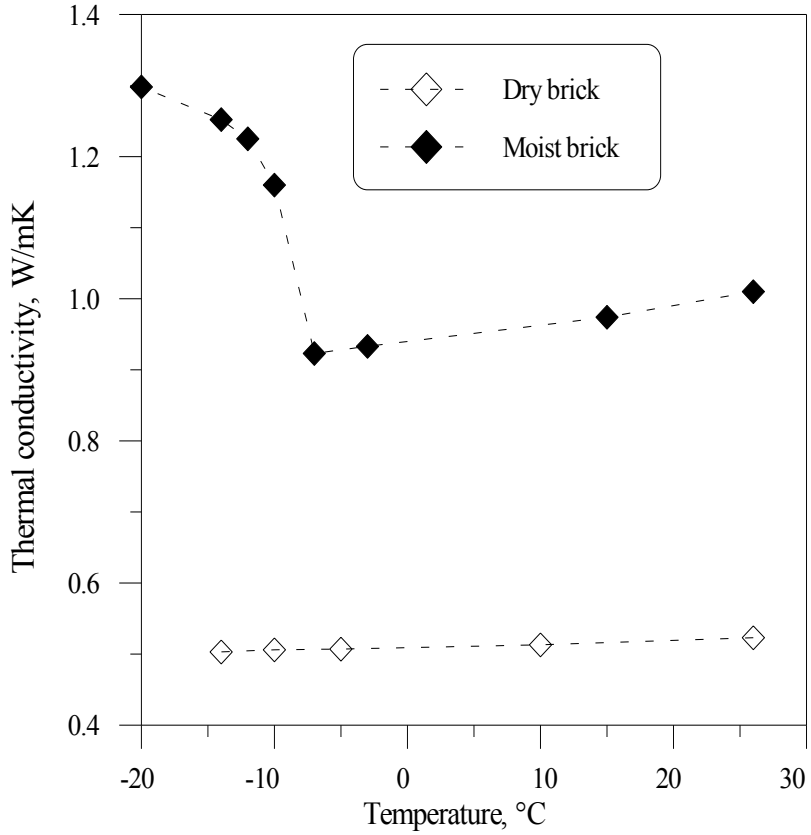

Figure 8.7: Measured thermal conductivity of dry and water-saturated bricks as function of temperature.

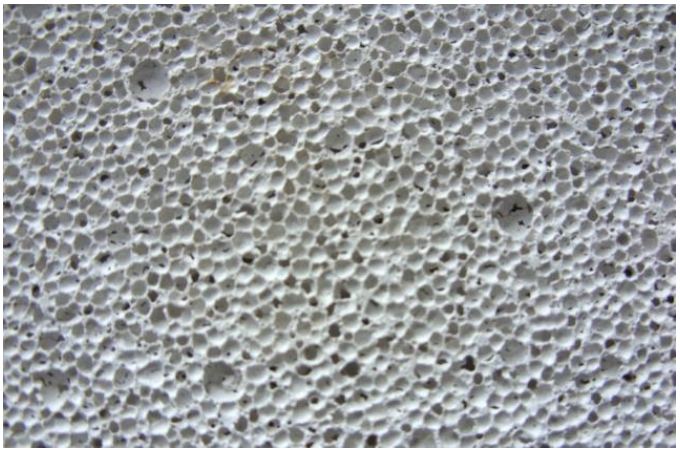

Figure 8.8: Surface image of cellular concrete sample.

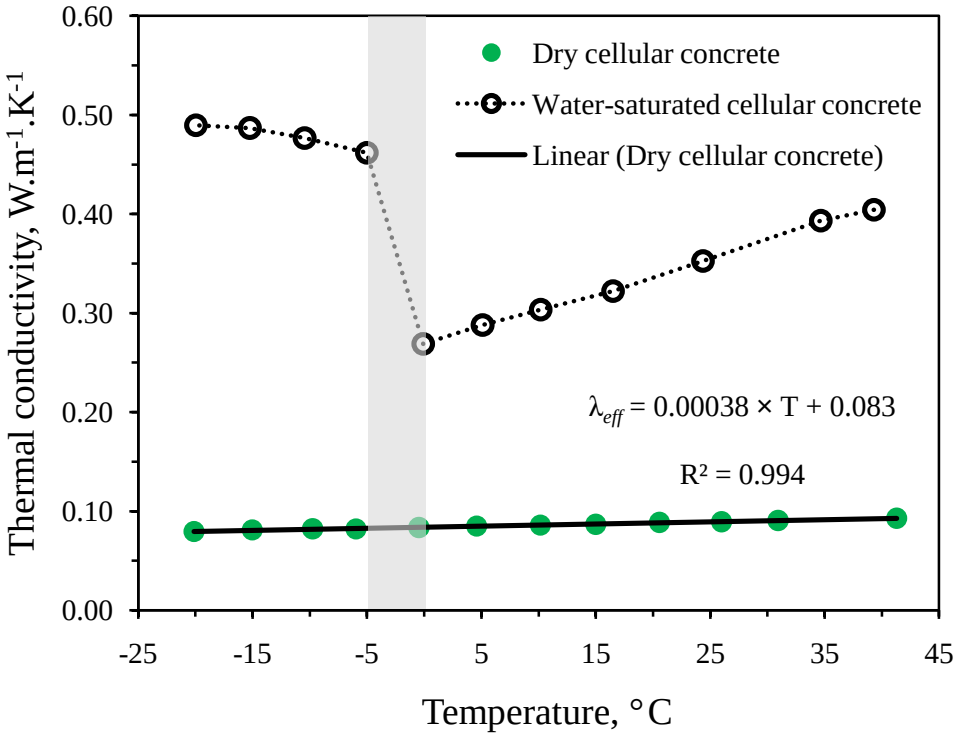

Figure 8.9: Thermal conductivity of dry and water-saturated cellular concrete as a function of temperature.

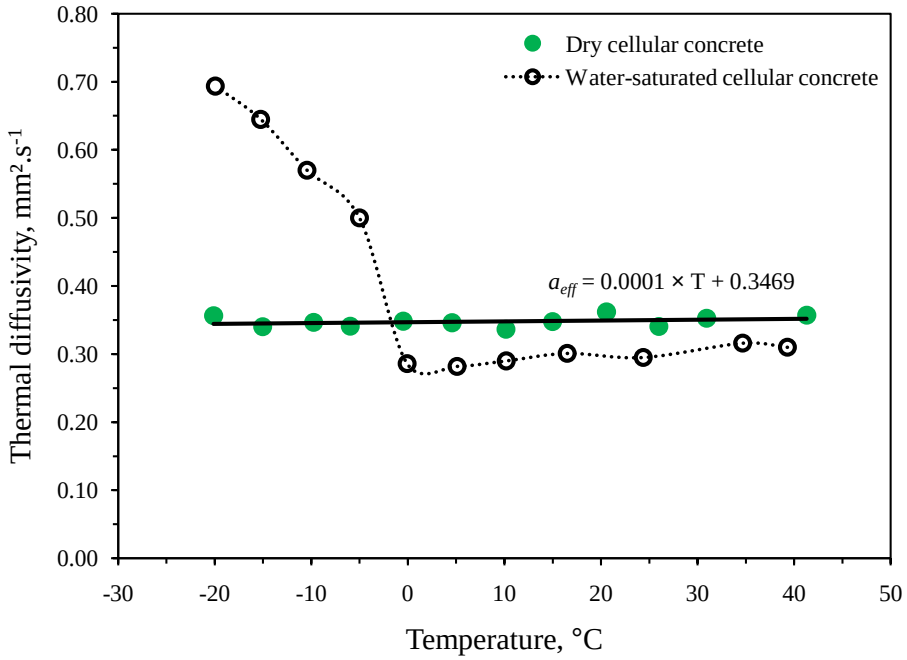

Figure 8.10: Thermal diffusivity of dry and water-saturated cellular concrete as a function of temperature.

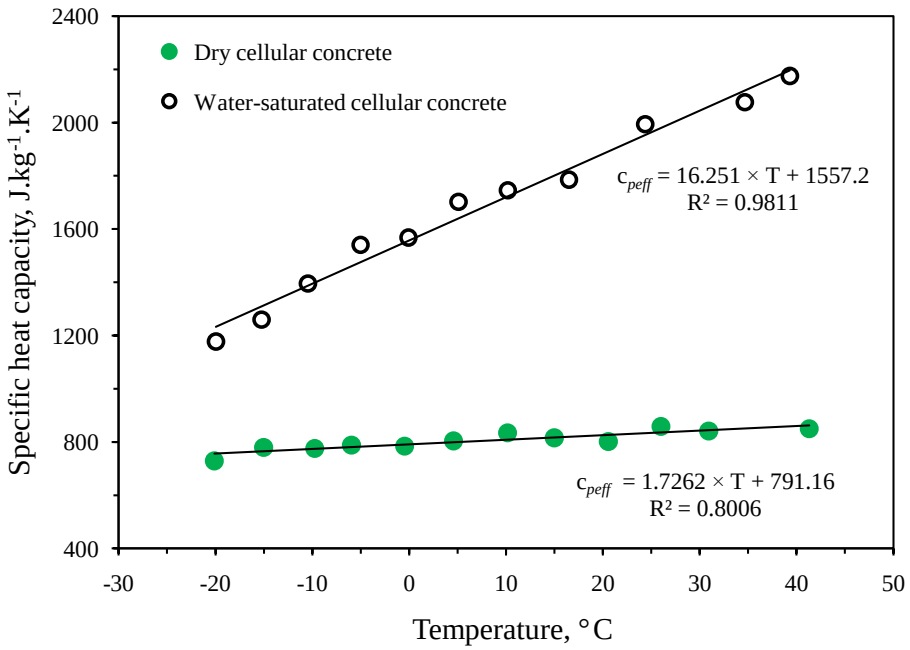

Figure 8.11: Specific heat capacity of dry and water-saturated cellular concrete as a function of temperature.

Chapter 9

Prediction of the Effective Thermal Conductivity of Porous Materials

Effective thermal conductivity of porous materials can also be predicted using mixing, empirical and theoretical models. Mixing law models depend solely on the component thermal conductivities and the volume fraction (porosity). These models (models without any adjustable parameters) do not take into account the structural characteristics of rocks/stones; however, these are very useful in predicting minimum and maximum values of the effective thermal conductivity for a given specific porous material. Second type of models is empirical. Empirical models are much better as compared to mixing laws because, these models take into consideration the geometrical parameters of porous materials. Unfortunately, these models are only applicable for a specific type of solids; therefore, we cannot consider these as general model for all types of porous structures. The third type of models are theoretical model that are based on the mechanism of heat transfer applicable to simplified geometries of solid/fluid systems. All of the above-mentioned three types of models are discussed in detail in this chapter. In the end, we will decide which model should be used for the prediction of the effective thermal conductivity of sandstone. Last but not least, an empirical model has been proposed to estimate the effective thermal conductivity of porous materials depending on simple geometrical parameters.

9.1 Mixing Law Models

Thermal conductivity of porous materials can be calculated indirectly from their mineral composition, pore filling fluids, porosity (ϕ) and density data. Numerous models

have been proposed [75; 76; 77] for estimation of the effective thermal conductivity. Some of these over-estimate while others under-estimate the true bulk thermal conductivity. Mixing law models combine values of thermal conductivities of rock matrix (solid part) (λ_s) with the thermal conductivity of the saturating fluid (λ_f) based on fractional porosity (ϕ)[16]. Few mixing law models are given in below subsections.

9.1.1 Parallel Model

For a two-phase porous structure containing low thermal conductivity porous phase and higher thermal conductivity solid phase, there are equal chances for their presence in series or in parallel to each other. In case of parallel model, direction of flow of heat is parallel to both phases as shown in figure 9.1. This model is also known as porosity-weighted arithmetic mean model.

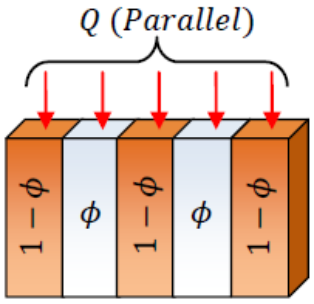

Figure 9.1: Parallel arrangement of components relative to the direction of heat flow.

According to this model, the effective thermal conductivity of a two phase sample can be predicted as,

$$\lambda_{eff}^{P} = \lambda_f \phi + (1 - \phi)\, \lambda_s \tag{9.1}$$

Equation 9.1 (parallel model) gives highest value of effective thermal conductivity of the rock/fluid system for all mixing law models.

9.1.2 Series Model

Series model is also known as porosity-weighted harmonic mean model. In this model, direction of heat flow is considered in series to the solid and fluid phase as shown in figure 9.2. This model gives lowest value of the effective thermal conductivity.

$$\lambda_{eff}^{S} = \left[\frac{\phi}{\lambda_f} + \frac{(1 - \phi)}{\lambda_s} \right]^{-1} \tag{9.2}$$

Equations 9.1 and 9.2 are also called Wiener's bounds [78]. These models are physically unrealistic, because a body consisting of alternating slabs of solid and

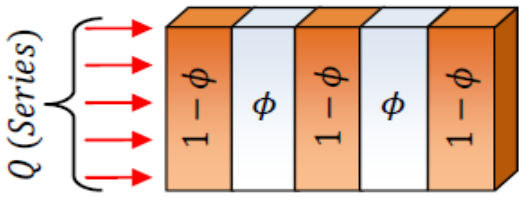

Figure 9.2: Series arrangement of components relative to the direction of heat flow.

fluid cannot sustain structural rigidity.

9.1.3 Geometric Mean Model

The geometric mean model is more realistic as compared to the above two models, because it assumes that there are grain-to-grain contact paths through the bulk solid rock. This model gives an intermediate value of the arithmetic and harmonic mean models [1].

$$\lambda_{eff}^{GMM} = \lambda_s \left(\frac{\lambda_f}{\lambda_s}\right)^{\phi} \tag{9.3}$$

9.1.4 Hashin-Shtrikman Bounds (H-S Bounds)

Weiner's bounds (series and parallel models) are too far from the real values of the effective thermal conductivity. There are also other bounds, called Hashin and Shtrikman bounds.

$$\lambda_{eff}^{HSU} = \lambda_s + \left[\frac{3\lambda_s(\lambda_f - \lambda_s)\phi}{3\lambda_s + (\lambda_f - \lambda_s)(1-\phi)}\right] \tag{9.4}$$

$$\lambda_{eff}^{HSL} = \lambda_f + \left[\frac{3\lambda_f(\lambda_s - \lambda_f)(1-\phi)}{3\lambda_f + (\lambda_s - \lambda_f)\phi}\right] \tag{9.5}$$

Equations 9.4 and 9.5 are called Hashin-Shtrikman upper and lower bounds respectively. H-S bounds are always tighter than Weiner's bounds and propose an upgrading in the prediction of the effective thermal conductivity of porous materials.

9.1.5 Maxwell-Eucken Models

Maxwell-Eucken upper and lower models provide us more tight limits resulting more close values to the true thermal conductivity [78]. Maxwell-Eucken models assume that the inclusions of the dispersed phase (fluid phase) do not encounter with similar neighboring inclusions as shown in figure 9.3. This means that the dispersed phase could never form continuous conduction pathways. In case, if thermal conductivity of the continuous phase (solid phase) is greater than dispersed phase (fluid phase) then

we get Maxwell-Eucken upper limit for the effective thermal conductivity, as given in equation 9.7. On the other hand, if thermal conductivity of the continuous phase (solid phase) is lower than the dispersed phase (fluid phase) then we get Maxwell-Eucken lower limit as given in equation 9.6 [79; 80]. Since the pore structure of most of the stones (especially Sander sandstone) consists of large and small pores interconnected through capillary tubes, therefore, Maxwell-Eucken upper and lower models do not provide us satisfactory results.

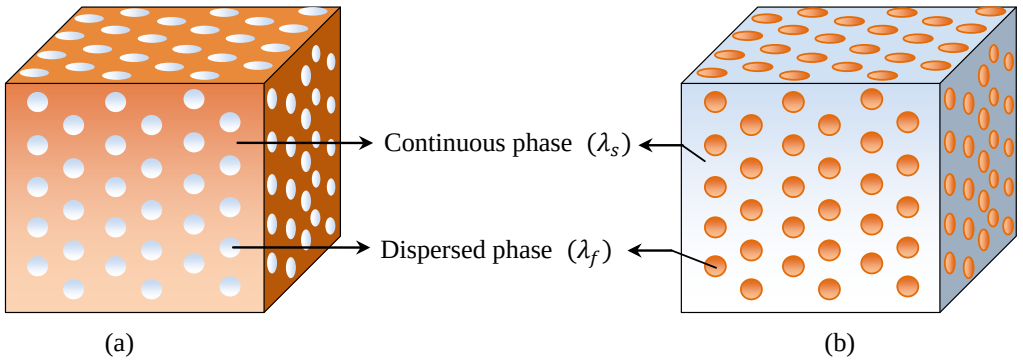

Figure 9.3: Dispersion of solid and liquid phases in Maxwell-Eucken model: (a) Maxwell-Eucken upper model, (b) Maxwell-Eucken lower model.

$$\lambda_{eff}^{MEL} = \lambda_f \left[\frac{2\lambda_f + \lambda_s - 2(\lambda_f - \lambda_s)(1-\phi)}{2\lambda_f + \lambda_s + (\lambda_f - \lambda_s)(1-\phi)} \right] \tag{9.6}$$

$$\lambda_{eff}^{MEU} = \lambda_s \left[\frac{2\lambda_s + \lambda_f - 2(\lambda_s - \lambda_f)(1-\phi)}{2\lambda_s + \lambda_f + (\lambda_s - \lambda_f)(1-\phi)} \right] \tag{9.7}$$

9.1.6 Landauer's Effective Medium Theory Model (EMT)

Effective medium theory is a statistical approach that is often used to model thermal conductivity of random mixtures of component materials, particularly when one component has higher thermal conductivity than the other component [81]. EMT is also applicable for the estimation of electrical resistances for a network of resistors [82]. Unlike, the Maxwell-Eucken structures, EMT do not have any continuous and dispersed phases as shown in figure 9.4. According to this theory, the effective thermal conductivity of a two-phase system can be estimated using equation 9.8 [83].

$$\lambda_{eff}^{EMT} = \frac{1}{4}\left[\lambda_f (3v_f - 1) + \lambda_s (3v_s - 1) + \sqrt{\{\lambda_f (3v_f - 1) + \lambda_s (3v_s - 1)\}^2 + 8\lambda_f \lambda_s} \right] \tag{9.8}$$

Where, v_f and v_s are the volumes contained by pores/fluid and solid matrix, respectively. EMT supposes a heterogeneous material in which the two material

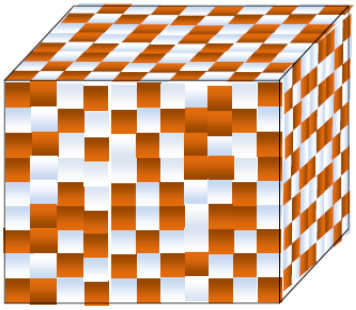

Figure 9.4: Randomly distributed phases in EMT model.

components (solid and fluid phases) are distributed randomly, with neither phase necessarily continuous or dispersed [76].

9.2 Empirical Models

Empirical models are developed by adding one or more adjustable parameters (coefficients or exponents) to the simple effective thermal conductivity measuring parameters. The values of these parameters can be determined by applying regression analysis to the laboratory data [84]. Few empirical models are briefly given below.

9.2.1 Asaad's Model

Asaad's model is very similar to the geometric mean model, the only difference is that Assad's model contain one additional coefficient "c" in the exponent. It can be represented as equation 9.9,

$$\lambda_{eff}^{A} = \lambda_s \left(\frac{\lambda_f}{\lambda_s}\right)^{c\phi} \tag{9.9}$$

Where, c is the empirical exponent. Asaad's model becomes identical to the geometric mean model by putting $c = 1$.

9.2.2 Pande and Chaudhary Model

For porous consolidated materials, Pande and Chaudhary (1984) propose an empirical model of the form as shown by equations 9.10 and 9.11.

$$\lambda_{eff}^{PC} = F(0.6132)\sqrt{\lambda_s \lambda_f}\left(1 - 1.545\zeta_f^{2/3}\right) \; for\; \zeta_f \; > \; 0 \tag{9.10}$$

$$\lambda_{eff}^{PC} = F(0.6132)\sqrt{\lambda_s \lambda_f}\left(1 + 3.844\zeta_s^{2/3}\right) \; for\; \zeta_s \; > \; 0 \tag{9.11}$$

Where ζ_f and ζ_s are geometrical parameters which depend on porosity and are equal to $\zeta_f = \phi$ - 0.5, $\zeta_s = 0.5$ - ϕ. F is an empirical coefficient determined in conformity with the material studied.

9.2.3 Sugawara and Yoshizawa's Model

Sugawara and Yoshizawa's model [87] is based on an adjustable parameter A and is given by equation 9.12,

$$\lambda_{eff}^{SY} = A\lambda_f + (1 - A)\lambda_s \tag{9.12}$$

Where,

$$A = [2^n(2^n - 1)^{-1}][1 - (1 + \phi)^{-n}] \; for \; n \; > \; 0 \tag{9.13}$$

and n is an empirical exponent depending on the porosity, shape, orientation and emissivity of the pores.

9.3 Theoretical Models

As mentioned before, empirical models are based on experimentally determined data and are useful when applied to a specific sort of rocks under investigation. Applying such models on different types of rocks may lead to significant errors. Therefore, models generally based on the elementary properties of rocks and basic heat transfer mechanisms are needed. Two theoretical models are briefly discussed in the next sections.

9.3.1 Gomaa Model

In 1973, Gomaa [85] developed a theoretical model for the thermal conductivity of uniform diameter spheres packed in a cube containing wetting and non-wetting fluids, based on the fundamental principles of heat transfer. This model assumes electrical resistance analogy to one-dimensional heat transfer through solid rock, wetting and non-wetting fluids. Geometry is kept fixed and contacts between two spheres are assumed flat as shown in figure 9.5. Distribution of fluid is dependent on the amount of saturation and dispersion of non-wetting fluid is supposed to be in the center of pore space.

If the fluid distribution is identified, resistances of the three regions (solid rock, solid rock and wetting fluid, non-wetting fluid) can be determined as resistors in series. Gomaa added a term of heat transfer coefficient between solid and two liquid phases. Heat transfer coefficient (h) is expressed in terms of dimensionless Biot number;

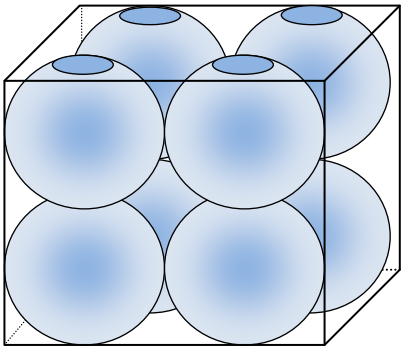

Figure 9.5: Cubic packing of spheres in Gomma model.

$B_i = 2R_p h/\lambda_s$. Where R_p is the radius of the sphere. This model is considered as a first step in the development of theoretical models [16].

9.3.2 Özbek Model

Özbek model [86] is a modified version of Gomaa model. In Gomaa's model, physical contacts between the spheres are considered flat only in vertical direction. Whereas, in the case of Özbek model both vertical and horizontal contacts are assumed to be flat. The unit cell is divided into five regions and contact resistances for the wetting fluid/solid contact (R_{ws}) and non-wetting fluid/solid contacts (R_{nws}) are included into the model. Özbek found that porosity is the most important parameter in his relation and after porosity thermal conductivity of the solid rock is important. In addition, conductivity of wetting phase is important while conductivity of non-wetting phase is less important. Özbek generated data for a large range of properties and applied multiple regression analysis to obtain the following expression 9.14 [16]:

$$\lambda_{eff}^{\ddot{O}} = 5.85e^{-3.3\phi} + 1.66\sqrt{S_w} + 19.4(0.01 \times \lambda_s)^{0.78} + 1.97e^{0.18\times\lambda_{wf}} + 1.60e^{0.86\times\lambda_{nwf}} - 5.14 \tag{9.14}$$

Where, S_w is the fractional wetting-phase saturation, λ_s is the thermal conductivity of solid rock, λ_{wf} is the thermal conductivity of wetting-phase and λ_{nwf} is the thermal conductivity of non-wetting phase. Thermal contact resistances are ignored due to their less influence.

9.4 Prediction of the Effective Thermal Conductivity as a Function of Temperature

There are a number of published data available correlating the effective thermal properties of rock (especially sandstone) with temperature. According to several authors [23; 52; 53; 54], dependence of the thermal conductivity on temperature may be divided into two parts. The first part correlates the thermal conductivity up to a temperature range of 1000 K, while second part becomes effective at temperatures higher than 1000 K when radiative heat transfer takes place. Dependence of thermal conductivity on temperature may be written as,

$$\lambda_T = \left(\frac{1}{A + BT}\right) + CT^3 \tag{9.15}$$

Where A (W^{-1}.m.K) and B (W^{-1}.m) are constants related to the scattering properties of phonons. According to Schatz and Simmons (1972) [88], constant A is related to the scattering of phonons by impurities and imperfections, while B is related to the phonon-phonon scattering. In this study on sandstone, experiments are done at temperatures lower than 1000 K, therefore only first term on R.H.S of equation 9.15 works. Thermal conductivity of most of the crystalline rocks decreases with increasing temperature. For high thermal conductivity rocks, this inverse relation ($\lambda \propto 1/T$) is faster as compared to the low thermal conductivity rocks. For example, in rocks containing high amount of quartz, thermal conductivity decreases more rapidly with temperature. In case of highly disordered or mixed crystalline rocks, thermal conductivity varies more slowly with reciprocal of temperature [89]. Effect of temperature on several sandstone samples were tested by Tikhomirov (1968) and a modified form of temperature dependent thermal conductivity relation is given by equation 9.16,

$$\lambda_T = \lambda_{20^\circ} - 10^{-3}(T - 293) \times (\lambda_{20^\circ} - 1.38) \times [\lambda_{20^\circ}(0.008T)^{-0.25\lambda_{20^\circ}} + 1.28](\lambda_{20^\circ})^{-0.64} \tag{9.16}$$

Where, λ_T is the thermal conductivity at measurement temperature T and λ_{20° is the known value of thermal conductivity at 20 °C of the same specimen. Tikhomirov's correlation was developed for dry rocks but it is seems to be equally applicable for liquid-saturated sandstones.

9.5 Effect of Radiation and Convection on Overall Heat Transfer

So far, we have restricted our discussion up to the conductive heat transfer mechanism. However, in porous rocks, heat may be subjected to radiation and conduction mechanisms depending on the temperature and pore size. According to Progelhof (1976) [90], heat transfer through radiation occurs at temperatures above 93.3 °C with a pore diameter of more than 1 mm. In this work, all experimentally analyzed samples (except cellular concrete samples, where pore diameter can be 1 mm) seldom have pore sizes greater than 1 mm and also the measurement temperature is kept lower than 93 °C. Therefore, we can ignore all the effects due to convection and radiation.

9.6 Comparison of the Experimental Results with Mixing Laws and Empirical Models

Experimental data on the effective thermal conductivity are compared with some of the important already existing mixing law and empirical models. Wiener's bounds (series and parallel models) provide us the minimum and maximum limits for thermal conductivity. Maxwell-Eucken's upper and lower models give us better results as compared to Weiner bounds [74]. Our results show that, data for multi-fluid-saturated porous structures is in good agreement with most of the models as far as the saturating fluid has thermal conductivity value lower than 2 $W.m^{-1}.K^{-1}$. The difference between the experimental values and the values calculated by mixing law models increases more and more as the thermal conductivity of the saturating fluid increases. Therefore, we can conclude that, already existing mixing law and empirical models are good for data comparison only for low thermal conductivity saturants in a porous structure. Comparison of the results is shown in figure 9.6.

9.7 Proposed Empirical Model

In this section, an empirical model [91] has been proposed which is based on simply series and parallel arrangements of the pores in a porous structure. Suppose, we have a porous structure containing pores as well as solid matrix. We suppose that the heat flow is in one direction and it has possibility to pass through three thermal paths, (1) — through the solid matrix, λ_1(mineral grains in case of sandstone), (2) — through the vacant space, λ_2 (pores) and (3) — in between both pore space and the solid

matrix (i.e., λ_1+λ_2). A sketch of the model is shown in figure 9.7.

According to this model, we suppose that heat flow is parallel to the direction of solid matrix and of the pore spaces. First term on right-hand-side of equation 9.17 shows the contribution in heat flow due to the solid grains of the material, second term shows the contribution due to the pore spaces and third term represents the part of heat flowing through both solid grains and pores.

$$\lambda_{eff} = \frac{S_1}{S}\lambda_1 + \frac{S_2}{S}\lambda_2 + \frac{S_3}{S}\left(\frac{\lambda_1\lambda_2}{\frac{d_1}{D}\lambda_2 + \frac{d_2}{D}\lambda_1}\right) \tag{9.17}$$

Where, S is the total surface area of the sample, S_1, S_2, S_3 are the surface areas contributed by the three path respectively, D is the total volume of the sample, d_1 and d_2 are the volume fractions occupied by the solid matrix (mineral grains) and the pore spaces (porosity), respectively. Equation 9.17 has two limiting cases,

Case I: If thermal conductivity of the pore filling fluid tends to zero, $\lambda_2 \to 0$ (i.e., there are no pore spaces) then equation 9.17 reduces to

$$lim_{\lambda_2 \to 0}\left\{\lambda_{eff} = \frac{S_1}{S}\lambda_1\right\} \tag{9.18}$$

Case II: If thermal conductivity of the pore filling fluid tends to infinity, $\lambda_2 \to \infty$ (i.e., very high thermal conductive fluid) then equation 9.17 reduces to

$$lim_{\lambda_2 \to \infty}\left\{\lambda_{eff} = \frac{S_1}{S}\lambda_1 + \frac{S_3}{S}\left(\frac{D}{d_1}\right)\lambda_1 = \lambda_{const}\right\} \tag{9.19}$$

It means if we fill the porous structure with a fluid having very high thermal conductivity (approaching infinity), then the overall thermal conductivity of the porous structure will not be infinity but it will tend to some constant higher values. Experimental data on thermal conductivity of liquid and gas-saturated Sander sandstone is compared with the above-proposed model and is shown in figure 9.8 and figure 9.9. The thermal conductivity of liquid and gas-saturated sandstone increases non-linearly as a function of thermal conductivity of the saturating fluids towards some highest value. On the other hand, the thermal conductivity of the moist sandstone shows an inverse effect (shown with a symbol of star in figure 9.10). Experimental data are fitted with a non-linear curve. The maximum deviation in the values of thermal conductivity between the experimental and the theoretically proposed model is 1.4 % and the converging limit approaches a maximum value of 2.82 $W.m^{-1}.K^{-1}$ for liquid-saturated case. For gas-saturated sandstone, the convergence is faster as compared to liquid-saturated sandstone and the maximum deviation between the experimental and the theoretical data is 2.3 %. The limiting value of the effective thermal

conductivity for gas-saturated case is 1.93 $W.m^{-1}.K^{-1}$.

It is clear from figure 9.10 that, the heat transfer mechanism shows similar trend for both liquid and gas-saturated cases but it is completely different for the moisture-saturation case. It means that, the mechanism of heat transfer in moisture-saturation case can not be co-related with the gas or liquid-saturated results for porous rocks like sandstone.

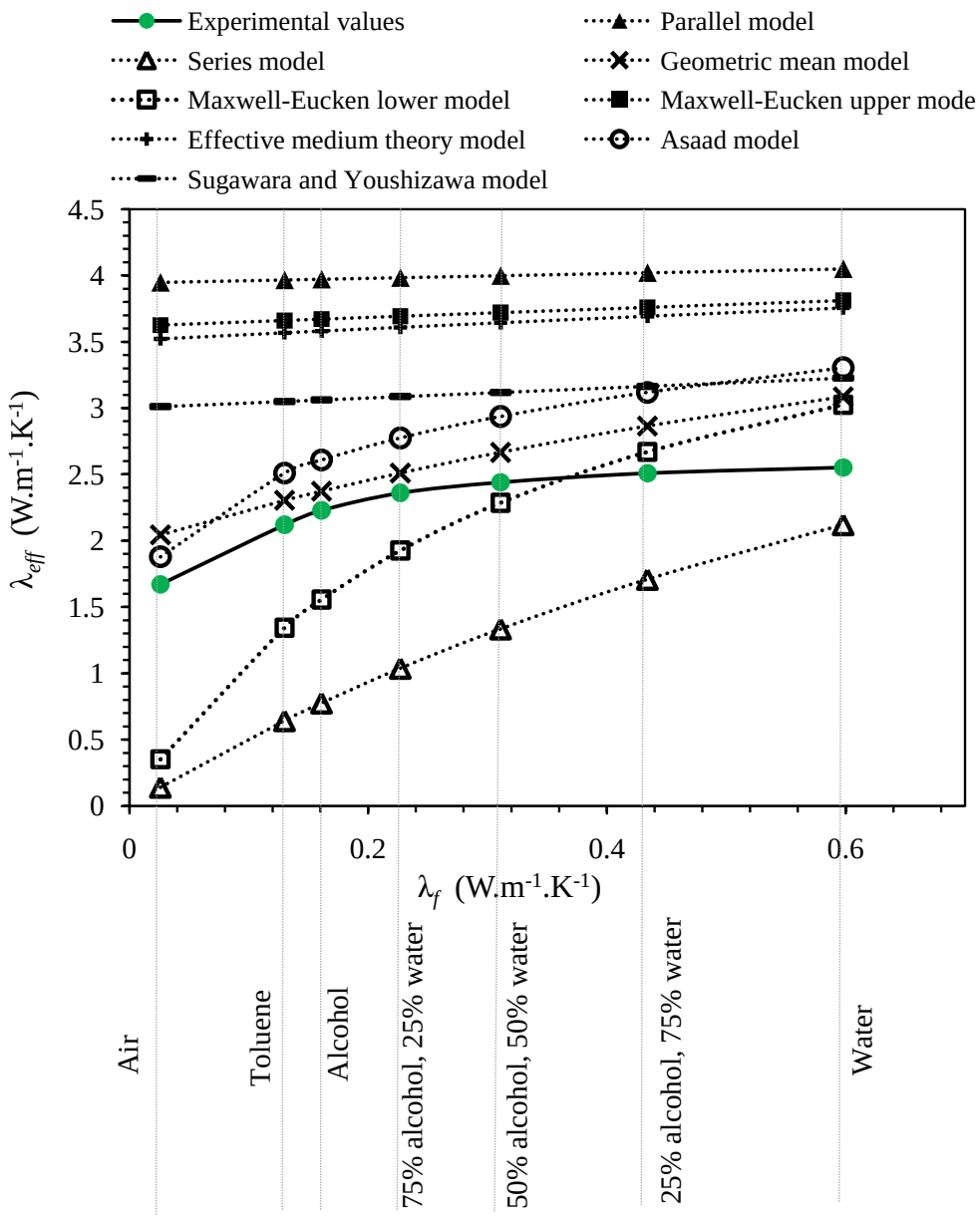

Figure 9.6: Comparison of the experimental results with the mixing law and empirical models.

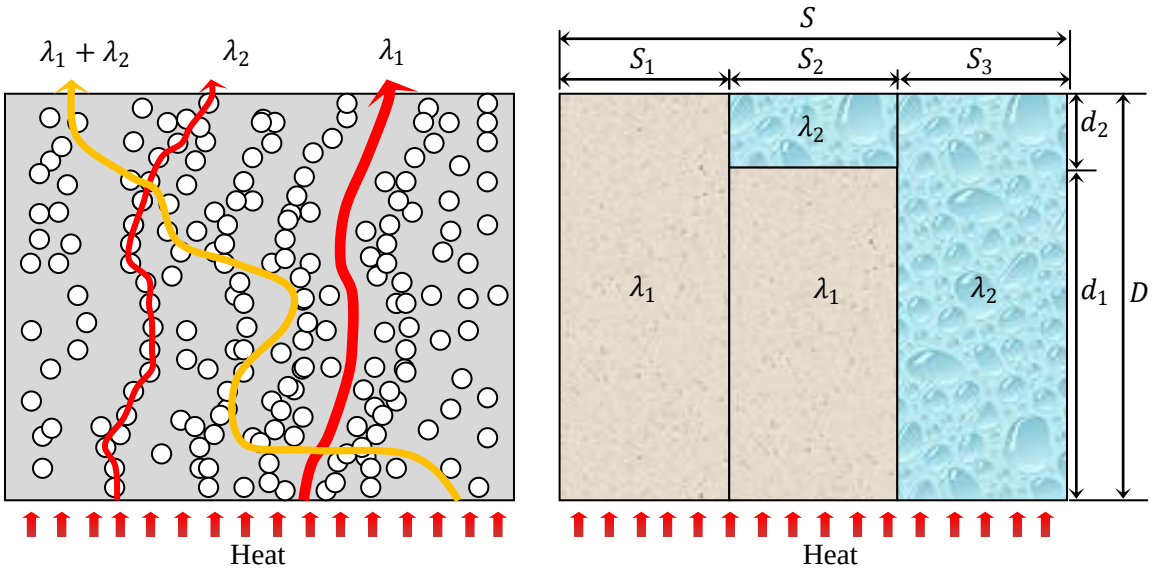

Figure 9.7: Schematic diagram of a proposed empirical model.

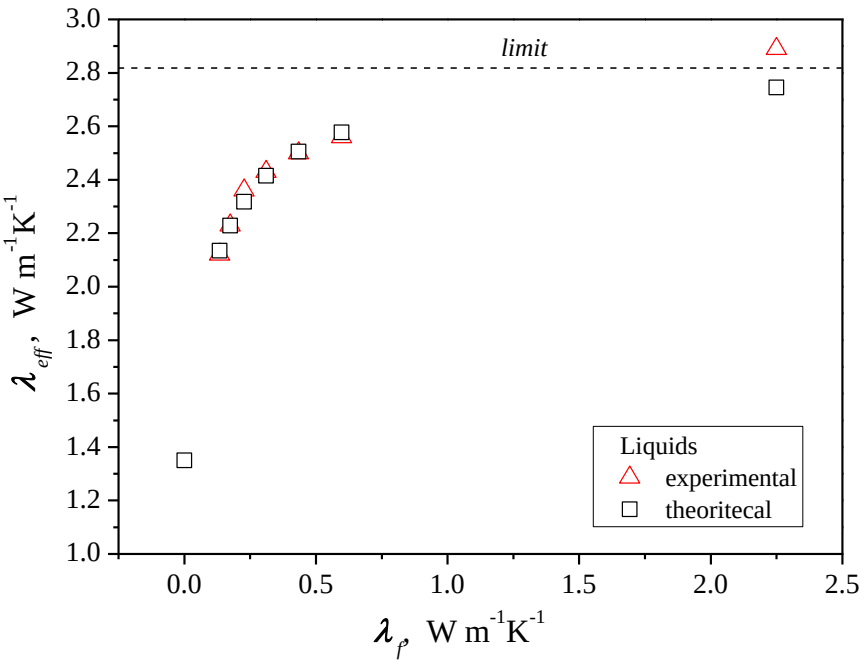

Figure 9.8: Comparison of the experimental and theoretical values of thermal conductivity of liquid-saturated sandstone.

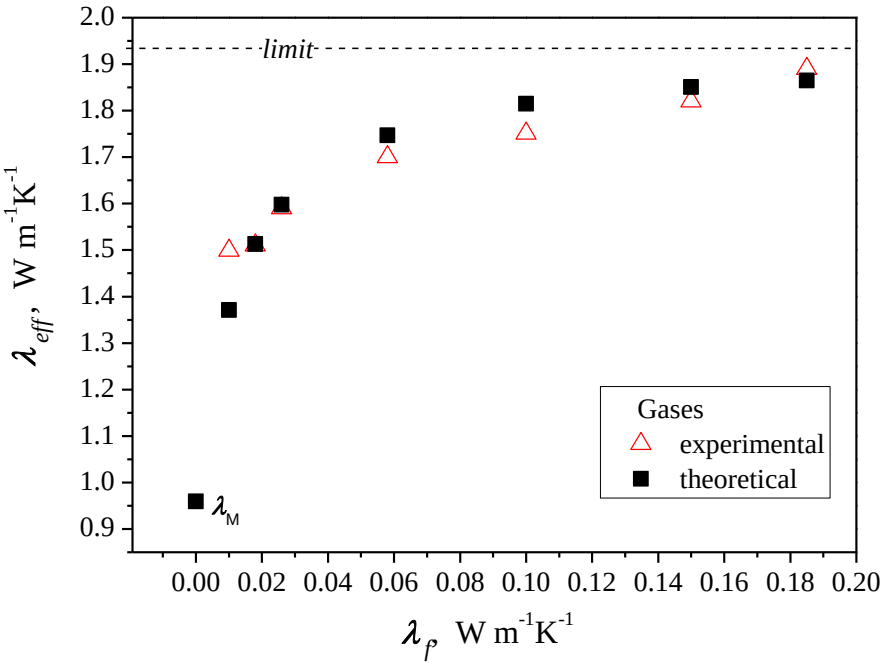

Figure 9.9: Comparison of the experimental and theoretical values of thermal conductivity on gas-saturated sandstone.

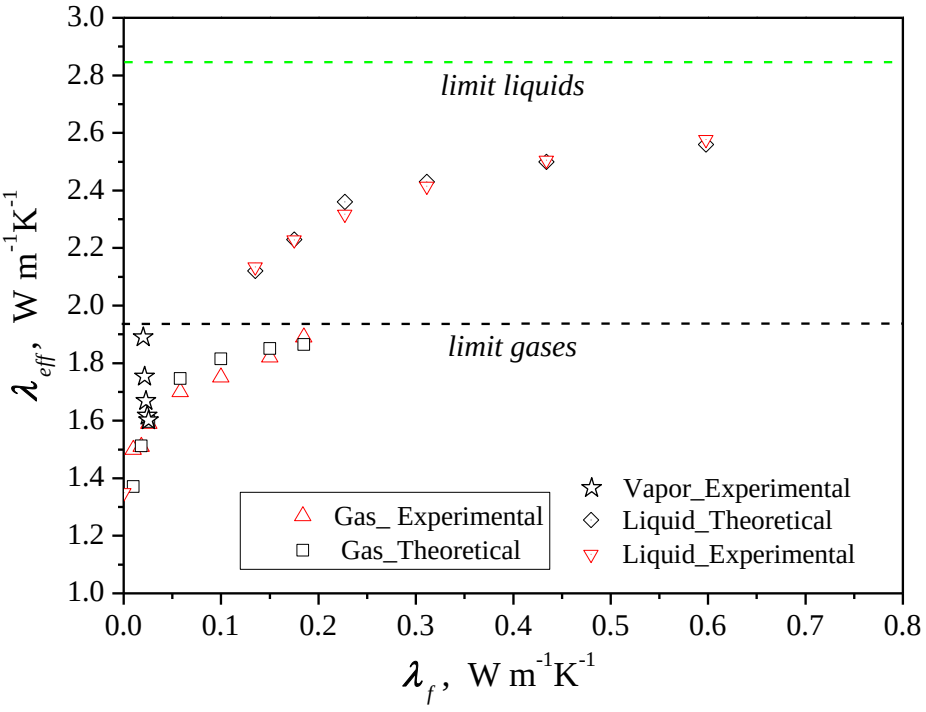

Figure 9.10: Comparison of experimental and theoretical values of thermal conductivity on gas, liquid and vapor-saturated sandstone.

Chapter 10

Conclusions

Thermophysical properties of consolidated and unconsolidated porous rocks/stones are needed in a wide variety of applications. To get reliable results on thermophysical properties, there is always need to measure these properties with some state of the art instrument. We have discussed a number of experimental methods to measure thermophysical properties. In the end, we decided to choose Transient hot-bridge method because of its excellent features like, short measurement time, maximum temperature rise up to 2 K, constant penetration depth, low uncertainty range and compensation of the end-effect problem. In this work, main thermophysical properties namely; thermal conductivity, thermal diffusivity and specific heat capacity of porous materials are experimentally measured using Transient hot-bridge sensor. Working validity of the THB sensor is successfully checked on a model porous material (Sander sandstone) experimentally as well as numerically. For numerical analysis on THB sensor, we used COMSOL Multiphysics version 3.4 software. Numerical simulations are performed using different thermal contact resistances between sensor and the sample in the form of a thin air gap. FEM results are compared with the experimentally determined values; both are in good agreement with a maximum deviation of 3 %. However, deviation in the values is more for time window of less than 0.5 s. This is because of the fact that, at very short initial times, heat accumulates on the strip and results a time-delayed curve in the end. We have also checked the contact resistance problem experimentally. We put successive loads of 1 kg on the top of the upper sample half to make a better thermal contact between sensor and the sample halves. Results show that the difference in the values of thermal properties for different runs remains within the uncertainty range of the sensor (i.e., ≤ 3 % for thermal conductivity and ≤ 9 % for thermal diffusivity).

Physical characterization of Sander sandstone is done according to the standard methods. Porosity and density of the sample is measured according to the ASTM standard (ASTM D 2216-05). Mineral composition is determined using XRD (X–

ray Diffraction) method. Results of this test show that main mineral component in Sander sandstone is quartz which is about 54 % of all minerals in it. A high-resolution scanning electron microscope (HRSEM JSM-6700F NT), is used for getting scanned images of the sample (Sander sandstone). Results of SEM images clearly show that Sander sandstone consists of a microscopic porous system. Few pores are captured in between mineral grains and have no connectivity to other pores. Estimated average grain size is 180 μm and pore sizes lie in the range of 1 μm to 100 μm. To determine the distribution of pores, we used Mercury Intrusion Porosimetry (Porosimeter Pascal 240) method. Porosity values of Sander sandstone as determined by this method are 19.54 % and 18.63 % for dry and wetted stone, respectively. Whereas, porosity of the sample as determined through water saturation method is 17 %.

Using transient hot-bridge sensor, we measured the key thermal transport properties of dry, aqueous alcohol-saturated, pure alcohol-saturated and water-saturated Sander sandstone in a temperature range of -20 °C to +40 °C. Effect of freeze-thaw process (before and after freezing point of water) on thermophysical properties is also analyzed. Results show that, the thermal conductivity and thermal diffusivity of Sander sandstone are inversely proportional to the temperature. However, anomalies are found during freeze-thaw process in the case of water-saturated sandstone. A shift in the thermal properties of this stone is noticeable because its thermal conductivity and thermal diffusivity values changes drastically up to 69 % and 51 % respectively before and after freezing point of water in its water-saturated state. In addition, an empirical relation is also proposed to predict the effective thermal conductivity of Sander sandstone depending on temperature. Experimental and empirically calculated results are pretty close to each other with a maximum deviation of 1.99 %.

Since, saturating fluid also play an important role in changing the thermal behavior of a porous stone, therefore; we have also investigated the dependence of the thermal transport properties of moist and multi-fluid saturated Sander sandstone. Results show that, the thermal conductivity of sandstone increases nonlinearly both for liquid and gaseous saturates. Thermal conductivity of gas-saturated sandstone exhibits lower values than liquid-saturated states. This trend holds even if we fill sandstone pores with a liquid and a gas both having similar values of thermal conductivity. Whereas, no major changes in thermal diffusivity values are found. It is seen that, the specific heat capacity of Sander sandstone increases linearly by increasing the specific heat capacity of the pore filling fluids and if no fluid is filled in sandstone pores then the net specific heat capacity will be very close the average (weighted) of the heat capacities of all its mineral constituents. Thermophysical properties of sandstone are also dependent on the applied interstitial pressure in the pores. Overburden pressure reduces the thermal contact resistance by increasing the

internal gas density in the pores and thus increases overall thermal conductivity and specific heat capacity of the stone. It is also seen that, influence of moist air on overall thermal conductivity of the stone is more as compared to the dry air (Nitrogen). Relative humidity in the air can also increase the thermal conductivity of the porous building stones (like Sander sandstone) by more than 20 percent which is a bad precursor for building made of stones in which thermal insulation is needed.

We have also experimentally analyzed the effective thermal conductivity of three different types of porous structures namely, a brick sample, a cellular concrete sample and sandstone powder sample. All the three types of samples are analyzed in dry and in water-saturated states at temperatures from -20 °C to +25 °C. Results on bricks show that, the thermal conductivity of water-saturated brick samples slightly decreases with decreasing temperature up to -7 °C and after that, it shows an abrupt change between -7 °C and -10 °C due to the phase transition of water into ice in the pores. Further below -10 °C, the thermal conductivity increases linearly with a relative slow rate. In addition, we noticed that, because of the large variation in pore sizes within the brick samples, crystallization process of ice formation proceeds slowly as compared to sandstone. Therefore, the phase transition of water into ice takes place towards more negative temperatures as compared to the cellular concrete and unconsolidated sandstone.

Thermal conductivity and thermal diffusivity values of cellular concrete also show abrupt increase after freezing point of water (in between -1 to -5 °C). However, specific heat capacity increases linearly with increasing temperature. It is seen that, thermal conductivity and thermal diffusivity values of water-saturated sandstone powder are much higher as compared to its dry powder and dry compact form. For the sake of confirmation, we have also compared our results with few other known thermal property measurement methods. We can conclude that, in comparison with other transient methods, the newly developed transient hot-bridge sensor is a good sensor to measure thermal transport properties of porous materials like sandstone.

In the end, we proposed an empirical model to estimate the effective thermal conductivity of a porous material similar in structure as Sander sandstone. The maximum deviation in the values of thermal conductivity between the experimental and the theoretically proposed model are 1.4 % and 2.3 % of liquid-saturated and gas-saturated sandstone, respectively. Based on our experimental results on sandstone, we have seen that, according to this model, the maximum thermal conductvity values of Sander sandstone can approach a value of 2.82 $W.m^{-1}.K^{-1}$ in the case of liquid saturants. Whereas, for gas-saturated sandstone, the maximum value can approach a value of 1.93 $W.m^{-1}.K^{-1}$. After having experimental results on moist sandstone, we noticed that, the heat transfer mechanism in a moist sandstone is completely different

from the heat transfer mechanism in liquid and gas-saturated sandstone. It means that, there involves some other heat transfer parameters which are responsible for an entirely different thermal behavior of the porous sandstone.

Bibliography

[1] W. Woodside and J. Messmer. Thermal conductivity of porous media. I. Unconsolidated sands. Journal of Applied Physics, 32(9):1668-1699, 1961.

[2] J. Shelton. Underground storage of heat in solar heating systems. Solar Energy, 17(2):137-143, 1975.

[3] B. Sanner, F. Kabus, P. Seibt and J. Bartels. Underground thermal energy storage for the German parliament in Berlin, system concept and operational experiences. Proceedings World Geothermal Congress, Antalya, Turkey, 24-29 April 2005.

[4] M. Spearing, G. P. Matthews. Modeling characteristic properties of sandstones. Transport in Porous Media, 6:71-90, 1991.

[5] Y. A. Çengel and R. H. Turner, Fundamentals of thermal-fluid sciences. (Boston Burr Ridge: McGraw-Hill) pages 604-613, 2001.

[6] J. E. Parrott and Audrey D. Stuckes. Thermal conductivity of solids. Page 2, 1975.

[7] Halliday, Resnick and J. Walker, Fundamentals of Physics, p. 624, 8th Edition, 2007.

[8] R. E. Pierls, Quantum Theory of Solids (Oxford: Oxford University Press), 1964.

[9] M. A. Wahab, 2005. Solid State Physics 2nd edn. (New Delhi: Narosa Publishing House) page 317.

[10] http://en.wikipedia.org/wiki/Debyemodel

[11] Terry. M. Tritt, Thermal Conductivity, Theory, Properties and Applications. Clemson University, 2004.

[12] N. G. Bäcklund, Thermal Conductivity 8, edited by C. Y. Ho and R. E. Taylor (Plenum Press, New York, 1969), page 355.

[13] W. Hemminger, International Journal of Thermophysics. 10:765-777, 1989.

[14] M. I. Abdel-Ati, O. M. Hemeda, M. M. Mosaad and D. M. Hemeda, Thermal properties of pure and doped (Polyvinyl-Alcohol) PVA. Journal of Thermal Analysis. 42:1113-1122, 1994.

[15] A. G. Whittington, A. M. Hofmeister and P. I. Nabelek. Temperature dependent thermal diffusivity of the Earth's crust and implications for magmatism. Nature, 458:319-321, 2009.

[16] W. H. Somerton, Thermal properties and temperature-related behavior of rock/fluid systems. page 6, 1992.

[17] V. Rzhevsky and G. Novik. The physics of rocks. Moscow: Mir, 4:140-148, 1971.

[18] D. Waples and J. Waples. A review and evaluation of specific heat capacities of rocks, minerals, and subsurface fluids. Part 2: Fluids and porous rocks. Natural Resources Research, 13(2):123-130, 2004.

[19] W. Conshocken, PA. ASTM Standard C 177-04, Standard test method for steady-state heat flux measurements and thermal transmission properties by means of the Guarded-hot-plate apparatus, Annual Book of ASTM Standards, ASTM International, 2004.

[20] H. Czichos, T. Saito and L. Smith. Springer handbook of materials measurement methods. s.l.: Springer, pages 402-408, 2006.

[21] U. Hammerschmidt. Guarded hot-plate method: Uncertainty assessment. International Journal of Thermophysics, 23(6):1551-1570, 2002.

[22] W. Hemminger and R. Jugel. A Guarded Hot-plate apparatus for thermal conductivity measurements over the temperature range -75 to 200 °C. International Journal of Thermophysics, 6(5):483-498, 1985.

[23] Z. Abdulagatova, I. M. Abdulagatov and V. N. Emirov. Effect of temperature and pressure on the thermal conductivity of sandstone. International Journal of Rock Mechanics and Mining Sciences, 46(6):1055-1071, 2009.

[24] A. Beck. A steady state method for the rapid measurement of the thermal conductivity of rocks. Journal of Scientific Instruments, 34:186-189, 1957.

[25] U. Hammerschmidt. Thermal transport properties of water and ice from one single experiment. International Journal of Thermophysics, 23(4):975-996, 2002.

[26] U. Hammerschmidt and V. Meier. New transient hot-bridge sensor to measure thermal conductivity, thermal diffusivity and volumetric specific heat. International Journal of Thermophysics, 27(3):840-8653, 2006.

[27] Evaluation of measurement data–Guide to the expression of uncertainty in measurement, First edition September 2008.

[28] U. Hammerschmidt and W. Sabuga. Transient hot wire (THW) method: uncertainty assessment. International Journal of Thermophysics, 21(6):1255-1278, 2000.

[29] S. E. Gustafsson, E. Karawacki and M. N. Khan. Transient hot-strip method for simultaneously measuring thermal conductivity and thermal diffusivity of solids and fluids. Journal of Physics D: Applied Physics, 12:1411-1421, 1979.

[30] W. A. Wakeham, A. Nagashima and J. V. Sengers. Measurement of the transport properties of fluids. Experimental Thermodynamics, III:7, 1991.

[31] Y. Nagasaka and A. Nagashima. Absolute measurement of the thermal conductivity of electrical conducting liquids by the transient hot-wire method. Journal of Physics E: Scientific Instruments, 14:1435-1440, 1981.

[32] Y. Song. Das transient heissdraht-verfahren und seine anwendung zur messung der wärmeleitfähigkeit bis nahe an den kritischen punkt. Institut für thermodynamik und wärmetechnik der universität Stuttgart. PhD thesis, pages 11-15, 1992.

[33] U. Hammerschmidt and W. Sabuga. Transient hot strip (THS) method: Uncertainty assessment. International Journal of Thermophysics, 21:217-248, 2000.

[34] U. Hammerschmidt. A linear procedure for analyzing transient hot strip signals. Proc. 24th International Thermal Conductivity Conference, pages 123-134, 1999.

[35] S. E. Gustafsson. Transient plane source technique for thermal conductivity and thermal diffusivity measurements of solid materials. Review of Scientific Instruments, 62(3)797-804, 1991.

[36] L. Kubicar. Pulse method of measuring basic thermophysical parameters. Vol. XII. s.l.: ELSEVIER, 1990.

[37] H. S. Carslaw and J. C. Jaeger. Conduction of heat in solids. 2nd edition, pages 255-263, 1959.

[38] W. J. Parker, C. P. Jenkins, C. P. Butler and G. L. Abbot. Flash method for determining thermal diffusivity, heat capacity and thermal conductivity. Journal of Applied Physics, 32(9):1679-1684, 1961.

[39] K. D. Maglic and R. E. Taylor. The apparatus for thermal diffusivity measurement by the laser pulse method. Compendium of Thermophysical Property Measurement Methods 2, New York: pages 281-314, 1992.

[40] L. Vozar and W. H. Boulder. Uncertainty of the thermal diffusivity measurement using the laser flash method. Tech. Dig. 15th Symposium on Thermophysical Properties, 2003.

[41] R. Model, R. Stosch and U. Hammerschmidt. Virtual experiment design for the transient hot-bridge sensor. International Journal of Thermophysics, 28(5):1447-1460, 2007.

[42] S. Grunert and J. Szilagyi. Petrophysical properties of a selection of dimensional stones from Germany in relation to the petrography of these rocks. Journal of Central European Geology, 56(1):39-82, 2010.

[43] L. Kubicar, V. Vretenar, V. Bohac and P. Tiano. Thermophysical analysis of sandstone by pulse transient method. International Journal of Thermophysics, 27(1):220-234, 2006.

[44] F. Brigaud, D. S. Chapman and S. Le Douaran. Estimating thermal conductivity in sedimentary basins using lithological data and geophysical well logs. AAPG Bulletin, 74:1459-1477, 1990.

[45] T. Hadgu, Clinton C. Lum, James E. Bean. Determination of heat capacity of Yucca mountain stratigraphic layers. International Journal of Rock Mechanics & Mining Sciences, 44:1022-1034, 2007.

[46] K. Horai and G. Simmons. Thermal conductivity of rock-forming minerals. Earth and Planetary Science Letters, 6:359-368, 1969.

[47] W. Waples and S. Waples. A review and evaluation of specific heat capacities of rocks, minerals and subsurface fluids. part 2: Fluids and porous rocks. Natural Resources Research, 13(2), 2004.

[48] M. Abid and U. Hammerschmidt. Thermophysical properties of Sander sandstone using Transient Hot-Bridge sensor. Arbeitskreis Thermophysik, Karlsruhe, Germany, 4-5 March 2010.

[49] W. Klose and A. Schinkel. Measurement and modeling of the development of pore size distribution of wood during pyrolysis. Fuel Processing Technology, 77-78:459-466, 2002.

[50] B. Meng. Determination and interpretation of fractal properties of sandstone pore system. Materials and Structures, 29:195-205, 1996.

[51] M. Abid, U. Hammerschmidt and V. Meier. Dependence of Thermophysical properties of Sander sandstone on multiple pore filling fluids. Thermophysics 2010, Valtice Chateu, Czech Republic. 3-5 November 2010.

[52] C. Clauser and E. Huenges. Thermal conductivtiy of rocks and minerals. Rock Physics and Phase Relations, A Handbook of Physical Constants, AGU reference shelf 3, 1995.

[53] H. Vosteen and R. Schellschmidt. Influence of temperature on thermal conductivity, thermal capacity and thermal diffusivity for different types of rocks. Physics and Chemistry of the Earth, 28:499-509, 2003.

[54] U. Seipold. Temperature dependence of thermal transport properties of crystalline rocks-a general law. Tectonophysics, 291:161-171, 1998.

[55] Sahrigi, Johan C. Harper and F. El Ahmed. Thermal conductivity of gas-filled porous solids. I & EC Fundamentals, 3:318-324, 1964.

[56] A. I. Shutov, S. V. Alekseev and T. V. Yashurkaev. Effect of pore size on heat flows in thermal treatment of foam glass. Glass and Ceramics, 63:213-214, 2006.

[57] U. Schärli and L. Rybach. Determination of specific heat capacity on rock fragments. Geothermics, 30:93-110, 2001.

[58] G. Buntebarth and J. Schopper. Experimental and theoretical investigations on the influence of fluids, solids and interactions between them on thermal properties of porous rocks. Physics and Chemistry of the Earth, 23:1141-1146, 1998.

[59] W. Douglas and S. Jacob. A review and evaluation of specific heat capacities of rocks, minerals, and subsurface fluids. Part 1: Minerals and nonporous rocks. Natural Resources Research, 13(2):97-122, 2004.

[60] U. Grigull and H. Sander. Wärmeleitung. s.l.: Springer-verlag, Berlin-Heidelberg-New York. 1979.

[61] M. J. Assael, E. Charitidou and W. A. Wakeham. Absolute measurements of the thermal conductivity of mixtures of alcohols with water. International Journal of Thermophysics, 10:793-803, 1989.

[62] J. Wang and M. Fiebig. Measurement of thermal diffusivity of aqueous solutions of alcohol by a laser-induced thermal grating technique. International Journal of Thermophysics, 16(6):1353-1361, 1995.

[63] R. Perry and D. Green. Perry's Chemical Engineers Handbook. 6. s.l. : McGraw-Hill, 1984.

[64] Heinz R. Trechsel. Moisture control in buildings, page 56, 1994.

[65] American Society of Testing and Materials. Standard test method for laboratory determination of water (moisture) content of soil and rock by mass. ASTM standard D2216-05. Philadelphia, PA. 2007.

[66] P. T. Tsilingiris. Thermophysical and transport properties of humid air at temperature range between 0 and 100 °C. Energy Conversion and Management, 49:1098-1110, 2008.

[67] K. M. Dijkema, J. C. Stouthart and D. A. De Vries. Measurements of the thermal conductivity of gases and gas mixtures, methods and results. Wärme-und Stoffübertragung, 5:47-55, 1972.

[68] R. Parsons. ASHRAE Fundamental Handbook (SI). pages 6-16, 1997.

[69] Y. S. Touloukian, P. E. Liley and S. C. Saxena. Thermophysical properties of matter, Thermal conductivity, Nonmetallic liquids and gases. Volume 3, 1970.

[70] A. Melling, S. Noppenberger, M. Still and H. venzke. Interpolation correlations for fluid properties of humid air in the temperature range 100 °C to 200 °C. Journal of Physical and Chemical Reference Data, 26(4):1111-1123, 1997.

[71] L. Wolf, M. Ludewig, L. Hahne and T. Kölbel. Environmental complaint planning of shallow geothermal district heating using numerical groundwater models, Proceedings World Geothermal Congress, Bali, Indonesia, 25-29 April 2010.

[72] F. Mzali, V. Meier, M. Abid and U. Hammerschmidt. Measurement of temperature dependent thermal conductivity of moist bricks using the transient hot-bridge sensor. Special Topics & Reviews in Porous Media–An International Journal, 1(2):87-94, 2010.

[73] S. Chatterji. Aspects of the freezing process in a porous material-water system: Part 1. Freezing and the properties of water and ice. Cement and Concrete Research, 29:627-630, 1999.

[74] S. Chatterji. Aspects of freezing process in porous material-water system: Part 2. Freezing and properties of frozen porous materials. Cement and Concrete Research, 29(5):781-784, 1999.

[75] A. Maqsood and K. Kamran. Thermophysical prperties of porous sandstones: Measurements and comparative study of some representative thermal conductivity models. International Journal of Thermophysics, 26(5):617-1632, 2005.

[76] M. S. Goual, A. Bali and M. Queneudec. Effective thermal conductivity of clayey aerated concrete in the dry state: Experimental results and modeling. Journal of Physics D: Applied Physics, 32:3041-3046, 1999.

[77] J. K. Carson, S. J. Lovatt, D. J. Tanner and A. C. Cleland. Predicting the effective thermal conductivity of unfrozen, porous foods. Journal of Food Engineering, 75:297-307, 2006.

[78] R. W. Zimmermann. Thermal conductivity of fluid-saturated rocks. Journal of Petroleum Science and Engineering, 3:219-227, 1989.

[79] M. M. Awad and Y. S. Muzychka. Effective property models of homogeneous two-phase flows. Experimental Thermal and Fluid Sciences, 33:106-113, 2008.

[80] R. A. Rocha and M. E. Cruz. Computation of the effective conductivity of unidirectional fibrous composities with an inter-facial thermal resistance. Numerical heat transfer Part A: Applications, 39(2):179-203, 2001.

[81] S. Kirkpatrick. Percolation and conduction. Reviews of Modern Physics, 45(4):574-588, 1973.

[82] R. Landauer. The electrical resistance of binary metallic mixtures. Journal of Applied Physics, 23(7):779-784, 1952.

[83] B. Nait-Ali, K. Haberko, H. Vesteghema, J. Absi, D. S. Smith. Thermal conductivity of highly porous zirconia. Journal of the European Ceramic Society, 26:3567-3574, 2006.

[84] B. Aurangzeb. Prediction of effective thermal conductivity of fluid saturated porous media: in situ thermophysical measurements. PhD thesis: Quaid-e-Azam university, Islamabad, Pakistan, 2009.

[85] E. Gomma, Thermal behavior of partially liquid saturated porous media. PhD thesis: University of California, Berkeley, 1973.

[86] H. Özbek, Thermal conductivity of multifluid-saturated porous media. PhD thesis: University of California, Berkeley, 1976.

[87] A. Sugawara and Y. Yoshizawa. An experimental investigation on the thermal conductivity of consolidated porous materials. Journal of Applied Physics, 33:31-35, 1962.

[88] J. Schatz and G. Simmons. Thermal conductivity of earth materials at high temperatures. Journal of Geophysical Research, 77(35):6966-6983, 1972.

[89] V. Tikhomirov. Conductivity of rocks and their relationship with density, saturation and temperature. Neftianoe Khoziaistra, 46(4):36, 1968.

[90] R. Progelhof, J. Throne and R. Reutsch. Methods for predicting the thermal conductivity of composite systems: A review. Polymer Engineering and Science, 16(9):615-625, 1976.

[91] U. Hammerschmidt. An empirical model to estimate the effective thermal conductivity of porous sandstone, Private Communication, to be published in 2012.

[92] J. Fricke, From Dewars to VIPs - one century of progress in vacuum insulation technology, in: M. Zimmerman (Ed.), Proceedings of the 7th International Vacuum Insulation Symposium, EMPA, Duebendorf, Switzerland. Pages 5-14, 28-29 September 2005.

[93] S. Q. Zeng, A. J. Hunt, W. Cao., and R. Grief. Pore size distribution and apparent gas thermal conductivity of Silica Aerogel, Trans. ASME 116:756, 1994.

[94] R. Baetens, B. Jelle, J. Thue, M. Tenpierik, S. Grynning, S. Uvsløkk and A. Gustavsen. Vacuum insulation panels for building applications: A review and beyond. Energy and Buildings 42:147-172, 2010.

[95] E.H. Kennard. Kinetic theory of Gases, with an introduction to statistical mechanics, Mc-Graw-Hill, New York, 1938.

[96] K. Raed, G. Barth, R. Wulf and U. Gross. Gas atmosphere and pore size distribution effects on the effective thermal conductivity of nano-scaled insulations. 17th European Conference on Thermophysical Properties. Bratislava, Slovakia, 5-8 September, 2005.

Appendix A

Nomenclature

Latin Characters

Symbol	Unit	Description
A	[m^2]	Cross-sectional area of the sample
a_f	[$mm^2.s^{-1}$]	Thermal diffusivity of the pore filling fluid
a_{efff}	[$mm^2.s^{-1}$]	Effective thermal diffusivity of the bulk material
a_w	[$mm^2.s^{-1}$]	Thermal diffusivity of the hot-wire
c_{p_f}	[$J.kg^{-1}.K^{-1}$]	Specific heat capacity of the pore filling fluid
c_v	[$J.m^{-3}.K^{-1}$]	Volumetric heat capacity
$c_{p_{eff}}$	[$J.kg^{-1}.K^{-1}$]	Effective specific heat capacity of the bulk material
c_{m_i}	[$J.kg^{-1}.K^{-1}$]	Specific heat capacity of a particular mineral in the Sample
D_i	[m]	Distance between heating strips of THB sensor
d	[m]	Thickness of the sample
$D(\tau)$	–	Characteristic time dependent function
F	–	Empirical coefficients
$f(t)$	–	Dimensionless function
h	[$W.m^{-2}.K^{-1}$]	Heat transfer coefficient
I_m	[A]	Measurement current applied to the THB sensor
L_S	[m]	Length of the short strip of the THB sensor
L_L	[m]	Length of the long strip of the THB sensor

L_{eff}	[m]	Effective length of THB sensor strips
l	[m]	Mean free path of gas molecules
m	–	Slope
m_{max}	[V.s^{-1}]	Maximum slope
n	–	Intercept
Q	[W.m^{-3}]	Heat pulse per unit volume
q	[W.m^{-2}]	Heat flux through the sample
R_{ws}	[$W^{-1}.m.K$]	Wetting-fluid to solid contact resistance
R_{nws}	[W^{-1}.m.K]	Non-wetting fluid to solid contact resistance
r	[m]	Radial distance from the hot-wire
r_w	[m]	Radius of the hot-wire
r_p	[m]	Radius of the pores
R_p	[m]	Radius of sphere
R_{eff}	[Ω]	Effective resistance of the THB sensor strips
R_0	[Ω]	Electrical resistance of the strip before heating
S_w	[%]	Fractional wetting-phase saturation
T_w	[K]	Temperature of the hot-wire
T_0	[K]	Equilibrium temperature at zero time
T_m	[K]	Maximum temperature
T_{inn}	[°C]	Temperature rise at the inner strips of THB sensor
T_{out}	[°C]	Temperature rise at the outer strips of THB sensor
ΔT	[°C]	Temperature difference between inner and outer strips of THB sensor
t_m	[s]	Measurement time of THB sensor time
t_{max}	[s]	Maximum time
V_{THB}	[V]	Output voltage signal of THB sensor
V_p	[m^3]	Volume contained by pores
V_t	[m^3]	Total volume of the bulk sample

$\overline{v}$	$[m.s^{-1}]$	mean velocity of the molecules
x_i	[%]	Weight fraction of a particular mineral in the sample

Greek Characters

Symbol	Unit	Description
α	$[K^{-1}]$	Temperature coefficient of resistance
γ	–	Euler constant
θ_D	[K]	Debye temperature
λ_f	$[W.m^{-1}.K^{-1}]$	Thermal conductivity of the pore filling fluid
λ_{eef}	$[W.m^{-1}.K^{-1}]$	Effective thermal conductivity of the bulk material
λ_s	$[W.m^{-1}.K^{-1}]$	Thermal conductivity of solid phase
λ_{matrix}	$[W.m^{-1}.K^{-1}]$	Thermal conductivity of solid matrix without pore spaces
λ_{wf}	$[W.m^{-1}.K^{-1}]$	Thermal conductivity of wetting phase
λ_{nwf}	$[W.m^{-1}.K^{-1}]$	Thermal conductivity of non-wetting phase
λ_{20°	$[W.m^{-1}.K^{-1}]$	Thermal conductivity value at 20 °C
λ_{air}	$[W.m^{-1}.K^{-1}]$	Thermal conductivity of moist air
ζ_f, ζ_s	–	Empirical coefficients
ρ_b	$[kg.m^{-3}]$	Bulk density of material
ρ_{matrix}	$[kg.m^{-3}]$	Density of the solid matrix
σ	$[N.m^{-1}]$	Surface tension of mercury
τ	–	Dimensionless parameter
ϕ	[%]	Porosity

Subscripts and Superscripts

Subscripts		Superscripts	
Symbol	Description	Symbol	Description
f	Fluid	P	Parallel
eff	Effective	S	Series
s	Solid	HSU	Hashin-Shtrikman upper
$matrix$	Matrix	HSL	Hashin-Shtrikman lower
wf	Wetting-fluid	MEL	Maxwell-Eucken lower
nwf	Non-wetting fluid	MEU	Maxwell-Eucken upper
ws	Wetting-solid	EMT	Effective Medium Theory
nws	Non-wetting solid	A	Asaad
20°	20 degree Celsius	PC	Pande and Chaudhary
b	Bulk	SY	Sugawara and Yoshizawa
D	Debye	GMM	Geometric Mean Model
0	Initial condition (zero time)	Ö	özbek
i	Number of components		
max	Maximum		
t	Total		
p	Pore		
THB	Transient hot-bridge		
m	Measurement		
L	Long		
S	Short		
inn	Inner		
out	Outer		
m_i	Particular mineral		
w	Wire		
v	Volume		

Appendix B

B.1 Differential Equation of Heat Conduction

The differential equation of heat conduction is needed for solving problems in which temperature in a solid may vary with time in more than one direction. Suppose we have a solid, isotropic element having constant value of thermal conductivity in all directions of heat flow. We take a differential element from this material to examine the conduction of heat in it. It is shown in figure B-I below. We suppose that rate of

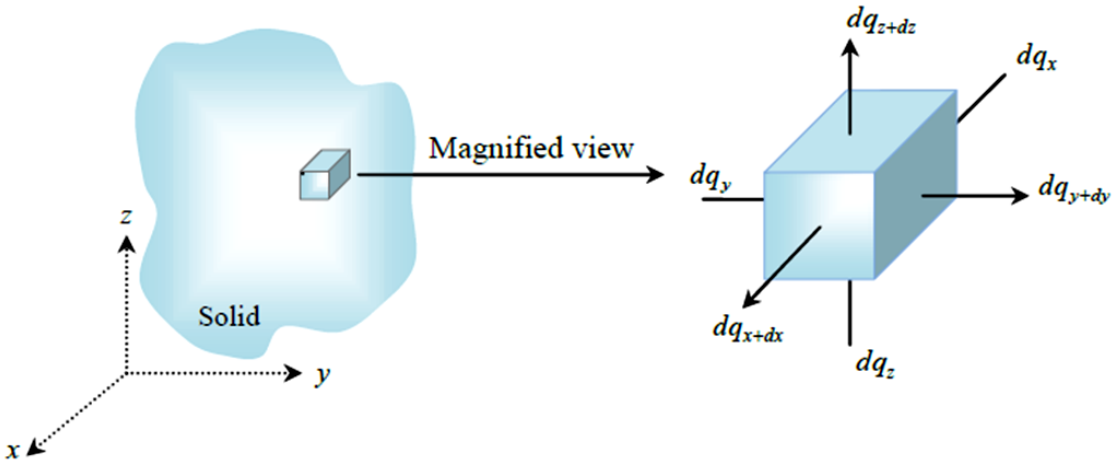

Figure B-I: Three-dimensional heat conduction in Cartesian coordinates of a solid body

heat flowing in the positive x-direction at face x is dq_x and flowing out after moving a distance dx at face $x + dx$ is dq_{x+dx}. Now we use Fourier's law of heat conduction to write down expressions for each of these quantities.

$$dq_x = -\left[\left(\lambda\frac{\partial T}{\partial x}\right) + \frac{\partial}{\partial x}\left(\lambda\frac{\partial T}{\partial x}\right)dx\right] \times dy.dz \tag{B-1}$$

The rate of heat flowing out at face x+dx will be simply an increment in the rate of heat flowing in at face x.

$$dq_{x+dx} = -\left(\lambda\frac{\partial T}{\partial x}\right) \times dy.dz \tag{B-2}$$

We assume that the thermal conductivity values and the surface area normal to the heat flow remains constant in the x-direction. Net amount of heat in x-direction can be deduced by subtracting equation B-2 from equation B-1.

$$dq_x - dq_{x+dx} = \lambda \left(\frac{\partial^2 T}{\partial x^2} \right) \times dx.dy.dz \tag{B-3}$$

Similarly we can write expressions for y and z-directions using Fourier's law of heat conduction as,

$$dq_y - dq_{y+dy} = \lambda \left(\frac{\partial^2 T}{\partial y^2} \right) \times dx.dy.dz \tag{B-4}$$

$$dq_z - dq_{z+dz} = \lambda \left(\frac{\partial^2 T}{\partial z^2} \right) \times dx.dy.dz \tag{B-5}$$

Total amount of heat per unit time conducted into the volume element will be the sum of equations B-3, B-4 and B-5.

$$net\ rate\ of\ heat\ conduction\ =\ \lambda \left(\frac{\partial^2 T}{\partial x^2} + \frac{\partial^2 T}{\partial x^2} + \frac{\partial^2 T}{\partial z^2} \right) \times dx.dy.dz \tag{B-6}$$

By conservation of energy principle, we know that "total change in internal energy of a small body is equal to the net rate of energy flow in the body plus heat generated within the body". We also assume that there is a heat generation within the body per unit time per unit volume, mathematically we can write it as,

$$Quantity\ of\ heat\ generated\ within\ the\ material\ per\ unit\ time\ =\ \overline{q} \times dx.dy.dz \tag{B-7}$$

The third quantity we need to fulfill the first law of thermodynamics for a closed system is the net change in internal energy of the system. When heat enters a differential element of a solid body, the body heats up due to molecular vibrations. A quantitative expression for molecular thermal vibrations can be expressed in terms of specific internal energy and it changes as heat enters or leaves the material. Change in internal energy of the closed system per unit time is given below,

$$\frac{\partial E}{\partial T} = m c_p \frac{\partial T}{\partial t} \tag{B-8}$$

Since, $\rho \times dx.dy.dz = m$, therefore equation B-8 may be re-written as,

$$\frac{\partial E}{\partial T} = \rho c_p \frac{\partial T}{\partial t} \times dx.dy.dz \tag{B-9}$$

Heat balance equation for this element may be written as,

$$\begin{aligned} &Rate\ of\ change\ of\ internal\ energy\ within\ the\ material\ = \\ &(Net\ rate\ of\ heat\ conduction\ in\ the\ material) \\ &+(Rate\ of\ heat\ generated\ within\ the\ material) \end{aligned} \tag{B-10}$$

Substituting equations B-6, B-7 and B-9 in equation B-10 we get,

$$\left(\frac{\partial^2 T}{\partial x^2}+\frac{\partial^2 T}{\partial x^2}+\frac{\partial^2 T}{\partial z^2}\right)+\frac{\overline{q}}{\lambda}=\frac{1}{a}\frac{\partial T}{\partial t} \tag{B-11}$$

Depending on the geometry of the heat source, we can choose spherical or cylindrical coordinates by changing Cartesian coordinates as following,

Cylindrical coordinate system

$$x = rcos\theta$$
$$y = rsin\theta$$
$$z = z$$

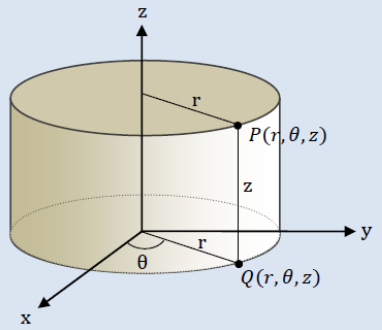

Spherical coordinate system

$$x = rsin\psi cos\phi$$
$$y = rsin\psi sin\phi$$
$$z = rcos\psi$$

Where ψ is zenith angle and ϕ is azimuth angle

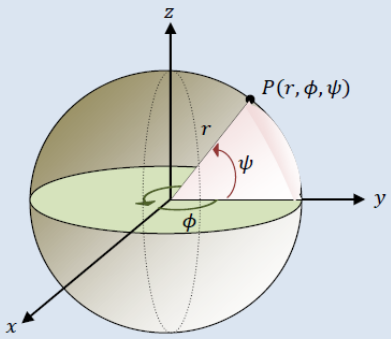

Similarly, we can derive differential equations of heat conduction in cylindrical and spherical coordinates as following: For cylindrical coordinates,

$$\lambda\left[\frac{1}{r}\frac{\partial}{\partial r}\left(r\frac{\partial T}{\partial r}\right)+\frac{1}{r^2}\frac{\partial^2 T}{\partial \theta^2}+\frac{\partial^2 T}{\partial z^2}\right]+\overline{q}=\rho c_p\frac{\partial T}{\partial t} \tag{B-12}$$

For spherical coordinates,

$$\lambda\left[\frac{1}{r}\frac{\partial^2 (rT)}{\partial r^2}+\frac{1}{r^2\sin\psi}\frac{\partial}{\partial \psi}\left(\sin\psi\frac{\partial T}{\partial \psi}\right)+\frac{1}{r^2\sin^2\psi}\frac{\partial^2}{\partial \psi^2}\right]+\overline{q}=\rho c_p\frac{\partial T}{\partial t} \tag{B-13}$$

Now we have all types of differential equations for heat conduction. We need to

solve appropriate heat equation depending on the geometry of the heat source using some conditions. These conditions are initial and boundary conditions. All initial conditions will represent temperature inside the body at time equal to zero and what is happening at the boundaries of the solid are called boundary conditions. Typically, there are three types of boundary conditions namely, 1) prescribed surface temperature, 2) prescribed heat flux incident on the surface, 3) prescribed heat transfer coefficient at the surface.

B.2 Solution of the Differential Equation of Transient Heat Conduction using Dimensional Analysis

Transient heat conduction depends on space and time variables at the same time, say $T = f(x, y, z, t)$. Determination of thermal conductivity using thermoelectric sensors is usually carried out using continuous point heat source, line heat source and plane heat sources. In all cases, we take the solution of the instantaneous point source as fundamental. By integrating with respect to time we obtain the solution for the continuous point source, corresponding to release of heat at a given point at a prescribed rate $q = Q/t$. If $Q = I^2R$ is constant (in case of electrically heated source) and supply of heat goes for a very long time, the solution becomes in the limit that for the steady point source. By integrating the solutions for point sources with respect to space variables, we obtain solutions for instantaneous and continuous line, plane, spherical surface, and cylindrical surface sources [37]. The differential equation of heat conduction in three dimensions in Cartesian coordinates without internal heat generation may be written as,

$$\left(\frac{\partial^2 T}{\partial x^2} + \frac{\partial^2 T}{\partial y^2} + \frac{\partial^2 T}{\partial z^2}\right) = \frac{1}{a}\frac{\partial T}{\partial t} \tag{B-14}$$

It is satisfied by following solution [37]

$$T = \frac{Q}{8(\pi a t)^{\frac{3}{2}}} e^{-\left\{(x-x')^2+(y-y')^2+(z-z')^2\right\}/4at} \tag{B-15}$$

Equation B-15 gives us temperature distribution from a heat source at some distance. Heat source may be in the form of a sphere, line, plane or cylinder. In this work, transient hot-bridge (THB) sensor is used that works on the basic principles of heat distribution due to a line heat source. Therefore, we will briefly derive equation for temperature distribution due to a line heat source. However, a short derivation on the temperature distribution due to a point heat source is also given.

B.2.1 Continuous Point Heat Source

Suppose we have a point heat source liberating heat at constant rate $q.\rho c$ per unit time from $t = 0$ to $t = t$ at a point $(x^{'}, y^{'}, z^{'})$. The temperature at point (x, y, z) at a distance r after some time t can be calculated by integrating equation B-15 with respect to time,

$$T = \frac{q}{8(\pi a)^{3/2}} \int_0^t e^{\frac{-r^2}{4a(t-t^{'})}} \frac{dt^{'}}{(t-t^{'})^{3/2}} \tag{B-16}$$

Where $r^2 = (x - x^{'})^2 + (y - y^{'})^2 + (z - z^{'})^2$. Using dimensional analysis and putting $\tau = (t - t^{'})^{-1/2}$ we get finally

$$T = \frac{q}{4(\pi a)^{3/2}} \int_{1/\sqrt{t}}^{\infty} e^{\frac{-r^2\tau^2}{4a}} d\tau \tag{B-17}$$

In terms of complementary error function we can write equation B-17 as,

$$T = \frac{q}{4\pi ar} \text{erfc}\left(\frac{r}{\sqrt{4at}}\right) \tag{B-18}$$

Where complementary error function can be defined as,

$$\text{erfc} = 1 - \text{erf}(x) = \frac{2}{\sqrt{\pi}} \int_{\infty}^{x} e^{-s^2} ds \tag{B-19}$$

If time $t \to \infty$, equation B-19 can be reduced to $T = q/4\pi ar$, a steady-state temperature distribution with a continuous heat generation at some point.

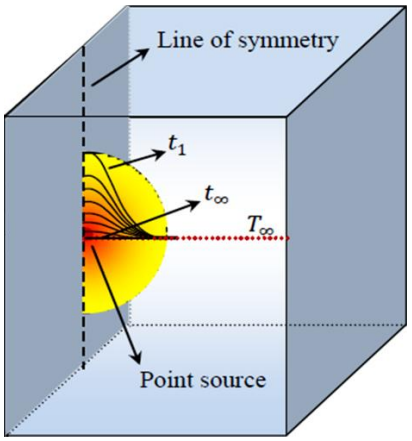

Figure B-II: Point heat source.

B.2.2 Continuous Line Heat Source

Suppose we have a thin line heat source passing through point $(x^{'}, y^{'})$ parallel to z-axis. It liberates heat at a rate of $q.\rho c$ per unit time per unit length. If heat generation starts at $t = 0$ when solid is at zero temperature, the temperature rise after some time t at some point $(x^{'}, y^{'})$ can be calculated from below given formula [37].

$$T = \frac{q}{4\pi at} e^{-\left\{(x-x^{'})^2 + (y-y^{'})^2\right\}/4at} \tag{B-20}$$

Now integrating over time from $t = 0$ to $t = t$ and putting $r^2 = (x-x^{'})^2+(y-y^{'})^2$

$$T = \frac{q}{(4\pi at)} \int_0^{\infty} e^{\frac{-r^2}{4a(t-t^{'})}} \frac{dt^{'}}{(t-t^{'})} \tag{B-21}$$

$$T = \frac{q}{(4a)} \int_{r^2/4a}^{\infty} \frac{e^{-u}}{u} du \tag{B-22}$$

$$T = -\frac{q}{4\pi a} \mathrm{Ei}\left(\frac{-r^2}{4at}\right) \tag{B-23}$$

Where, $-\mathrm{Ei}(-x) = \int_x^{\infty} \frac{e^{-u}}{u} du$ is called exponential integral. For small values of x it is expanded as,

$$\mathrm{Ei}(-x) = \gamma + \ln(x) - x + \frac{1}{4}x^2 + \cdots\cdots \tag{B-24}$$

Where γ=0.5772 is Euler's constant. Thus, for large value of time t, we get following approximate solution.

$$T = \frac{q}{4\pi a} \ln\left(\frac{4at}{r^2} - \gamma\right) \tag{B-25}$$

This solution is of great importance in calculating thermal conductivities of different materials. It gives temperature rise of an infinitely long line heat source, for instance let say, a thin metal wire carrying electric current and liberating heat to its surroundings at constant rate in semi infinite (one surface fixed at constant temperature) solid at is kept initially at zero temperature and is heat using a line heat source at a distance a from the surface and parallel to it, then the solution may be obtained as,

$$T = -\frac{q}{4\pi a}\left[\mathrm{Ei}\left(-\frac{r^2}{4at}\right) - \mathrm{Ei}\left(-\frac{r_1^2}{4at}\right)\right] \tag{B-26}$$

Where r and r_1 are the distances of the point from the line source and its image with respect to the surface.

We assume only conductive heat transfer mode during dissipation of thermal energy from the line source. The temperature rise ΔT(K) in the fluid at a distance r from the heat source is,

$$\Delta T(r,t) = T(r,t) - T_0 \tag{B-27}$$

Where T_0 is the equilibrium temperature of the fluid with its surroundings. Since we are considering a cylindrical shape of the heat source, therefore, the differential equation of heat conduction (in cylindrical co-ordinates) in radial direction of a body having constant thermal conductivity, density and heat capacity can be written as,

for wire

$$a_w = \left(\frac{\partial^2 T_w}{\partial r^2} + \frac{\partial T_w}{r\partial r}\right) + \frac{\overline{q_v}}{(\rho c_p)_w} = \frac{\partial T_w}{\partial t}, \quad \text{for } 0 < r < r_w \tag{B-28}$$

For specimen

$$a = \left(\frac{\partial^2 T}{\partial r^2} + \frac{\partial T}{r\partial r}\right) = \frac{\partial T}{\partial t}, \quad \text{for } r_w < r < \infty \tag{B-29}$$

To solve this differential equation, we need to impose few initial and boundary conditions given below, For initial conditions when $t \leq 0$,

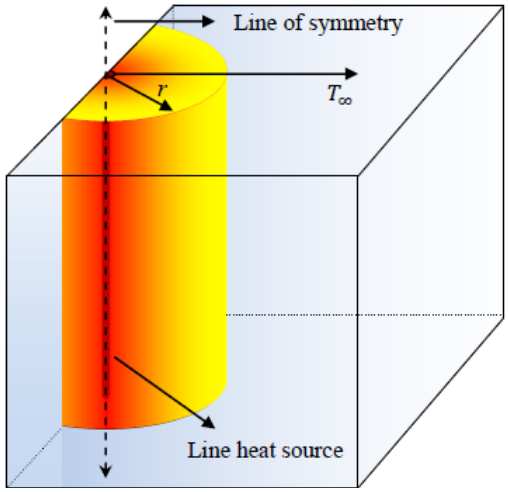

Figure B-III: A continuous line heat source.

$$T_w = T_0 = T \quad \text{at any} \quad r \tag{B-30}$$

$$\Delta T(r,t) = 0 \quad \text{at any} \quad r \tag{B-31}$$

For boundary conditions when $t > 0$

$$T = T_0 \quad \text{at } r \to \infty \tag{B-32}$$

$$T = T_w \quad \text{at } r = r_w \tag{B-33}$$

$$\lambda_w \frac{\partial T_w}{\partial r} = \lambda \frac{\partial T}{\partial r} \quad \text{at } r = r_w \tag{B-34}$$

$$\frac{\partial T_w}{\partial r} = 0 \quad \text{at } r = 0 \tag{B-35}$$

By using above given initial and boundary conditions, we come to result;

$$\Delta T(r,t) = T(r,t) - T_0 = -\frac{q}{4\pi\lambda}\text{Ei}\left(-\frac{r^2}{4at}\right) \tag{B-36}$$

Here, $\text{Ei}(-x)$ is the exponential integral function. Wire acts as a heat source and produces a time-dependent temperature field within the test specimen. The temperature

rise at a radial distance r from the hot-wire is given by [30; 31]

$$\Delta T(r,t) = \frac{q}{4\pi\lambda}\ln\left(\frac{4at}{r_w^2 C}\right) \tag{B-37}$$

Appendix C

C.1 Working Principle of Transient Techniques

A line or semi-infinite strip heat source is surrounded by a material which is initially at uniform temperature $T = T_0$. The resulting time-dependent temperature rise at a cylindrical surface at a distance r from the reference axis ($r = 0$) is governed by following equation:

$$\Delta T(t) = T(t) - T_0 = \frac{q}{\sqrt{4\pi}L\lambda} f(\tau) \tag{C-1}$$

The signal $\Delta T(t)$ is a measure of the thermal conductivity λ and thermal diffusivity a of the sample. In a transient hot wire (THW) experiment, the temperature increase of the wire ($T(t)$) is monitored with time t. As temperature rises, the voltage drop $V(T(t))$ across a current-carrying metal wire also rises. It can be represented as:

$$V(T(t) = V_0 \left(1 + \alpha \Delta T(t)\right) \tag{C-2}$$

Substituting value of ΔT from equation C-1 we get,

$$V(T(t) = V_0 \left(1 + \alpha \frac{q}{\sqrt{4\pi}L\lambda} f(\tau)\right) \tag{C-3}$$

The initial voltage drop V_0 is the voltage before starting the experiment at time zero. α denotes the temperature coefficient of the electrical resistance of the sensor (wire) of length L. $f(\tau)$ specifies the shape of the output signal and is called the sensor function. For a hot-wire, $f(\tau)$ is given as below:

$$f(\tau) = -\frac{1}{\sqrt{4\pi}} \mathrm{Ei}(-\tau^{-2}) \tag{C-4}$$

Where, τ is a dimensionless time defined as;

$$\tau = \frac{\sqrt{4at}}{r} \tag{C-5}$$

The sensor function $f(\tau)$ is nonlinear and implicit in real time t. For practical purposes ($\tau^{-2} << 1$), first-order approximations which are linear in $\ln(t)$ can be obtained. This is based on the related series expansions of equation C-4. It can be expressed as;

$$f(\tau) \approx \frac{1}{\sqrt{4\pi}}(-\gamma + \ln(\tau^2)) \tag{C-6}$$

Where, $\gamma = 0.5772$ is the Euler's constant.

By substituting equation C-6 into equation C-3 and putting $q = IV_0$ we can get the working equation of the transient hot wire technique:

$$\Delta V(t) = V(t) - V_0 \approx \frac{\alpha(V_0)^2 I}{4\pi\lambda L}\left(\ln(t) + \ln\left(\frac{4a}{Cr^2}\right)\right) \tag{C-7}$$